



UNIVERSITY OF SALERNO
DEPARTMENT OF PHARMACEUTICAL SCIENCES



PhD Course in Pharmaceutical Sciences
IX-Course N.S (XXIII)
2007-2010

DESIGN AND SYNTHESIS OF NEW POLYCYCLIC COMPOUNDS
WITH POTENTIAL ANTICANCER ACTIVITY

Tutor
Prof. Pio Iannelli

PhD Student
Simona Musella

Coordinator
Prof. Nunziatina De Tommasi

INDEX

ABSTRACT	I
CHAPTER I:	1
INTRODUCTION	
Proliferation, cell cycle and Apoptosis in cancer	
1.1 Evolution of cancers	2
1.2 The commonality of cancers	5
<i>1.2.1. Carcinogenesis</i>	5
1.3 The cell cycle and its regulation	7
<i>1.3.1 Cancer as a disease of deregulated cell proliferation</i>	11
1.4. Apoptosis in health and disease	12
<i>1.4.1 The apoptotic process</i>	13
<i>1.4.2 Cancer as a disease of deregulated survival</i>	15
1.5 Therapeutic targeting of cell proliferation and apoptosis	19
CHAPTER II:	22
INTRODUCTION	
Target for cancer therapy	
2.1. p53 network	23
<i>2.1.1 Role of p53: normal versus cancer cells</i>	23
2.2 The role of p53 in human cancer	25
<i>2.2.1 p53; the guardian of the genome</i>	26
<i>2.2.1.1. p53; The policeman of the oncogenes</i>	29
2.2. p53 co-activators	30
2.3. Downstream events of the p53 pathway	32
<i>2.3.1 Growth arrest</i>	32
<i>2.3.2 DNA repair</i>	33
<i>2.3.3 Apoptosis</i>	34
<i>2.3.3.1 Cell cycle arrest or apoptosis</i>	34
<i>2.3.4 p53 role in transcription dependent apoptosis</i>	36
<i>2.3.5 p53 role in mitochondrial mediated apoptosis</i>	39

CHAPTER III:	41
SEARCH SETTING	
3. AIMS OF THE STUDY	42
CHAPTER IV:	44
DESIGN AND SYNTHESIS OF A SERIES OF CARBAZOLE-BASED DERIVATIVES	
4.1. Background and design	45
4.2. Results and discussion	48
<i>4.2.1. Chemistry</i>	48
<i>4.2.2. Biological results</i>	53
CHAPTER V:	56
DESIGN AND SYNTHESIS OF SPIROTRIPROSTATIN-INSPIRED DIKETOPIPERAZINE SYSTEMS AS POTENTIAL CELL CYCLE MODULATORS	
5.1. Background and design	57
5.2 Results and discussion	59
<i>5.2.1 Chemistry</i>	59
<i>5.2.2 Biological results</i>	72
CHAPTER VI:	74
DESIGN OF POTENTIAL p53 MODULATORS	
6.1. Background and design	75
6.2 Results and discussion	78
<i>6.2.1 Chemistry</i>	78
6.4. Biology and Pharmacology	81
<i>6.4.1. Phase-Contrast Microscopic Analysis of Cell Morphology and Apoptosis</i>	86
<i>6.4.2. Cell Cycle Effects and Expression of p53</i>	88
<i>6.4.3. Inhibition of p53-MDM2 Interaction.</i>	90
CHAPTER VII:	92
CONCLUSIONS	

CHAPTER VIII:	96
EXPERIMENTAL SECTION	
8.1. Materials and methods	97
8.2. General Procedure for the Synthesis of 1a, 1b, 1c derivatives	100
8.3. General Procedure for the Synthesis of 2, 3, 4 derivatives	101
8.4. General Procedure for the Synthesis of 2a, 2b, 3a, 3b, 4a, 4b derivatives	102
8.5. General procedure for the synthesis of 29a,b–32a,b derivatives	104
8.6. General procedure for the synthesis of 26a–b, 27a, 28a–b derivatives	108
8.7. General procedure for the synthesis of 29a,b–32a,b derivatives	113
8.8. General Procedure for the Synthesis of 42a-e/45a-e derivatives	118
8.9. General Procedure for the Synthesis of 46f-i/47f-I derivatives	127
8.10. Biology.	132
CHAPTER IX:	134
REFERENCES	

ABSTRACT

p53 is best known as a tumor suppressor that transcriptionally regulates, in response to cellular stresses such as DNA damage or oncogene activation, the expression of various target genes that mediate cell-cycle arrest, DNA repair, senescence or apoptosis—all of these cellular responses are designed to prevent damaged cells from proliferating and passing mutations on to the next generation. In 50% of human cancers, p53 is defective due usually to somatic mutations or deletions primarily in its DNA-binding domain and, to a lesser extent, to posttranslational modifications such as phosphorylation, acetylation and methylation that affect p53 function and stability. Altered p53 fails to regulate growth arrest and cell death upon DNA damage, directly contributing to tumor development, malignant progression, poor prognosis and resistance to treatment. Conversely, restoring endogenous p53 activity can halt the growth of cancerous tumors in vivo by inducing apoptosis, senescence, and innate inflammatory responses. cycle arrest, apoptosis, or senescence. While p53 plays a protective role in normal somatic tissues by limiting the propagation of damaged cells, its powerful growth suppressive and proapoptotic activity could be turned into a powerful weapon against cancer cells that have retained the functionality of the p53 pathway.

Searching for small-molecules that activate the transcriptional activity of p53 would be expected to lead to the discovery of both DNA-damaging agents and compounds that are specific for the p53 pathway, including agents that interact directly with p53 or that inhibit MDM2 a negative regulator of p53 activity and stability. MDM2 is overexpressed in many human tumors and effectively impairs the function of the p53 pathway. Therefore, restoration of p53 function by antagonizing MDM2 has been proposed as a novel approach for treating cancer, and studies using macromolecular tools have shown its validity in vitro.

According to these findings, and as part of a wide medicinal chemistry program aimed at identifying small-molecules endowed with antitumor activity, different series of natural compound-inspired derivatives were designed as potential p53 modulators. Specifically, my PhD thesis work has been centered on two projects: the first was based on the design and synthesis of carbazole derivatives as DNA- damaging agents; while the second was based on the valuation of natural product analogues designed as both cellular cycle modulators and p53-MDM2 interaction inhibitors. The final aim of this study was to identify of suitable leads which allow us to deep on the molecular complexity of p53 network, improving the antitumor therapeutic arsenal

The role of natural products as a source for remedies has been recognized since ancient times. Despite major scientific and technological progress in combinatorial chemistry, drugs derived from natural product still make an enormous contribution to drug discovery today. The development of novel agents from natural sources presents obstacles that are not usually met when one deals with synthetic compounds. For instance, there may be difficulties in accessing the source of the samples, obtaining appropriate amounts of the sample, identification and isolation of the active compound in the sample, and problems in synthesizing the necessary amounts of the compound of interest. An analysis of the number of chemotherapeutic agents and their sources indicates that over 60% of approved drugs are derived from natural compounds.

During my PhD thesis work three different structural motives present in natural products have been considered to be suitable scaffold in the design of new antitumoral agents: carbazoles, acridines and spirooxindole derivatives.

Carbazoles either in a pure substituted or in an annellated substituted form, represent an important and heterogeneous class of anticancer agents, which has grown considerably over the last two decades. Recently, Wong et al. have described a particular activity of a series of acridine derivatives characterized

by a polycyclic planar system and by a side chain ending with a tertiary amine, act stabilized p53 protein by blocking its ubiquitination, without phosphorylation of ser15 or ser20 on p53. Furthermore, these derivatives induced p53-dependent cell death, activating p53 transcriptional activity. Based on the structural cytotoxic requirements for these class of products my first PhD project was centered on synthesis of two series of compounds in which a carbazole skeleton were linked by an alkyl chain to an amine (series 1) or substituted amide (series 2) groups.

In the other hand, small molecule natural products containing spirooxindole derivatives have demonstrated to be invaluable tools in the discovery and characterization of critical events for the progression and the regulation of the cell cycle. Based on the spirotryprostatin-A structure, during my PhD project II I designed, synthesized, and evaluated different series of compounds belonging to the diketopiperazine structural class as potential cell cycle modulators and cytotoxic agents. Starting from the spirooxindolthiazolidine scaffold, amide coupling with Pro derivatives and intramolecular cyclization reactions are suitable synthetic methods to generate chemically diverse diketopiperazine system, such as hexahydropyrrolo[1,2-a][1,3]thiazolo[3,2-d]pyrazine-5,10-dione (structure I), hexahydropyrrolo[1,2-a][1,3]thiazolo[3,4-d]pyrazine-5,10-dione (structure II) and, spiroindol-2-one[3,30]hexahydro-5,10H-pyrrolo[1,2-a][1,3]thiazolo[3,4-d]pyrazine-5,10-dione (structure III). Some of these compounds, especially those who belong to the series I and II, showed interesting cytotoxic activity.

In the last part of my project, I have designed and synthesized two libraries of compounds based on the spirooxindol-thiazolidine moiety, analogues of spirooxindol-pyrrolidine template as p53-MDM2 inhibitors.

Compounds (3R,7aR)-6-(4-chlorobenzyl)-1H-spiro[imidazo[1,5-c]thiazole-3,3'-indoline]-2',5,7(6H,7aH)-trione (**42c**) and (3R,7aR)-50-methyl-6-(3,4,5-trimethoxybenzyl)-1H-spiro[imidazo-[1,5-c]thiazole-3,3'-indoline]-

2',5,7(6H,7aH)-trione (**43d**) are the most potent compounds of this series, inhibiting cell growth of different human tumor cells at submicromolar and micromolar concentrations, respectively. Compound **42c** induces apoptotic cell death in human melanoma cell line M14 at 24 h, while in the same condition, treatment with **43d** shows a clear arrest at G2/M phase inducing delay of cell cycle progression. Possibly, these activities may be due to inhibition of p53-MDM2 interaction and subsequent p53 release and activation.

CHAPTER 1:
INTRODUCTION

Proliferation, cell cycle and Apoptosis in cancer

1. PROLIFERATION, CELL CYCLE AND APOPTOSIS IN CANCER

1.1 Evolution of cancers

Since its inception, the study of the molecular basis of cancer has carried with it the promise of more refined, more effective cancer therapies. It has generally been assumed that because cancers are derived from numerous tissues with multiple etiologies, and as tumor progression carries with it a bewildering and seemingly endless combination of genetic and epigenetic alterations giving rise to a hugely disparate series of diseases, cures for cancer must be as diverse as the diseases themselves.

Although neoplasia involves many other processes that also present targets for cancer therapy,¹ in almost all instances, deregulated cell proliferation and suppressed cell death together provide the underlying platform for neoplastic progression. The challenge before the research community is to identify and understand the molecular anatomy of such pivotal steps in tumor progression and to develop therapies that directly these points of convergence.

Cancers are diseases in which unremitting clonal expansion of somatic cells kills by invading, subverting and eroding normal tissues. Driving cancer development are stochastic somatic cell mutations in genes that govern and regulate the diverse aspects of metazoan growth control. Evolution of cancer is more complex than the straightforward linear accumulation of oncogenic mutations. Potentially oncogenic proliferative signals are coupled to a variety of growth-inhibitory processes, such as the induction of apoptosis, differentiation or senescence, each of which restricts subsequent clonal expansion and neoplastic evolution. Tumor progression occurs only in the

very rare instances where these growth-inhibitory mechanisms are thwarted by compensatory mutations (Figure 1).

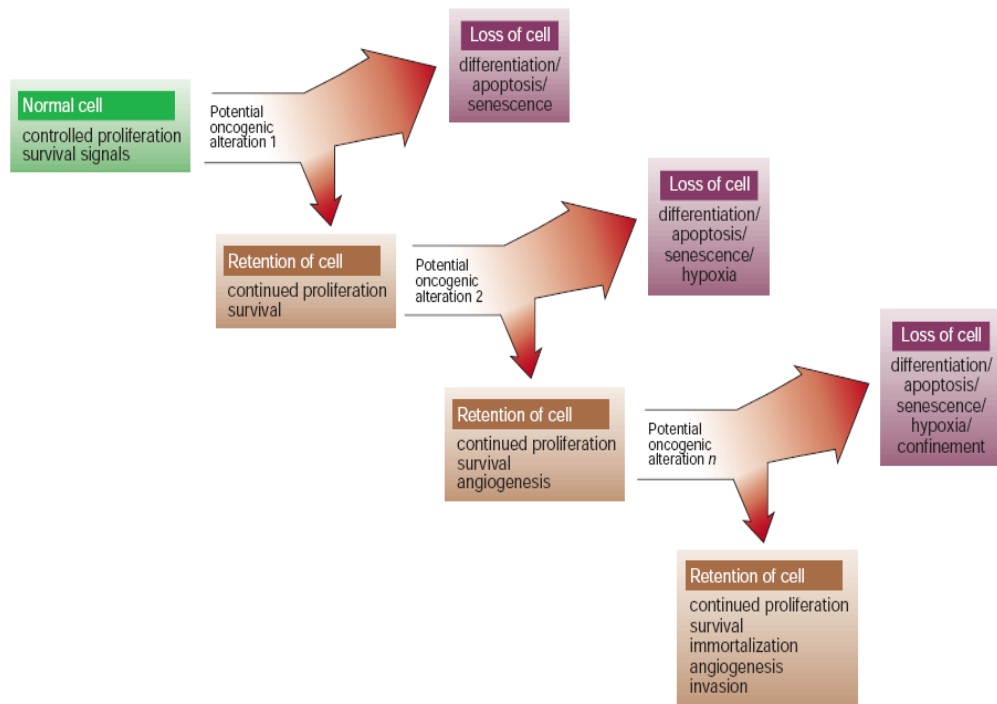


Figure 1: *Evolution of cancer*

The processes governing the genesis and progression of cancers are evolutionary ones in which natural selection acts upon the inherent or acquired diversity of various somatic clones, fostering the outgrowth of those with some form of propagative advantage. Metazoans must restrain this tendency of individual somatic cells to establish their own autonomous colonies, yet at the same time sanction sufficient somatic cell proliferation to build and maintain the whole organism.

Unfortunately, long-lived organisms such as vertebrates need substantial and continuous cell proliferation throughout their extended lives, both for

development and long-term maintenance and repair. In teleological terms, the evolutionary imperative of vertebrates has been to find a way to allow cell proliferation when needed, while at the same time efficiently suppressing the genesis of mutated cells leading to deregulated growth. When such measures fail, cancer is the inevitable consequence.

Awareness of the evolutionary nature of cancer offers a number of important insights into the malignant process. First, and perhaps most striking, is the rarity of the cancer cell. With an estimated mutation rate of some 1 in 22107 per gene cell division², some 1014 target cells in the average human, and an abundant repertoire of genes regulating all aspects of cell expansion, it is remarkable that cancers arise in only 1 in 3 lifetimes. This is even more striking when one considers that oncogenic mutations, by their nature, foster clonal expansion of the affected cell, so propagating the initial mutation and thereby increasing the number of target cells available for (and hence the probability of) further oncogenic mutation. The rarity of cancer highlights the efficacy of potent anti-tumorigenic mechanisms presiding over somatic cells. Cancers prevail only when these mechanisms have failed.³

Second, cancers ‘progress’ for the same reason organisms seem to — we see only the successes, not the failures. This distorts our statistical view of cancer progression. No matter how rare the genesis and evolution of a cancer cell or how effective the anti-cancer therapy administered, our perception is only of the rare surviving clones that beat all the odds and appear as clinical disease. Our inability to discern the mechanisms that thwart the vast majority of inchoate tumors deprives us of great insight into how these mechanisms break down in cancer and, correspondingly, how we might best reactivate them.

Third, evolutionary trajectories of cancers are shaped by the selective pressures they encounter. Tumors evolve within differing somatic environments, each of which imposes its own unique constraints.

Fourth, evolution is an ongoing process. As a neoplasm progresses, expands and spreads, it confronts shifting selective pressures. The heterogeneity and diversity seen in cancers are vestiges of a dynamic and stochastic evolutionary force that varies with differing somatic environments.

1.2 The commonality of cancers⁴

Tumors are diverse and heterogeneous, but all share the ability to proliferate beyond the constraints limiting growth in normal tissue. Aberrations in the regulation of a restricted number of key pathways that control cell proliferation and cell survival are mandatory for establishment of all tumors. Deregulated cell proliferation together with suppressed apoptosis constitute the minimal common platform upon which all neoplastic evolution occurs. The critical issue is to identify how tumor cells differ from normal cells and how those differences can be exploited therapeutically.

1.2.1. Carcinogenesis

The transformation of a normal cell into a cancerous cell is a complex and multi-step process that include initiation, promotion, and progression (Figure 2). A number of factors such as diet, toxins, smoking, alcohol, obesity and infections are attributed to the development of cancer.

These factors help in the carcinogenesis process by inducing oxidative damage to the DNA. If a cell containing damaged DNA divides before the DNA can be repaired, the result is likely to be a permanent genetic alteration constituting a first step in carcinogenesis. Body cells that divide rapidly are more susceptible to carcinogenesis because there is less opportunity for DNA repair before cell division. Factors as the variation in epigenetic code or aberrations in tumor suppressor genes, oncogenes, and genes involved in repair machinery leads to uncontrolled growth by recessive loss of tumor

suppressor genes or dominant gain of oncogenes and/or aneuploidy. Viruses, or mutagenic spontaneous changes in the components of signaling pathways lead also to cellular transformation and have also been implicated in the cause of cancer.

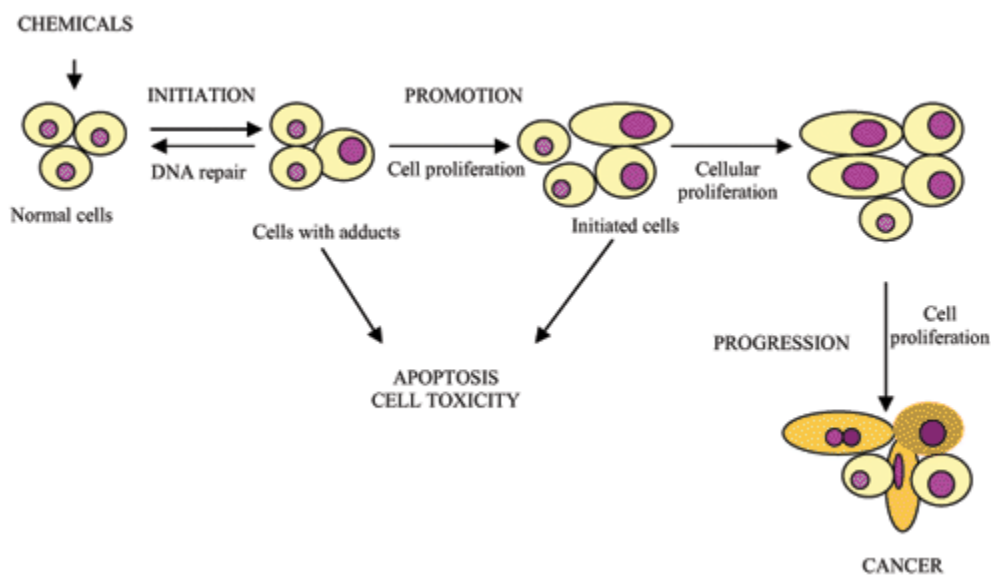


Figure 2. Carcinogenesis is initiated with the transformation of the normal cell into a cancer cell (initiated cell).

Causative factors may vary among different cancers but the basic hypothesis that a normal human cell has to acquire at least six essential alterations to become a malignant cancerous cell in case of solid tumors. These six alterations include: *the ability to sustain autonomous growth; the ability to avoid growth inhibitory signals; the evasion of apoptosis; the potential to replicate infinitely; sustained angiogenesis; and finally, for the malignant tissue to be invasive and metastatic.*¹

Cancer cells contain many altered and/or mutated genes. These almost always include: mutations in genes that are involved in mitosis; that is, in genes that

control the cell cycle. Their mutated or over-expressed products stimulate mitosis even though normal growth signals are absent. Example: *many tyrosine kinase receptors* including epidermal growth factor receptor (*EGFR*), the gene encoding the receptor for epidermal growth factor (EGF) (*EGFR* is also known as *HER1*). Moreover, for altering cell homeostasis in favor of cellular immortality cell has to by pass cell signals, which inhibit uncontrolled cell proliferation, they are tumor suppressor genes, and these genes normally inhibit mitosis. Example: the *p53* gene product normally senses DNA damage and either halts the cell cycle until it can be repaired or, if the damage is too massive; triggers apoptosis. During the course of cellular immortalization different cell signaling pathways are altered in favor of tumorogenesis and understanding of these altered cell signaling pathways in detail helps to design anticancer therapies

1.3 The cell cycle and its regulation

With advancements in our understanding of the basic mechanisms of oncogenesis, we have gained a greater appreciation for the critical role that cell cycle regulation plays in malignant transformation and in the development of resistance to chemotherapy. Perturbations in the cell cycle are described commonly in carcinogenesis. Furthermore, with our improved understanding of the effects of chemotherapy on healthy and cancerous cells, it is increasingly apparent that the cell cycle also plays a critical role in the development of resistance to chemotherapy. These observations have led to the development of a new class of anticancer therapeutics in clinical development today.⁵

The fundamental task of the cell cycle is to ensure that DNA is faithfully replicated once during S phase and that identical chromosomal copies are distributed equally to two daughter cells during M phase.⁶ The machinery for

DNA replication and chromosome segregation is insulated from interruption by extracellular signals, and its essential and autonomous nature implies that damage to the pivotal components would be highly debilitating, if not fatal, to cells. Therefore, genes commanding these processes should not be frequent targets of mutation, deletion, or amplification in cancer. Oncogenic processes exert their greatest effect by targeting particular regulators of G₁ phase progression.⁷ During the G₁ phase, cells respond to extracellular signals by either advancing toward another division or withdrawing from the cycle into a resting state (G₀).⁸ Unlike transit through the S, G₂, and M phases, G₁ progression normally relies on stimulation by mitogens and can be blocked by antiproliferative cytokines. Cancer cells abandon these controls and tend to remain in cycle, and because cell cycle exit can facilitate maturation and terminal differentiation, these processes are subverted as well. The decision to divide occurs as cells pass a restriction point late in G₁, after which they become refractory to extracellular growth regulatory signals and instead commit to the autonomous program that carries them through to division. An appreciation of restriction point control is central to our understanding of how and why cancer cells continuously cycle.

The cell cycle is a critical regulator of the processes of cell proliferation and growth as well as of cell division after DNA damage. It governs the transition from quiescence (G₀) to cell proliferation, and through its checkpoints, ensures the fidelity of the genetic transcript. It is the mechanism by which cells reproduce, and is typically divided into four phases. The periods associated with DNA synthesis (S phase) and mitosis (M phase) are separated by gaps of varying length called G₁ and G₂ (Figure 3). Progression of a cell through the cell cycle is promoted by a number of CDKs which, when complexed with specific regulatory proteins called cyclins, drive the cell forward through the cell cycle. There exist corresponding cell cycle inhibitory proteins (CDK inhibitors [CDKIs]) that serve as negative regulators of the cell

cycle and stop the cell from proceeding to the next phase of the cell cycle (Fig 1). The INK4 (for inhibitor of cdk4) class of CDKs, notably p16lnk4a, p15lnk4b, p18lnk4c, and p19lnk4d, bind and inhibit cyclin D-associated kinases (CDK2, -4, and -6). The kinase inhibitor protein (KIP) group of CDK inhibitors, p21waf1, p27kip1, and p57kip2, negatively regulate cyclin E/CDK2 and cyclin A/CDK2 complexes.⁹

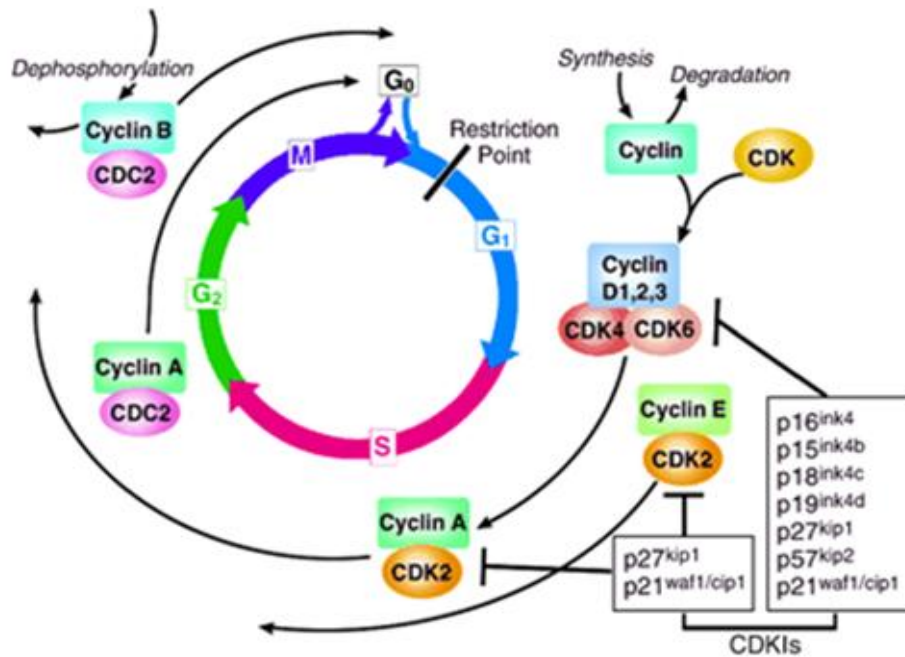


Figure 3. The cell cycle. The cell cycle is divided into four phases (G₁, S, G₂, and M). Progression through the cell cycle is promoted by cyclin-dependent kinases (CDKs), which are regulated positively by cyclins and negatively by CDK inhibitors (CDKIs). The restriction point is the point at which cells progress through the cell cycle independent of external stimuli.

The pattern of cyclin expression varies with a cell's progression through the cell cycle, and this specific cyclin expression pattern defines the relative position of the cell within the cell cycle.¹⁰ At least nine structurally related CDKs (CDK1- CDK9) have been identified, though not all have clearly defined cell cycle regulatory roles. A considerable number of cyclins have been identified to date (cyclin A–cyclin T). CDK/cyclin complexes themselves become activated by phosphorylation at specific sites on the CDK by cdk7/cyclin H, also referred to as CDK-activating kinase (CAK).¹¹ Cyclin D isoforms (cyclin D1-D3) interact with CDK2, -4, and -6 and drive a cell's progression through G1. The association of cyclin E with CDK2 is active at the G1/S transition and directs entry into S phase. S phase progression is directed by the cyclin A/CDK2 complex, and the complex of cyclin A with CDK1 (also known as cdc2) is important in G2. CDK1/cyclin B is necessary for mitosis to occur.

1.3.1 Cancer as a disease of deregulated cell proliferation

Each of the pathways that constrains the proliferative response in normal cells is perturbed in most cancers. One class of mutations required for tumor development acts by short circuiting the normally obligate requirement of somatic cells for external mitogenic signals.¹² Such mutations may involve autocrine production of a normally limiting mitogen, activating mutations of the mitogen RTKs or G-protein signal transducers such as Ras, or mutations affecting one of the many intermediary signal transducing molecules that convey mitogenic information to its intracellular targets. A second class of growth-deregulating mutations comprises those that target the principal late-G1 cell-cycle checkpoint regulated by pRB.¹³ Defects in this pathway, which may be universal in human cancers, include deletion of the *RB* gene itself and deregulation of the CDKs that phosphorylate and functionally inactivate pRB,

either through direct over-activation of CDKs or through genetic loss of their inhibitors.¹⁴ Another frequent proliferative lesion that has the effect of deregulating the cell cycle is uncontrolled expression of Myc.¹⁵ Myc expression is tightly controlled by mitogen availability in normal cells, but it is usually expressed in a deregulated or elevated manner in tumor cells. Myc seems to be a strategic controller of cell proliferation that acts pleiotropically to coordinate both cell growth¹⁶ and concomitant progression through the cell cycle.¹⁷

The presence in individual tumors of multiple mutations that affect each of the pathways discussed above suggests that each pathway contributes a discrete type of proliferative function to the neoplastic phenotype. But precisely what such functions are and how and why they interact, remains unknown.

In addition to driving aberrant cell division, mutations in the various proliferative control pathways have a profound impact on other cell functions. For example, many of the proliferative lesions in tumor cells also contribute to the inhibition of differentiation, thereby preventing the elimination of progeny cells from the proliferative compartment of many types of tissue. pRB, for example, is essential in differentiation of several tissue types through interactions with factors such as the helix–loop–helix proteins MyoD²⁶¹⁸ and Id2. Loss or inhibition of pRB function prevents normal differentiation, a contribution to tumor development distinct from the direct deregulation of cell-cycle progression. Deregulated Myc expression also inhibits differentiation, in part by activation of Id2 expression.¹⁹

1.4. Apoptosis in health and disease²⁰

Apoptosis, or programmed cell death, is a normal component of the development and health of multicellular organisms. Cells die in response to a

variety of stimuli and during apoptosis they do so in a controlled, regulated fashion. This makes apoptosis distinct from another form of cell death called necrosis in which uncontrolled cell death leads to lysis of cells, inflammatory responses and, potentially, to serious health problems. Apoptosis, by contrast, is a process in which cells play an active role in their own death (which is why apoptosis is often referred to as cell suicide).

Apoptosis occurs during the normal development of multicellular organisms and continues throughout adult life. The combination of apoptosis and cell proliferation is responsible for shaping tissues and organs in developing embryos. For example the apoptosis of cells located in-between the toes allows for their separation. Apoptosis is also an important part of the regulation of the immune system. T lymphocytes are cells of the immune system that are responsible for destroying infected or damaged cells in the body. They mature in the thymus, but before they can enter the bloodstream they are tested to ensure that they are effective against foreign antigens and are also not reactive against normal, healthy cells. Any ineffective or self-reactive T-cells are removed through the induction of apoptosis. Problems with the regulation of apoptosis have been implicated in a number of diseases. Cancer is a disease that is often characterized by too little apoptosis. Cancer cells typically possess a number of mutations that have allowed them to ignore normal cellular signals regulating their growth and become more proliferative than normal. Under normal circumstances damaged cells will undergo apoptosis, but in the case of cancer cells mutations may have occurred that prevent cells from undergoing apoptosis. In these cases there is no check on the cellular proliferation and consequently the disease can progress to the formation of tumors. In many cases these tumors can be difficult to kill as many cancer treatments rely on damaging the cells with radiation or chemicals and mutations in the apoptotic pathway often produce cells that are resistant to this type of attack.

*1.4.1 The apoptotic process*²⁰

Upon receiving specific signals instructing the cells to undergo apoptosis a number of distinctive changes occur in the cell. A family of proteins known as caspases are typically activated in the early stages of apoptosis. These proteins breakdown or cleave key cellular components that are required for normal cellular function including structural proteins in the cytoskeleton and nuclear proteins such as DNA repair enzymes. The caspases can also activate other degradative enzymes such as DNases, which begin to cleave the DNA in the nucleus.

There are a number of mechanisms through which apoptosis can be induced in cells. The sensitivity of cells to any of these stimuli can vary depending on a number of factors such as the expression of pro- and anti-apoptotic proteins (eg. the Bcl-2 proteins or the Inhibitor of Apoptosis Proteins), the severity of the stimulus and the stage of the cell cycle. Some of the major stimuli that can induce apoptosis include virus infection, cell stress and DNA damage.

In some cases the apoptotic stimuli comprise extrinsic signals such as the binding of death inducing ligands to cell surface receptors called death receptors. These ligands can either be soluble factors or can be expressed on the surface of cells such as cytotoxic T lymphocytes. The latter occurs when T-cells recognize damaged or virus infected cells and initiate apoptosis in order to prevent damaged cells from becoming neoplastic (cancerous) or virus-infected cells from spreading the infection. Apoptosis can also be induced by cytotoxic T-lymphocytes using the enzyme granzyme. In other cases apoptosis can be initiated following intrinsic signals that are produced following cellular stress. Cellular stress may occur from exposure to radiation or chemicals or to viral infection. It might also be a consequence of growth factor deprivation or oxidative stress caused by free radicals. In general intrinsic signals initiate apoptosis via the involvement of the mitochondria. The relative ratios of the

various bcl-2 proteins can often determine how much cellular stress is necessary to induce apoptosis.

1.4.2 Cancer as a disease of deregulated survival

Survival of all somatic cells requires the continuous input of survival and trophic signals to suppress apoptosis. The central engines of apoptosis are the caspases, cascades of cysteine aspartyl proteases that implement cell death by cleaving a variety of intracellular substrates that trigger cell dissolution. Caspases are synthesized as latent zymogens that are activated by proteolytic cleavage: typically through the action of upstream apical caspases. One such pathway is mediated by transmembrane death receptors of the CD95 (Apo-1 or Fas)/TRAIL/tumor-necrosis factor (TNF) receptor 1 family, whose ligation triggers recruitment and assembly of multiprotein complexes that activate apical caspase 8.²¹ The other principal death-signaling pathway involves the mitochondrion, which acts as an integrating sensor of multiple death insults by releasing cytochrome *c* into the cytosol where it triggers caspase activation. The mitochondrial pathway is thought to be the principal target of survival signaling pathways, which act by stabilizing mitochondrial function and integrity and suppressing release of cytochrome *c*.²² Once cytochrome *c* has been released from the mitochondrion, it orchestrates assembly of an intracellular apoptosome complex that recruits apical caspase 9 via the adaptor protein Apaf-1.²³ The anti-apoptotic oncoproteins Bcl-2 and Bcl-xL, which exert their principal effects through stabilization of the mitochondrion, are found to be overexpressed in several tumor types and recent analyses have indicated that loss of Apaf-1 is a relatively frequent event in malignant melanoma that presumably confers resistance to apoptosis.²⁴ A particularly potent driving force for the suppression of apoptosis in tumor cells is the coupled relationship between cell proliferation and cell death, a phenomenon

exemplified by the Myc protein. In addition to its well documented growth-promoting property, Myc was found to be a powerful inducer of apoptosis, especially under conditions of stress, genotoxic damage or depleted survival factors.²⁵ Consideration of such observations led to the proposal that the innate apoptotic potential of Myc serves as an inbuilt foil to its oncogenic capacity (Figure 4).

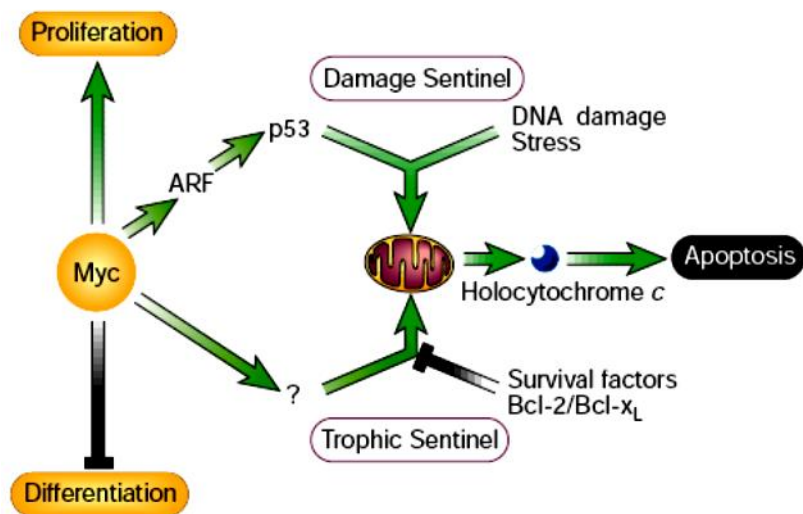


Figure 4 Activation of growth-deregulating lesions triggers ‘sentinel’ functions that guard the cell against acquiring mutations or propagating into an inappropriate somatic compartment.

In this example, the oncoprotein Myc is shown activating a p53 damage sentinel through the ARF/MDM-2 pathway, thereby sensitizing the cell to any DNA damage. Myc also promotes release of holocytochrome c from the mitochondrion into the cytosol where it triggers apoptosis. Release of holocytochrome c is inhibited by paracrine ‘survival’ signals that are typically restricted both in supply and location. Clonal outgrowth driven by relentless Myc expression outstrips survival factor availability, triggering the ‘trophic sentinel’ to kill the cell.

Another common pathway through which a wide variety of proliferative signals influence the apoptotic program is through induction of ARF, an alternate product of the *INK4a* locus, one of whose functions is to trigger upregulation of p53 through its inhibitory action on MDM-2.²⁶

Another potent selective pressure in cancers to suppress apoptosis arises from the fact that programmed cell death is the typical response of somatic cells to many forms of stress and damage; in particular damage to cell DNA (a fact exploited by most classical cancer therapeutics). Stress-associated signals that activate apoptosis include many of those encountered by the incipient tumor cell, including hypoxia and nutrient deprivation, as well as DNA damage arising from telomere erosion, defective repair, oncogene deregulation and therapy. The p53 protein is important in transducing such diverse signals into tumor-suppressive apoptotic or growth-arresting responses, which implies that there is strong selection for tumor cells to lose p53 function.²⁷ Importantly, differing p53-activating stresses tend to arise at different stages of carcinogenic progression. For example, oncogene deregulation occurs early, as it is a prerequisite for clonal expansion, whereas hypoxia is significant only after the tumor reaches macroscopic size. Consequently, p53 exerts a tumor-suppressive role at multiple stages of carcinogenic progression (Figure 5), offering an explanation for why loss of p53 has such a profound effect on tumor development.

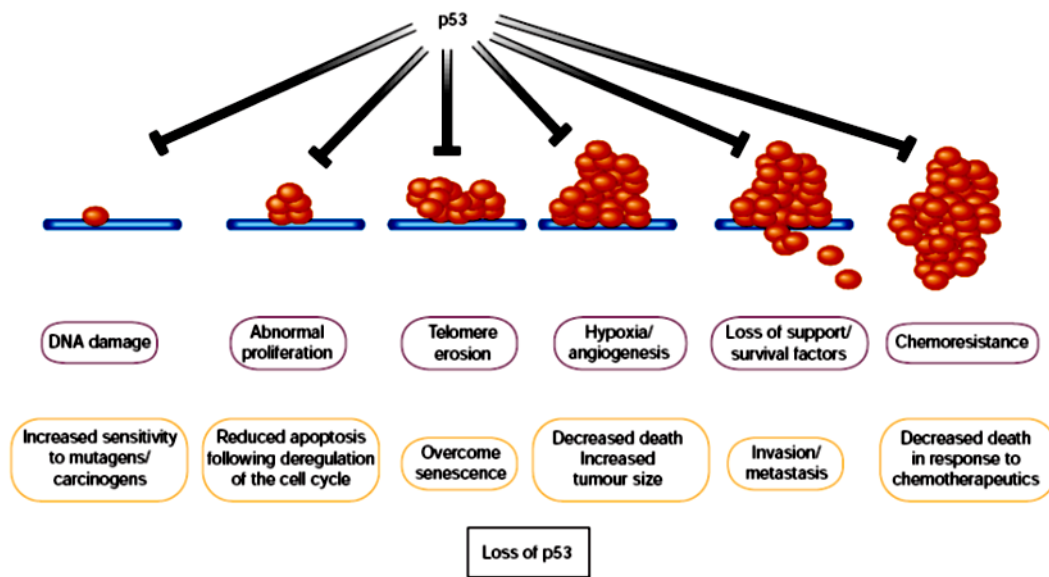


Figure 5. Many *stress signals encountered during tumor progression activate p53, resulting in apoptosis or growth arrest.*

Loss either of the ability to activate p53 or of p53 function itself has considerable impact on the ‘success’ of the carcinogenic process, as it increases the chances of a tumor cell surviving progressively adverse conditions. Inability to activate p53 in response to stress signals encountered early during tumor development, such as deregulated proliferation, may be sufficient to allow the formation of preneoplastic lesions. However, lesions that suppress activation of p53 in response to such oncogene-associated stress signals do not necessarily block activation of p53 by subsequent events encountered during malignant progression, such as DNA damage. Consequently, additional alterations in pathways that activate or respond to p53, or loss of p53 by direct mutation of the gene itself, may be selected during progression to more malignant cancers.

1.5 Therapeutic targeting of cell proliferation and apoptosis

Because deregulated proliferation and inhibition of apoptosis lie at the heart of all tumor development, they present two obvious targets for therapeutic intervention in all cancers. Clearly there are numerous mechanisms through which these two defects can occur, and the success of targeted therapy will depend to a large part on the molecular fingerprinting of individual tumours.²⁸ Although most existing cancer drugs are anti-mitotic, they act not by targeting the specific lesions responsible for deregulated tumor growth, but by crudely interfering with the basic machinery of DNA synthesis and cell division. Moreover, we now know that the surprising selectivity of such crude agents results largely from the increased sensitivity to apoptosis afforded to tumor cells by their oncogenic lesions. Drugs designed to specifically inhibit growth-deregulating lesions are currently being tested in clinical trials, and include inhibitors of RTKs, Ras, downstream signaling kinases such as the mitogen-activate protein kinase and Akt pathway, and CDKs.

At first glance, targeted inhibition of growth-deregulating lesions in cancer would be seem to have limited therapeutic efficacy, as they would at best be cytostatic. However, unexpected therapeutic bonuses may emerge from such an approach because growth deregulation induces a plethora of downstream activities in affected cells and their adjacent tissues. Therapeutic inhibition of the offending oncoprotein in tumors arising from cell lineages where terminal differentiation has been blocked could be sufficient to trigger a resumption of that differentiation program, permanently expelling the tumor cell from the proliferating compartment.²⁹

The second obvious strategy for cancer therapy is to target the lesions that suppress apoptosis in tumor cells. The potent proapoptotic effects of growth-deregulating mutations mean that tumors are peculiarly dependent upon their particular suite of antiapoptotic mutations for continued survival. Thus,

although apoptosis in tumor cells is sufficiently suppressed to below a critical threshold to enable them to survive, they remain acutely sensitized to apoptosis. In most, if not all, cancer, this ability to survive results in part from inhibition of the p53 pathway, either by inactivating mutations in p53 itself, perturbation of the signaling pathways that allow activation of p53 in response to stress, or defects in the downstream mediators of p53-induced apoptosis. Reintroduction of p53 function is sufficient to induce apoptosis in many tumor cells, and several mechanisms to reactivate p53 are being considered as therapeutic strategies. These include introduction of wild-type p53 into tumors expressing a mutant protein, or inhibition of negative regulators of p53, such as MDM-2, in those tumors that retain wild-type p53.³⁰

Regardless of efficiency in cell killing, the success of repairing the apoptotic response in tumor cells depends on the extent to which such therapies confine death to the cancer cells, and allow survival of normal tissue. Many conventional chemotherapies induce significant toxicity, particularly in tissues that normally maintain a proliferative compartment, such as gut epithelium and the hematopoietic system. This DNA damage-induced toxicity is mediated in part through p53, leading to the suggestion that inhibition of p53 in these normal tissues may protect against drug-induced toxicity, thereby improving the tolerance of conventional cancer therapies. However, implicit in the development of drugs that target specific lesions responsible for tumor cell growth is the prediction that these approaches will show significantly more specificity for tumor cell killing than conventional therapies.

Although activation of apoptotic pathways can lead to the death of untransformed cells, a process that is essential in normal development, a fundamental difference exists between tumor cells and their normal counterparts, as normal cells neither have to sustain the pro-apoptotic onslaught that is inherent in deregulated proliferation, nor survive away from

their usual environment in the absence of requisite survival signals. Repair or replacement of a single apoptotic signal, be it reactivation of p53 or removal of a survival signal, could well prove too much for a tumor cell already burdened with a heavy apoptotic load. By contrast, the same perturbation may scarcely ruffle the equilibrium of a normal cell, safely buffered in its appropriate soma and enjoying the full gamut of trophic support that ensures normal cell survival.

CHAPTER 2:
INTRODUCTION
Target for cancer therapy

2. p53: TARGET FOR CANCER THERAPY

2.1 p53 network

p53, (53KD) also known as tumor protein 53 (TP53), is a transcription factor that regulates the cell cycle and apoptosis, in case of cellular insults, and hence functions as a tumor suppressor. p53 has been described as "the guardian of the genome", "the guardian angel gene", or the "master watchman", referring to its role in conserving stability by preventing genome mutation. The transcription factor p53 responds to diverse cellular stresses to regulate target genes that induce cell cycle arrest, apoptosis, senescence, DNA repair, or changes in metabolism.³¹ In addition, p53 appears to induce apoptosis through nontranscriptional cytoplasmic processes.³² In unstressed cells, p53 is kept inactive essentially through the actions of the ubiquitin ligase MDM2, which inhibits p53 transcriptional activity and ubiquitinates p53 to promote its degradation.³² Numerous posttranslational modifications modulate p53 activity, most notably phosphorylation and acetylation. Several less abundant p53 isoforms also modulate p53 activity. Activity of p53 is ubiquitously lost in human cancer either by mutation of the p53 gene itself or by loss of cell signaling upstream or downstream of p53

2.1.1 Role of p53: normal versus cancer cells

Activation of p53 can result in a number of cellular responses, and it is possible that different responses are induced by different stress signals. There is evidence that p53 can play a part in determining which response is induced through differential activation of target-gene expression. Although the importance of these responses to tumor suppression is clear, previously unanticipated contributions of these responses to other aspects of human

health and disease are being uncovered. The role of p53 in tumor suppression, development and ageing is likely to depend on which cellular response is activated and on the context in which the activation occurs. p53 is an intensively studied protein, its fame stemming mainly from its clear role as a tumor suppressor in humans and other mammals.³³ Loss or mutation of p53 is strongly associated with an increased susceptibility to cancer, and most functions of p53 have been considered in the light of how p53 might protect from malignant progression.³⁴ Some *p53*-null mice can develop normally³⁵ an observation that has been taken to rule out major functions for p53 in normal physiology. But recent studies are questioning whether p53 is truly such a single-minded protein, and other functions of p53 that might be profoundly important during normal life are being uncovered. These include roles for p53 in regulating longevity and ageing, glycolytic pathways that might determine endurance and overall fitness, and apoptotic responses during ischaemic and other types of stress. Evidence for genetic variations in the activity of the p53 pathway in humans gives these ideas extra relevance.³⁶ One of the major mechanisms by which p53 functions is as a transcription factor that both positively and negatively regulates the expression of a large and disparate group of responsive genes (Figure 6).³⁷ Although some of these p53-responsive genes have an important role in mediating cell-cycle arrest, senescence and apoptosis (the best understood activities of p53), it is now evident that the ability of p53 to influence gene expression has wider reaching effects. Numerous studies have identified p53-regulated genes that could have a role in a number of different and sometimes unexpected responses.³⁸ Although some of these still need to be fully validated, there is now clear evidence for a role of p53 in the regulation of glycolysis,³⁹ and autophagy,⁴⁰ the repair of genotoxic damage,⁴¹ cell survival and regulation of oxidative stress,⁴² invasion and motility,⁴³ cellular senescence,⁴⁴ angiogenesis,⁴⁵ differentiation,⁴⁶ and bone remodeling.⁴⁷ The cellular pathways in which p53

is involved, are schematically represented in Figure 6. In these aspects, it is worthy to analyze whether any cancer cells are expressing wild type p53, and if they are expressing, its role in cancer cells has to be studied before clinical use of p53 mediated gene therapy as an anticancer therapy.

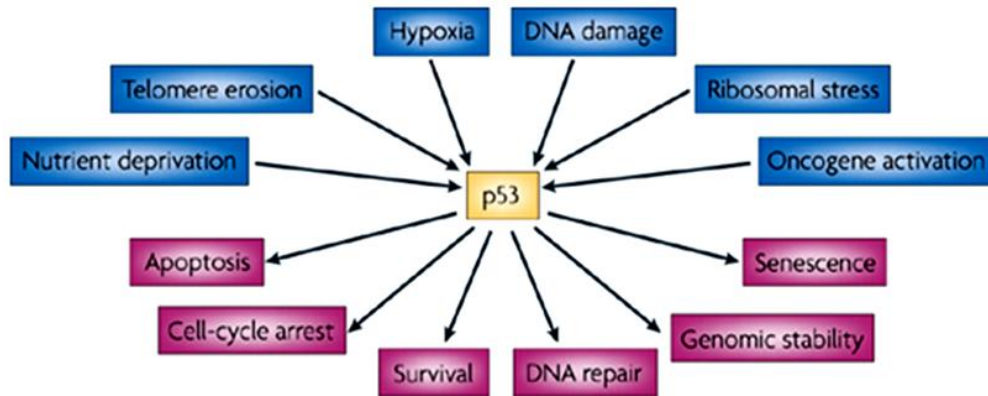


Figure 6. Activation and functions of p53. p53 has a key role in integrating the cellular responses (pink arrows) to different types of stress (blue arrows).

2.2 The role of p53 in human cancer

In the two decades since its original discovery, p53 has found a singularly prominent place in our understanding of human cancer. Although the biochemistry of p53 has been worked out in some detail, our knowledge of the biologic consequences of p53 dysfunction is still quite rudimentary. p53 dysfunction in cancer cells are mainly due to its mutation (50%), epigenetic modulation at expression level and low persistence of p53 protein level due to its enhanced turnover. Most p53 mutations found in human cancers are not null mutations but rather encode mutant version of the p53 protein that may have unwanted activities such as a gain-of-function or be dominant negative inhibitors of wt p53 activity. In this regard, it will be important to determine how best to harness the complex properties of p53's ability to induce cellular growth arrest and cell death to generate novel, effective approaches to cancer

therapy. Furthermore, a clearer appreciation of the direct interaction epigenetic factors with p53 will lead to development of strategies to inhibit tumor initiation and progression.

2.2.1 p53; the guardian of the genome

DNA damage was the first type of stress found to activate p53 and, based on this, p53 has been widely regarded as “the guardian of the genome”.⁴⁸ Extensive characterization of the signaling routes that connect DNA damage with p53 have identified a cascade of Ser/Thr kinases that includes ATM, ATR, Chk1 and Chk2, which phosphorylate p53.⁴⁹ This signaling cascade is permanently activated in human cancer, suggesting that the cancerous state is intrinsically associated to the generation of DNA damage.⁵⁰ The constitutive DNA damage present in cancer cells is thought to emanate primarily from the strong generation of reactive oxygen species,⁵¹ as well as, from the aberrant firing of DNA replication origins.⁵²

.Recent characterization of mice genetically manipulated with a knocked-in p53 that cannot be phosphorylated at two of the main residues targeted by ATM/ATR/Chk1/Chk2, namely, Ser18 and Ser23 (Ser15 and Ser20 in human p53), indicates an important role of these phosphorylation sites in some, but not all, the DNA damage induced and p53-dependent responses.⁵³ In agreement with this, mice carrying p53S18A/S23A alleles are tumor prone,⁵⁴ although this phenotype is considerably milder than in the case of p53-null mice.⁵⁵

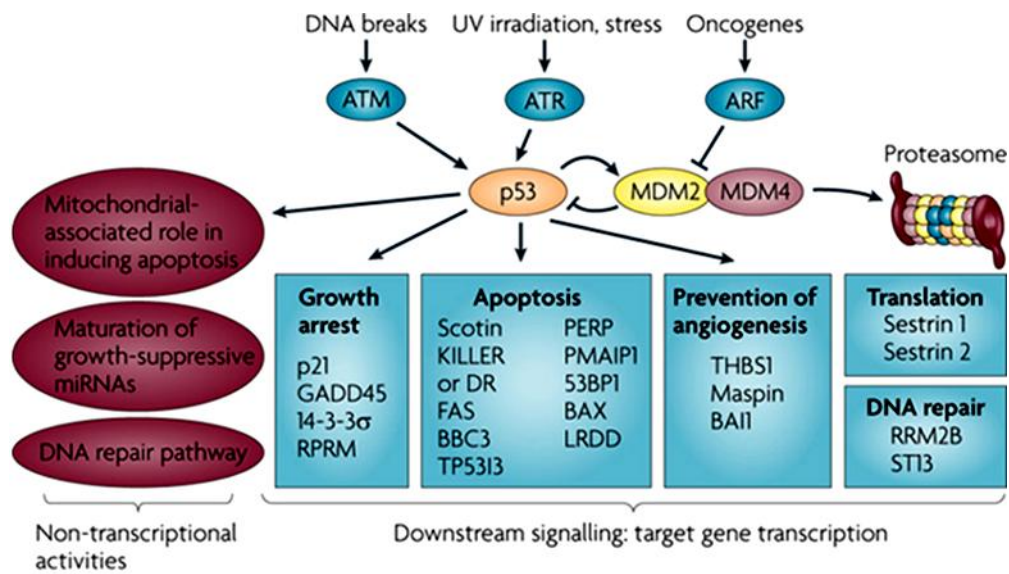


Figure 7. *p53 is at the center of a complex web of biological interactions that translates stress signals into cell cycle arrest or apoptosis²⁶. 53BP1, p53 binding protein 1; ATM, ataxia telangiectasia mutated; ATR, ataxia telangiectasia and Rad3 related; BAI1, brain-specific angiogenesis inhibitor 1; BAX, BCL2-associated X protein; BBC3, BCL2 binding component 3 (also known as PUMA); DR, death receptor; GADD45, growth arrest and DNA-damage-inducible 45; KILLER, p53-regulated DNA damage-inducible cell death receptor (also known as TNFRSF10B); LRDD, leucine-rich repeats and death domain containing; mRNA, microRNA; PMAIP1, phorbol-12-myristate-13-acetate-induced protein 1 (also known as NOXA); RPRM, reprimo; RRM2B, ribonucleotide reductase M2 B; ST13, suppression of tumorigenicity 13 (also known as p48); TP53I3, tumor protein p53 inducible protein 3; THBS1, thrombospondin 1; UV, ultraviolet.*

These data suggest that the activation of p53 in response to DNA damage occurs through multiple pathways, which in addition to the well-established kinase cascade of ATM/ATR/Chk1/Chk2, probably include other kinases such as p38, JNK/SAPK and c-Abl (Figure 7).⁵⁶ Regarding human cancer, the

available information gathered from the analysis of epigenetic aberrations indicates that the aforementioned DNA damage signaling kinases are not, in general, significant targets of genetic and epi-genetic inactivation.⁵⁷ The only exception to this is found in hematological malignancies, which present a high incidence of mutations in ATM (13–40% depending on the particular type of malignancy).⁵⁸ In line with this, a recent large-scale sequencing effort of 210 diverse human cancers has identified ATM among the three most frequently mutated kinases (5% incidence).⁵⁹ Based on the above genetic evidence, it can be concluded that DNA damage is conveyed to p53 through multiple redundant pathways in which many transducers participate, but none of them plays a critical role and, therefore, alteration of a single component does not have a significant impact on p53 function.

According, upstream signaling to p53 increases its level and activates its function as a transcription factor in response to a wide variety of stresses, whereas downstream components execute the appropriate cellular response (see below). The principal sensors seem to be MDM2 and MDM4 and their interaction with p53.⁶⁰ In non-stressed conditions these proteins bind p53, ubiquitylate it and target it for degradation by the proteasome. In stressed conditions the function of the MDM2–MDM4 complex is blocked by phosphorylation, protein-binding events and/or enhanced degradation. Hence, phosphorylation of MDM4 is essential for the p53 response to ionizing radiation, and the response to oncogene activation depends on the binding of ARF to MDM2. Many p53-activating small molecules function by causing the release of ribosomal proteins from the nucleolus to the nucleoplasm, where they bind to MDM2 and MDM4 and inhibit their function. Molecules that activate wild-type p53 in tumors by disrupting MDM2 activity can compensate for any missing upstream components of the p53 pathway, for example the loss of ARF expression that is frequent in cancer cells¹⁴². However, defective downstream p53 signaling might substantially decrease

their effectiveness. Therefore, the ability to identify tumors in which downstream p53 signaling is unaffected is important. The development of strategies to ensure that the desired p53 response is initiated when it is reactivated might be necessary and could require the judicious use of drug combinations.

2.2.1.1. p53; The policeman of the oncogenes

Among the many and varied stimuli that have been reported to activate p53, oncogenic signaling⁶¹ has gained much attention because, as DNA damage, is also universally present in cancer. Therefore, analogous to the title of “guardian of the genome”, we can also assign to p53 the function of “policeman of the oncogenes”. Oncogenic signaling activates p53 through ARF,⁶² which, in turn, interacts with MDM2 inhibiting its p53-ubiquitin ligase activity.

In this manner, ARF-dependent stabilization of p53 results in a dramatic increase in p53 activity. Many transcription factors activate ARF in response to oncogenic signaling, most notably, Dentin matrix acidic phosphoprotein (DMP1).⁶³ Mice lacking ARF have a remarkable tumor-prone phenotype,⁶⁴ although not as severe as p53-deficient mice,⁶⁵ and there is good genetic evidence in mice supporting the relevance of the ARF/MDM2/p53 axis in tumor suppression.⁶⁶ Importantly, mice deficient in ARF present a normal DNA damage response, indistinguishable from ARF-proficient mice.⁶⁷ Regarding human cancer, the analysis of (epi)genetic alterations indicate that ARF is indeed inactivated with an extraordinary high frequency (~30%).⁶⁸ However, inactivation of ARF almost invariably occurs in combination with the loss of p16INK4a, the cell cycle inhibitor, thus generating an ambiguity about which is the key targeted tumor suppressor. In this regard, it should be mentioned the existence of germline point mutations that inactivate ARF alone (i.e., sparing p16INK4a) in human kindreds predisposed to cancer.⁶⁹

Nonetheless, the number of germline mutations that inactivate p16INK4a only (i.e., sparing ARF) outnumbered by a factor of ~20 those that inactivate ARF alone.⁷⁰ Together, currently available evidence indicates that ARF is an important upstream regulator of p53, whose lack of activity has a significant impact on cancer.

2.2 p53 co-activators

The interaction between p53 and transcriptional co-activators also influences its affinity for promoters. It is therefore plausible that the specific co-factors expressed in a particular cellular context determine the repertoire of p53-target genes induced, and consequently whether the cell undergoes growth arrest or apoptosis, or even a particular apoptotic pathway, may be subject to the availability of co-activators.⁷¹

The Myc protein has been implicated as an important determinant of the choice between p53-induced growth arrest or apoptosis. Myc inhibits growth arrest in response to UV light, g-irradiation and DNA damage inflicted by reactive oxygen species.⁷² In the absence of Myc, cells that are exposed to UV light arrest in a p53- and Miz-1 (DNA-binding Myc-interacting zinc-finger 1)-dependent manner through activation of *p21*. However, when Myc is present, exposure to UV triggers its recruitment by Miz-1 to the proximal promoter region of *p21*. This interaction effectively represses *p21* induction by p53 and other activators.⁷³ Intriguingly, this repression appears to be specific for *p21*, because other p53-target genes, such as p53 upregulated modulator of apoptosis (*PUMA*) and *PIG3*, are induced. This block in *p21* induction shifts the balance away from growth arrest towards apoptosis.^{73b} It should be noted, however, that arrested cells are not necessarily protected from apoptosis. For example, normal thymocytes and mature lymphocytes undergo p53-mediated apoptosis under certain stress conditions.⁷⁴ Interaction of p53 with several

other proteins specifically enhances the induction of apoptotic target genes. The apoptosis stimulating proteins of p53 (ASPP), for example, increases the DNA binding and transactivation activity of p53 on the promoters of apoptotic genes (e.g. *Bax* and *PIG3*), while failing to promote binding to the *p21* promoter by a mechanism that remains to be defined.⁷⁵ A novel insight into the interplay between p53 and its family members, p63 and p73, in the induction of apoptosis has been recently revealed by Flores et al.⁷⁶ Their study of the effect of p63 and p73 on p53 transcriptional activity, using a selection of knockout mouse embryo fibroblasts (MEFs), defined two distinct classes of target gene. Whereas p53 alone is sufficient for the induction of *p21* and *Mdm2*, the induction of the apoptotic genes *PERP*, *Bax* and *Noxa* requires p53 together with p63 and p73. This finding demonstrates an essential role for both p63 and p73 in the efficient induction of apoptotic target genes by p53. The mechanism of this cooperation is currently unknown, but it may involve an enhanced binding to and/or stabilization of the transcription complex on the promoters of p53 apoptotic target genes by the cooperative action of all three members.⁷⁷ In addition to the contribution of p63 and p73 to the apoptotic function of p53, they play an important role in the precise control of cell death during normal mouse development. p73 also plays a role in the induction of cell death in response to DNA damage, a process involving cooperation between the Abl tyrosine kinase and p73.⁷⁸

2.3 Downstream events of the p53 pathway

Once the p53 protein is activated, it initiates a transcriptional program that reflects the nature of the stress signal, the protein modifications and proteins associated with the p53 protein. The p53 protein binds to a specific DNA

sequence, termed the p53- responsive element (RE),⁷⁹ and induces the expression of downstream genes. An algorithm that identifies p53-responsive genes in the human and mouse genome has been utilized to detect a number of new genes regulated by the p53 protein.⁸⁰ The genes in this p53 network mainly initiate one of three programs that result in cell cycle arrest, DNA repair or apoptosis.

2.3.1 Growth arrest

p21*WAF1/CIP1* is known to be a p53-downstream gene, and has been suggested to mediate p53-induced growth arrest triggered by DNA damage. The p21 protein is a cyclin-dependent kinase inhibitor that associates with a class of CDKs and inhibits their kinase activities. This will facilitate the accumulation of hypophosphorylated form of pRB that in turn associates with E2F inhibiting its transcriptional activity, leading to cell cycle arrest. As long as pRb is bound to E2F, the cell is prevented from entering into S phase. This G1 arrest affords the cell time to repair the DNA damage. Should repair be unsuccessful, P53 levels drop and CDK-cyclin protein kinase activity resumes, leading to entry into S phase. In the event that the DNA is not repair, p53 triggers apoptosis.⁸¹

2.3.2 DNA repair

Soon after having established TP53 as the most frequently altered gene in human tumors in the 1990s,⁸² p53 was understood as a major component of the DNA damage response pathway.^{48,83} After the introduction of DNA injuries the level of p53 protein rises, which in turn induces a transient cell cycle arrest or apoptotic cell death. DNA damage activates p53 through post-

translational modifications by specific kinases, such as the strand break sensor ataxia telangiectasia mutated protein (Atm), by acetyltransferases like CREB-binding protein (Cbp)/p300, and by the poly (ADPribose) polymerase 1 (Parp-1), which prevent proteolysis via the Arf-mouse double minute 2 (Mdm2) pathway and/or enhance binding of p53 to consensus sequences within the genome.⁸⁴ Initially, investigations on a direct participation of p53 in DNA repair were spurred by a number of biochemical observations. Thus, the C-terminal 30 amino acids of p53 were shown to recognize several DNA damage-related structures, such as DNA ends, gaps, and insertion/deletion mismatches.⁸⁵ p53 was also demonstrated to catalyze reannealing of short stretches of single- and double-stranded DNA and to promote strand exchange between them.⁸⁶ Further, p53 binds to three-stranded heteroduplex joints and four-stranded Holliday junction DNA structures with localization specifically at the junction, suggesting that p53 directly participates in recombinational repair.⁸⁷ Moreover, several groups demonstrated a Mg²⁺-dependent 3'–5' exonuclease activity intrinsic to p53.⁸⁸ Noticeably, the same central region within p53, where tumorigenic mutations are clustered, recognizes DNA sequence specifically, is required for junction specific binding of heteroduplex joints and is necessary and sufficient for the 3'–5' exonuclease activity on DNA.⁸⁹ In addition to p53's biochemical activities, numerous reports on physical and functional protein interactions further strengthened the proposal of a direct role of p53 in nucleotide excision repair (NER), base excision repair (BER), and double-strand break (DSB) repair.⁹⁰

2.3.3 Apoptosis

Pivotal to the tumor-suppressor activity of p53 is its ability to activate apoptosis via multiple different pathways. Since the most-studied function of p53 is its role as a transcription factor that can activate transcription of an ever-increasing number of target genes, its transcriptional activation of pro-

apoptotic genes, as well as its transcriptional repression of anti-apoptotic genes, has been widely analyzed.⁹¹ However, although a large number of genes regulated by p53 during induction of apoptosis are known no single target gene has been identified whose altered expression alone can sufficiently explain p53 mediated transcription dependent apoptosis, and whose genetic deficiency phenocopies p53 deficiency in vivo. As an additional mode of p53's pro-apoptotic activity, recent studies have placed non transcriptional pro- apoptotic activities of p53 at the center of an active debate that aims to establish a comprehensive understanding of p53- mediated apoptosis.⁹²

2.3.3.1 Cell cycle arrest or apoptosis?

The exact criteria that influence p53 to stimulate cell cycle arrest or apoptosis are only partially understood and are the subject of intense study. Several general factors that influence this decision include p53 expression levels, the type of stress signal, the cell type and the cellular context at the time of exposure to stress. Several intriguing observations have recently provided insight into the apparent intricacies of such cell fate determination. The examples described below involve the binding of p53 to its canonical binding sequence in target genes. Note, however, that p53 can also activate target genes through a non-canonical sequence. The first such example is in the p53-induced gene 3 (*PIG3*), which has been implicated in the accumulation of reactive oxygen species and apoptosis induction. *PIG3* can be induced by p53 through a microsatellite sequence within its untranslated region.⁹³ Another recently described example is the gene encoding the pro-apoptotic phosphatase PAC1, which is induced through binding of p53 to a novel palindromic binding site.⁹⁴ This might represent a new mechanism for transcriptional regulation of apoptotic genes by p53, which differs from that already described (see below). Exacting discrimination between p53 arrest and apoptotic functions has been critical to the identification of the importance of

the latter in tumor suppression. A strong link between the apoptotic function of p53 and tumor suppression has been demonstrated using transgenic mice bearing an SV40 large T antigen (LT) mutant, which inhibited pRb function without directly compromising p53 activity.⁹⁵ p53-mediated growth arrest is however impaired in these mice owing to pRb loss of function, but the apoptotic activity is functional. These mice develop choroid plexus tumors, but at a slow rate owing to continuous p53-dependent apoptosis. Elimination of p53 from these mice, by crossbreeding with p53-null mice, resulted in aggressive tumor development. This finding suggested that tumor suppression is primarily due to p53-mediated apoptosis. The most compelling insight into this fundamental question came from a recent study using the *Em-myc*-mediated lymphoma mouse model.⁹⁶ The apoptotic pathway of the lymphoma cells was blocked either by retroviral expression of *bcl-2* or a dominant negative *caspase-9*. The effect of this block on the growth of these lymphomas was then tested in recipient mice. In the apoptosis-impaired cells there was no selection for p53 mutations, in contrast to cells that had intact apoptotic pathways. Remarkably, in the apoptosis-impaired lymphoma cells expressing functional p53, the integrity of the genome and the cell cycle checkpoints were maintained. Taken together these studies support the notion that apoptosis is the critical function of p53 in tumor suppression.

2.3.4 p53 role in transcription dependent apoptosis

The past twenty-five years have seen intensive and varied investigations to better understand the functions that p53 uses to mediate apoptosis. The first indication of the role of p53 in apoptosis was obtained using the M1 mouse myeloid leukemia cell line lacking endogenous p53. Using M1 cells stably transfected with a temperature-sensitive mutant that acquires the conformation of wild-type p53 at permissive temperature (32°C), it was observed that upon downshift to the permissive temperature, the transfectants underwent rapid

loss of viability with the characteristics of apoptosis.⁹⁷ Several mechanisms have been implicated in p53-mediated apoptosis. One is p53 activation to up-regulation of pro-apoptotic Bax and down-regulation of pro-survival Bcl-2.^{92b,98} More recently it's determined that p53-mediated apoptosis of M1 cells involves rapid activation of the pro-apoptotic Fas/CD95 death pathway-via up-regulation of membrane bound Fas⁹⁹ and the intrinsic mitochondrial pathway, which results in activation of caspases 8, 9 and 10. Either Fas blocking antibody or inhibition of the apical caspases 8 and 10, were each almost as effective as IL-6 in abrogating p53 mediated apoptosis. These observations argue that p53 regulation of the bcl-2 members Bax and Bcl-2, associated with the intrinsic mitochondrial apoptotic pathway, is ancillary to the extrinsic Fas/CD95 apoptotic pathway in mediating p53 induced apoptosis of M1 myeloid leukemia cells.¹⁰⁰

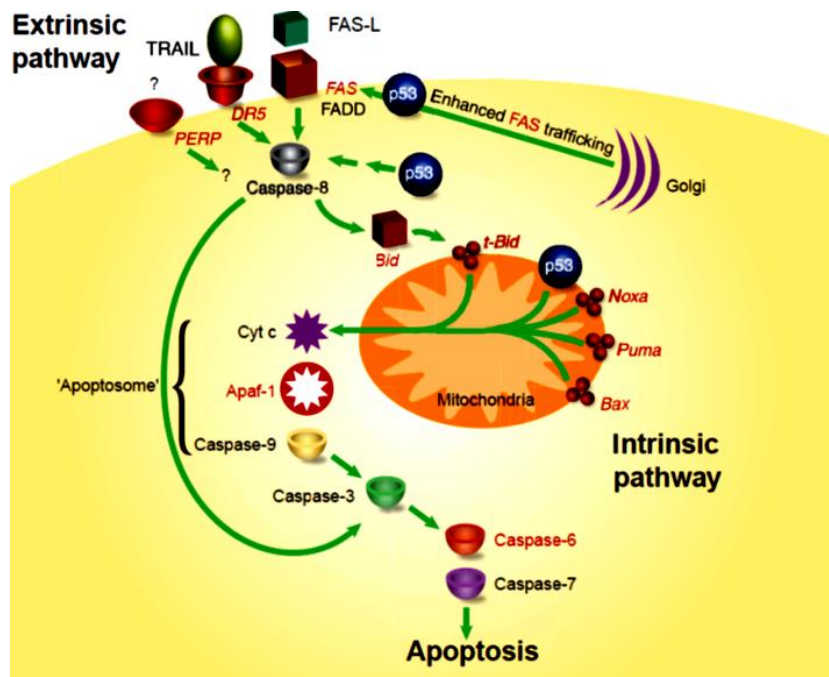


Figure 8. A model for p53-mediated apoptosis. This model depicts the involvement of p53 in the extrinsic and intrinsic apoptotic pathways. p53 target genes are shown in red. The convergence of the two pathways through Bid is shown.

In other cell types up-regulation IGF-BP3,¹⁰¹ which sequesters the cell survival factor insulin-like growth factor-1 has been associated with p53 mediated apoptosis.¹⁰² The gene encoding for the cathepsin-D protease,¹⁰³ PAG608 which encodes a nuclear zinc finger protein¹⁰⁴ and the human homolog of the Drosophilasina gene¹⁰⁵ have also been implicated as mediators of p53 induced apoptosis in various cell types. Furthermore, a series of p53-induced genes (PIG genes) were documented to encode proteins that respond to oxidative stress, suggesting that p53-mediated apoptosis involves activation of redox- controlling targets followed by increase in ROS, oxidative damage to mitochondria and caspase activation.^{93, 106} Along this research line it was recently observed that p53 suppresses Nrf2-dependent transcription of

antioxidant response genes, presumably to prevent the generation of antioxidants that could hinder induction of apoptosis.¹⁰⁷ Clearly established is p53's role as a nuclear transcription factor with the ability to activate, or repress, the expression of many genes. A number of p53 transcriptional targets, such as the p53-induced genes BAX, PUMA, NOXA, and the p53-repressed genes BCL2 and SURVIVIN, represent genes with the potential to promote or inhibit apoptosis, respectively, in stressed cells. Puma and Noxa are thought to indirectly induce mitochondrial outer membrane permeabilization (MOMP), known to be induced by the activation of Bax and Bak, via interfering with Bax and Bac interaction with prosurvival Bcl-2 family members.¹⁰⁸ Interestingly, it was observed that Puma and Noxa differentially contribute to the regulation of p53-mediated apoptotic pathways. In normal cells, Puma was found to induce mitochondrial outer membrane permeabilization via an ER-dependent pathway; however, upon E1A oncoprotein expression, cells also became susceptible to mitochondrial outer membrane permeabilization induction by Noxa via an ER-independent pathway.¹⁰⁹ In several instances, transcriptional activation by p53 was observed to be dispensable for p53-dependent apoptosis, since mutants p53 which fail to activate transcription could still induce apoptosis.¹¹⁰ In addition, p53-dependent apoptosis could occur in the presence of inhibitors of transcription and translation.¹¹¹ In recent years it has become clear that p53 also harbors a direct proapoptotic function at the mitochondria via engaging in protein-protein interactions with anti- and pro-apoptotic Bcl2 family members, including BclXL and Bak .¹¹²

2.3.5 p53 role in mitochondrial mediated apoptosis

It has been reported, certain transcriptionally inactive mutants of p53 can still induce apoptosis when over expressed in tumor cells.¹¹³ Also, in response to some stresses, such as hypoxia, p53 induces apoptosis but does not function as a transactivator.¹¹⁴ Intriguingly, Moll and al,¹⁰⁸ demonstrated that during p53-dependent apoptosis a fraction cellular p53 protein localizes to mitochondria and induces cytochrome c release; however, this is not observed during p53-mediated cell cycle arrest.¹¹⁵ Additional support for the concept that p53 has a cytoplasmic role in apoptosis induction resulted from functional analysis of polymorphic variants of p53 (Within exon 4 of the p53 gene, a common single-nucleotide polymorphism (SNP) at codon 72 leads to the incorporation of either an arginine (R72) or a proline (P72) at this position of the protein. When explored the potential mechanisms underlying the observed functional difference between the two p53 variants, made the initially surprising discovery that the greater apoptotic potential of the R72 form correlated with its much better ability to traffic to mitochondria. Based on these data, therefore concluded that the enhanced apoptosis-inducing activity of the R72 protein related, at least in part, to its greater mitochondrial localization. An analysis of whole cell or mitochondrial extracts by immune precipitation-western blot analysis, demonstrated the R72 form of p53 binds better to the mitochondrial death-effectors protein BAK than does the P72 variant, correlating with the difference in apoptotic potential of the two p53 variants. In healthy cells, Bak resides at mitochondria as an inactive monomer. In response to various death stimuli, it undergoes an activating allosteric conformational change that promotes homo-oligomerization. This leads to formation of a pore in the outer mitochondrial membrane, and allows the release of cytochrome c and other caspase cascade (Figure 4).¹¹⁶ Recently, like BAK, the BCL2 family members BAX and BCL-XL have also been implicated in mitochondrial apoptosis induction by p53 (Figure 9)¹¹⁷

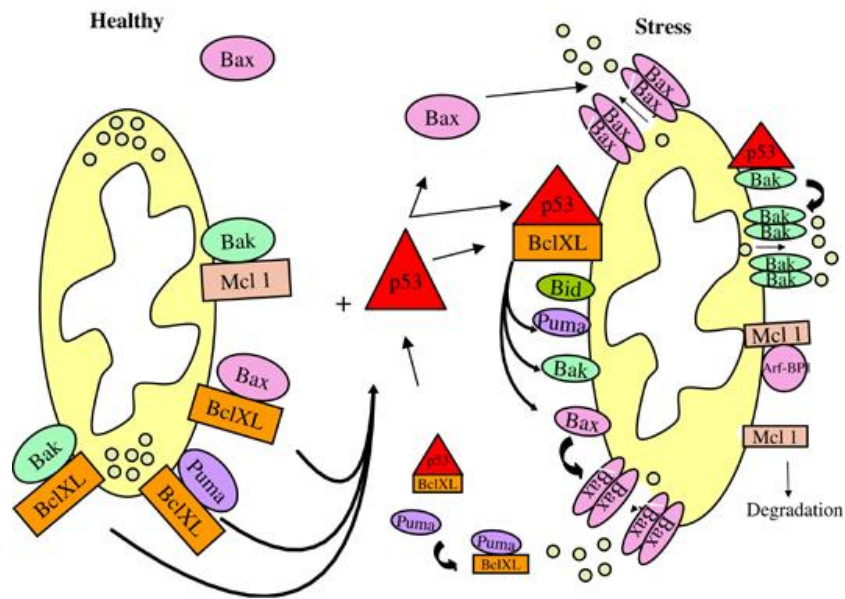


Figure 9. The mitochondrial pro-apoptotic activities of p53. In healthy cells (left), the proapoptotic BH3-only and effector BH123 proteins (ovals) exist either in complex with antiapoptotic proteins Bcl2 family proteins such as BclXL, Bcl2 and Mcl-1 (rectangles). Death stimulus induced mitochondrial p53 (triangle) forms a complex with BclXL and Bcl2, liberating pro-apoptotic BH3-only proteins (derepression by inhibiting their survival function) and BH123 proteins, resulting in Bax and Bak homo-oligomerization, activation and mitochondrial membrane permeabilization (MMP) to release a host of apoptotic activators. Moreover, translocated p53 can bind to Bak by disrupting the inhibitory Bak/Mcl1 complex, enabling Bak to ultimately undergo homo-oligomerization and MMP. In addition, in cells with a cytosolic BclXL fraction, p53 might activate cytoplasmic Bax through a 'hit and run' mechanism involving an intermediate cytosolic p53/BclXL complex that is disrupted by cytosolic Puma, which results in Bax conformational change, mitochondrial translocation, oligomerization and MMP.

CHAPTER 3
SEARCH SETTING

3. AIMS OF THE STUDY

p53 is best known as a tumor suppressor that transcriptionally regulates, in response to cellular stresses such as DNA damage or oncogene activation, the expression of various target genes that mediate cell-cycle arrest, DNA repair, senescence or apoptosis—all of these cellular responses are designed to prevent damaged cells from proliferating and passing mutations on to the next generation.^{82, 118} In 50% of human cancers, p53 is defective due usually to somatic mutations or deletions primarily in its

DNA-binding domain and, to a lesser extent, to posttranslational modifications such as phosphorylation, acetylation and methylation that affect p53 function and stability. Altered p53 fails to regulate growth arrest and cell death upon DNA damage, directly contributing to tumor development, malignant progression, poor prognosis and resistance to treatment.^{33b} Conversely, restoring endogenous p53 activity can halt the growth of cancerous tumors in vivo by inducing apoptosis, senescence, and innate inflammatory responses.^{34,85}

p53 protein network in cancer biology has attained much importance because of its redundant functions in normal versus cancer cells as well as this redundancy influences to different modes of anti-cancer therapy. p53 is the most frequently altered protein in human cancer. Approximately 50% of all human malignancies harbor mutations or deletions in the TP53 gene that disable the tumor suppressor function of the encoded protein.^{82,118} This high rate of genetic alterations underscores the important cellular function of p53. The tumor suppressor controls a signal transduction pathway evolved to protect multicellular organisms from cancer development that could be initiated by diverse stresses including DNA damage. p53 is a potent transcription factor capable of activating multiple target genes, leading to cell cycle arrest, apoptosis, or senescence.^{34,85} While p53 plays a protective role in normal somatic tissues by limiting the propagation of damaged cells, its

powerful growth suppressive and proapoptotic activity could be turned into a powerful weapon against cancer cells that have retained the functionality of the p53 pathway.

Searching for small-molecules that activate the transcriptional activity of p53 would be expected to lead to the discovery of both DNA-damaging agents and compounds that are specific for the p53 pathway, including agents that interact directly with p53¹¹⁹ or that inhibit MDM2 a negative regulator of p53 activity and stability.¹²⁰ MDM2 is overexpressed in many human tumors and effectively impairs the function of the p53 pathway.⁸ Therefore, restoration of p53 function by antagonizing MDM2 has been proposed as a novel approach for treating cancer, and studies using macromolecular tools have shown its validity *in vitro*.¹⁵²

According to these findings, and as part of a wide medicinal chemistry program aimed at identifying small-molecules endowed with antitumor activity, different series of compounds were designed as potential p53 modulators. Specifically, my PhD thesis work has been centered on two projects: the first was based on the design and synthesis of acridine derivatives as DNA-damaging agents; while the second was based on the valuation of natural product analogues designed as both cellular cycle modulators and p53-MDM2 interaction inhibitors

The final aim of this study was to identify of suitable leads which allow us to deep on the molecular complexity of p53 network, improving the antitumor therapeutic arsenal.

CHAPTER 4.
DESIGN AND SYNTHESIS OF A SERIES OF CARBAZOLE-
BASED DERIVATIVES

4. DESIGN AND SYNTHESIS OF A SERIES OF CARBAZOLE-BASED DERIVATIVES

4.1 Background and design

Natural and synthetic carbazoles, either in a pure substituted or in an annellated substituted form, represent an important and heterogeneous class of anticancer agents, which has grown considerably over the last two decades.¹²¹ Many natural carbazoles, such as Murraquinone A and B, and Ellipticine (Figure 10) have been tested for cytotoxic activity, some of them have entered clinical trials,¹²² but only very few have been approved for the treatment of cancer so far, since the clinical application of many carbazoles has encountered problems like severe side effects or multidrug resistance. Its planar fused ring system can intercalate into the DNA of tumor cells, thereby altering the major and minor groove proportions. These alterations to DNA structure inhibit both DNA replication and transcription by reducing association between the affected DNA and DNA polymerase, RNA polymerase and transcription factors. For many carbazoles cytotoxicity can be related to DNA-dependent enzyme inhibition such as topoisomerase I/II and telomerase. But also other targets such as cyclin-dependent kinases and estrogen receptors have emerged.^{122a}

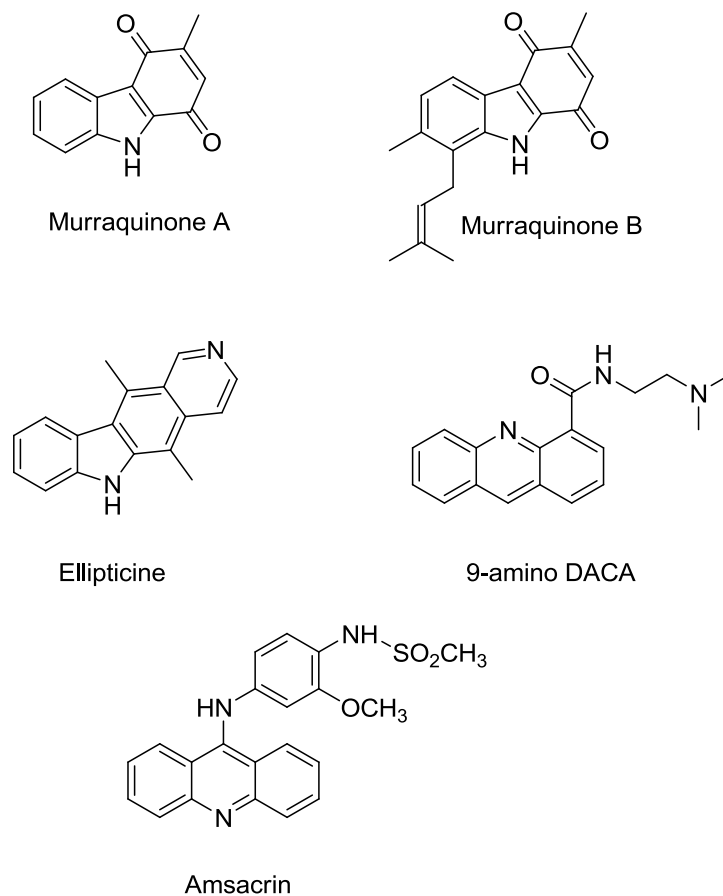


Figure 10. Carbazoles and acridines with antitumor activity

However it has been shown that the presence of a basic side chain improves the affinity to the double strand of DNA. One example is the carbazole analogue 9-amino-DACA which presents into its structure an acridine core¹²³ linked to protonable amino group. This compound establishes an important interaction with phosphate group of guanine G-2. Through recent study has been suggested that basic chain established initially an interaction with the groove of DNA and then the aromatic *core* intercalates the double strand.¹²⁴ An other acridine-based derivative, amsacrin was used combined with etoposide as therapy in acute lymphoblastic leukemia.¹²⁵ Intercalation of these

compounds causes relaxation of DNA and consequent alteration of its three-dimensional properties. This creates a lack of recognition of enzymes involved in transcription, duplication and repairing errors. Recently, Wong et al. have described a particular activity of a series of acridine derivatives (Figure 11).¹²⁶ These compounds, characterized by a polycyclic planar system and by a side chain ending with a tertiary amine, act stabilized p53 protein by blocking its ubiquitination, without phosphorylation of Ser¹⁵ or Ser²⁰ on p53. Furthermore, these derivatives induced p53-dependent cell death, activating p53 transcriptional activity.

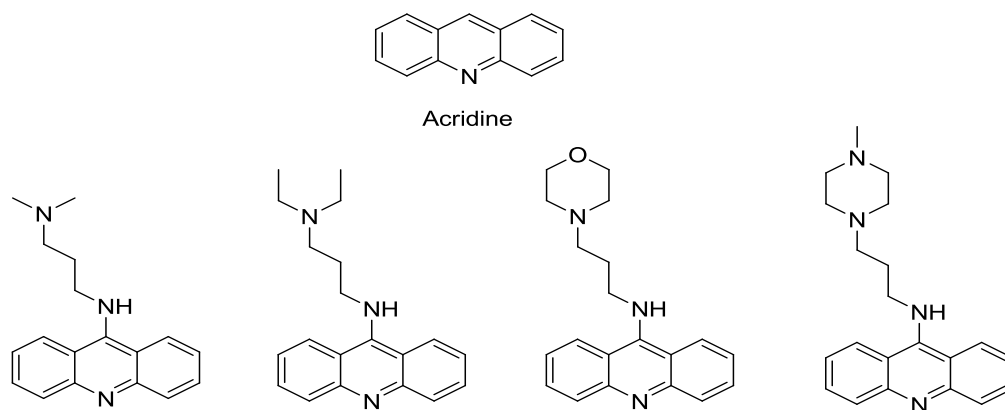


Figure 11. *Acridine derivatives*

Based in these findings, we have designed and synthesized two series of compounds in which a carbazole skeleton were linked by an alkyl chain to an amine (series 1) or substituted amide (series 2) groups. Compounds of series 1 incorporate an ethyl-, propyl- or butyl- *N,N*-diethylamino group as substituents at position N-9, while the more complex compounds of series 2 contain an aliphatic or aromatic amide in the same position (Figure 12).

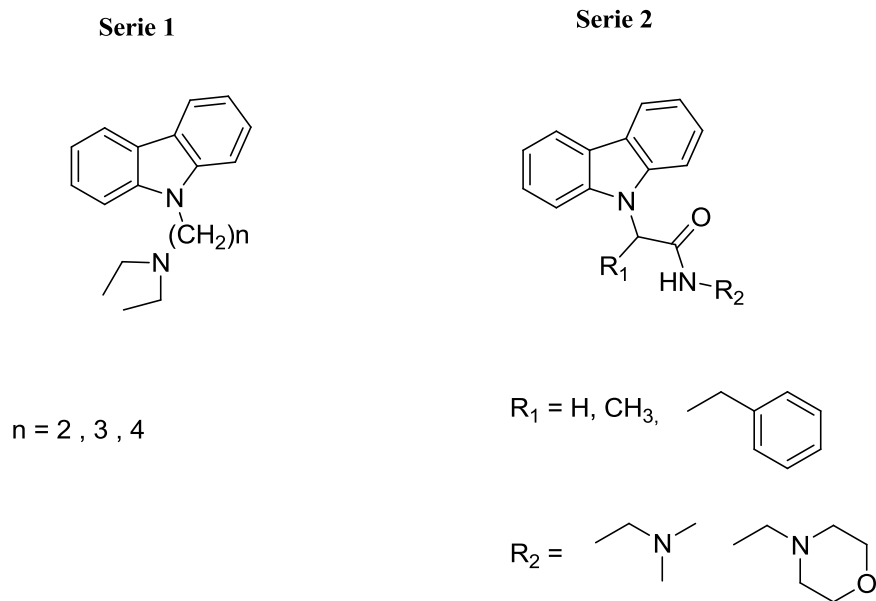
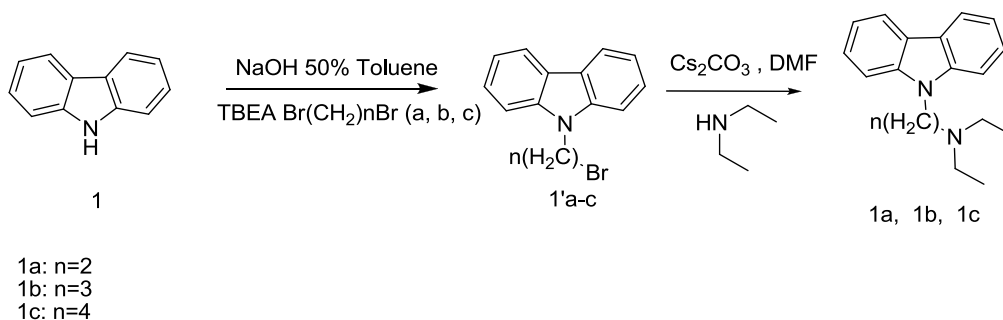


Figure 12. *Compounds synthesized (series 1-2)*

4.2 Results and discussion

4.2.1 Chemistry

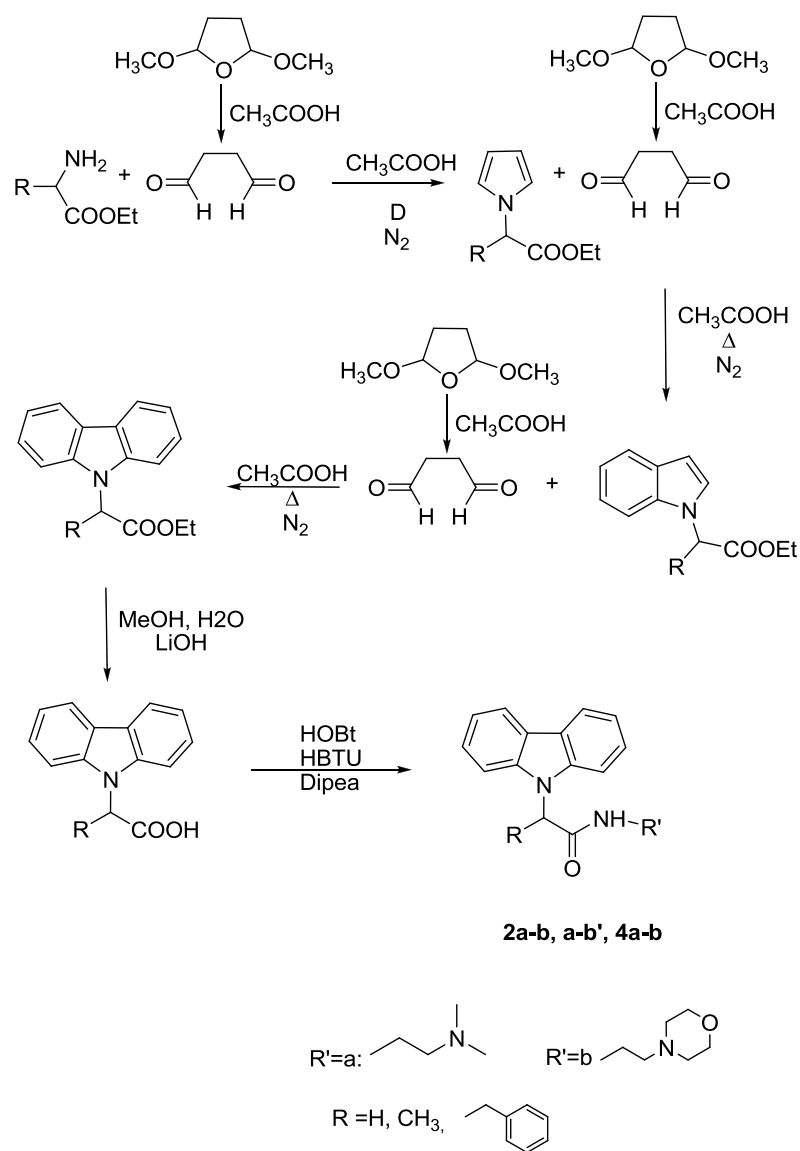
For the synthesis of final compounds, N-[(9H-carbazol-9-yl)alkyl]-N,N-(diethyl)amine (serie 1) and N-[(9H-carbazol-9-yl)alkyl]-N,N-(diethyl)amine (serie 2) derivatives we using two different strategies. The first series of compounds was obtained starting from carbazole **1** through the introduction at N-9 position of a bromo alkyl side chain. The reaction was carried out in 50% toluene solution containing (Br)₂alkyl chains of different lengths such as 1,2-dibromoethane (a), 1,3-dibromopropane (b), and 1,4-dibromobuthane (c) and using NaOH as base (Scheme 1).



Scheme 1. Synthesis of compounds **1a-c**

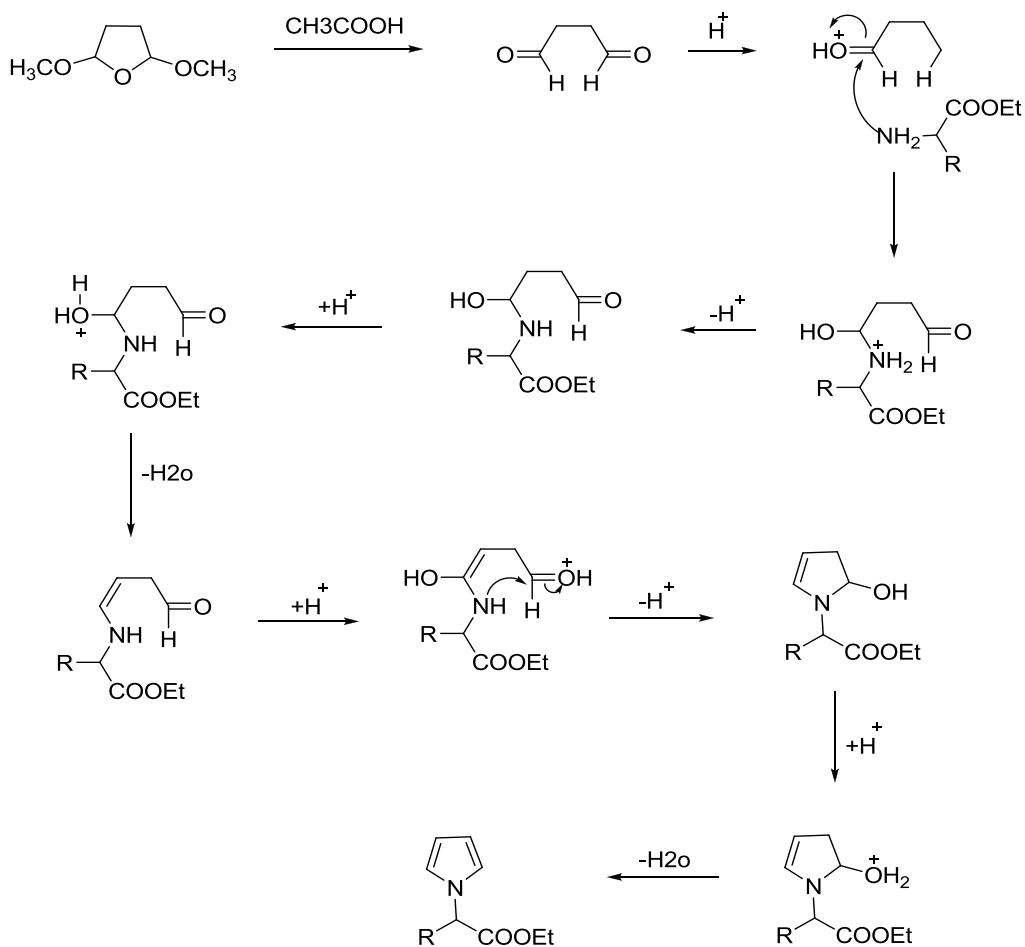
Then, the corresponding intermediates **1'a-c** were treated with diethylamine in DMF and CsCO₃ to generate the final compounds **1a-1c**.

Our approach to the synthesis of series 2 compounds involves the formation of carbazole derivatives *via* Clauson Kaas reaction¹²⁷ between an appropriate enantiopure amino acid such as Gly-OEt, L-Ala-OEt, L-Phe-OEt and 2,5-dimethoxytetrahydrofurane (Scheme 2).



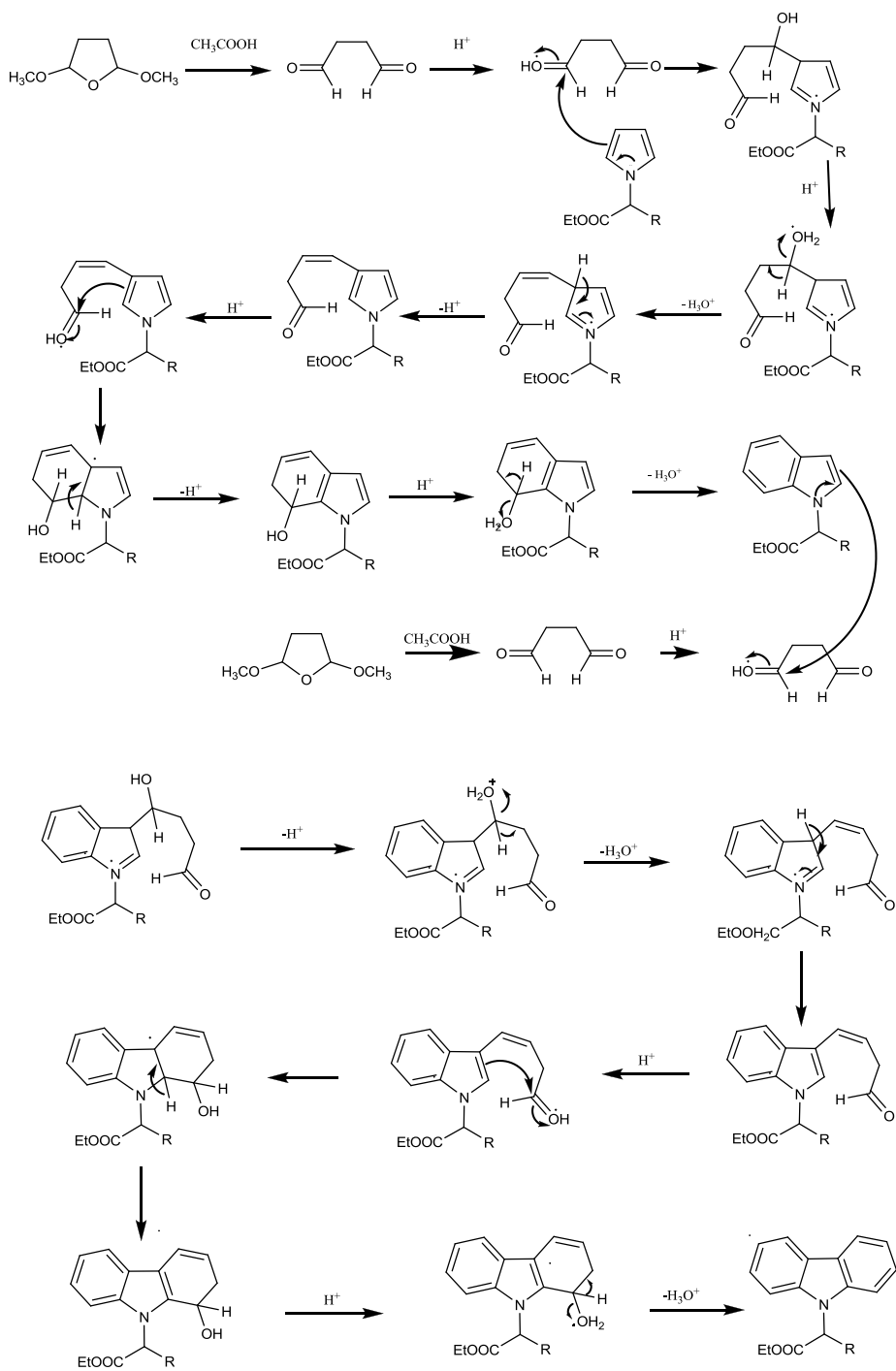
Scheme 2. *Synthesis of carbazole derivatives via Clauson Kaas reaction*

In this step of reaction the acetic acid promote the opening of dimethoxytetrahydrofuran to succinyl aldehyde. Reaction of this dialdehyde with the amino group of corresponding amino acids and then Clauson Kaas rearrangement give the pyrrole ring as shown in the scheme 4.



Scheme 3. *Clauson Kaas reaction*

The attack of other two succinyl aldehyde molecules to pyrrole system, through a Fiedel-Craft reaction, leads to the formation first of indole ring and successively of carbazole ring as show in scheme 4.



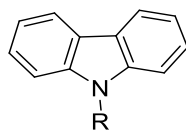
Scheme 4. Fiedel-Craft reaction

After hydrolysis of ester group in MeOH/H₂O using LiOH as base., the carboxylic function was funzionalized with two different amine: N,N'-dimehyletilendiamine and N-ethylmorpholyne using HOBt, HBTU as coupling agents and DIPEA as base (Fig 2, Table 1).

The use of different length side chain permits evaluation the optimal distance between the aromatic core and amino group to interact with the target.

4.2.2. Biological results

The target compounds were tested in vitro for tumor cell-growth inhibition on human breast carcinoma MCF-7 cell lines (Table 1).



Comp.	R	IC ₅₀ (μ M)
1 a		1.1 \pm 0.7
1 b		1.8 \pm 0.5
1 c		0.7 \pm 0.2
2 a		2.2 \pm 0.2
2 b		8.0 \pm 0.1
3 a		1.8 \pm 0.5
3 b		10.2 \pm 0.4
4 a		12.2 \pm 0.5
4 b		15.1 \pm 0.3

Table 1. Cytotoxic activity of series **1** and **2**

As shown in Table 1, compound **1a-1c** (series 1) showed an equipotent cytotoxic activity on the MCF-7 cell lines. These data seem indicated a weak influence of alkyl side length on the activity profile of these compounds.

Unfortunately the introduction of an amino acid side chain reduce the activity of corresponding derivatives. Compounds **2a** and **2b** containing un glycyl residue are more powerful than corresponding alanyl (**3a-b**) and phenylalanyl (**4a-b**) derivatives. The presence of a methyl or a benzyl group led to significant loss of activity. This data suggest that steric factors might affect the activity. In addition, compounds substituted with N,N'-dimehyletilendiamine function (series 1) are more active than N-ethylmorpholyne derivatives (series 2), demonstrating that the N,N-dimethyl group is an appropriate substituent for the interaction with DNA.

Due to the small structural differences in the more active compounds, a rigorous determination of structure–activity relationships is not possible at the moment. However, it seems that benzyl side chains was deleterious for any activity (compounds **4a, 4b**), as well as the introduction of N-ethylmorpholyne (**2a** versus **2b** and **3a** versus **3b**). Our research on these compounds will continue by modifying and developing the most promising cytotoxic active compounds.

CHAPTER 5

Design and synthesis of spirotriprostatin-inspired diketopiperazine system as potential cell cycle modulators

5. DESIGN AND SYNTHESIS OF SPIROTRIPROSTATIN-INSPIRED DIKETOPIPERAZINE SYSTEMS AS POTENTIAL CELL CYCLE MODULATORS¹²⁸

5.1 Background and design

The progress in understanding the molecular mechanisms of the mammalian cell cycle and its involvement in cancer development has shown that cell cycle regulators have a huge prospective both as molecular probes into the process as well as potential antitumor agents². Small molecule natural products have demonstrated to be invaluable tools in the discovery and characterization of critical events for the progression and the regulation of the cell cycle. Therefore, the development of new and specific inhibitors of signal transduction cascade pathways will continue to be extremely important in the knowledge of the regulatory mechanism of the cell cycle.¹³⁰

In this context, the isolation of the spirotryprostatins A and B (Fig. 13) from the fermentation broth of *Aspergillus*¹³¹ *fumigates* and the discovery of their activity as cell cycle inhibitors has challenged numerous investigators to develop concise total syntheses and analogues with superior biological activity.¹³²⁻¹³⁴

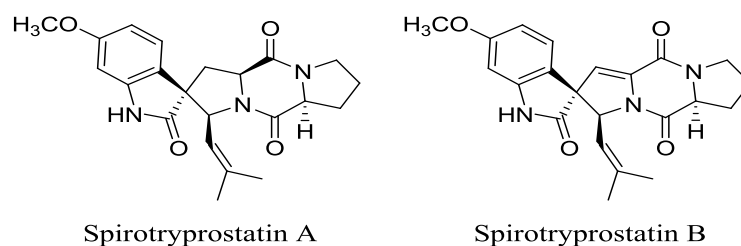
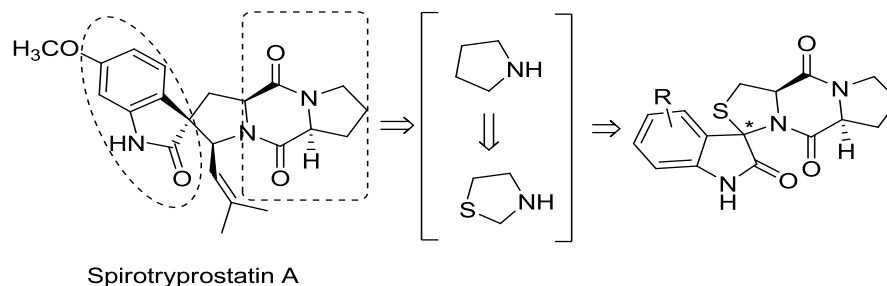


Figure 13. Structure of spirotryprostatin A and B.

Spirotryprostatins A and B cause G2/M phase cell cycle arrest in tsFT210 cell at IC₅₀s of 197.5 and 14.0 μ M, respectively, according to the therapeutic potential of this class of compounds and as part of a wide program centered on the development and individuation of new modulators of cell cycle, we have focused our attention on the Spirotryprostatin A core as inspiration of biologically useful diketopiperazine analogues.¹³⁵ Thus, our initial design implicated the modification of the spirocyclic structure replacing the pyrrolidine nucleus with a thiazolidine moiety and maintaining unaltered both the oxindole and the indolizidindione fragments (Scheme 5).



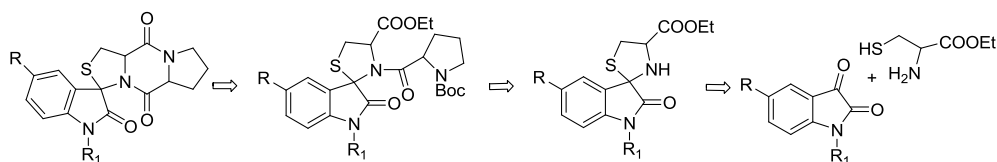
Scheme 5. Design of spirooxindolethiazolidine derivatives.

Previous work in our group on the synthesis of quinone-based cytotoxic agents, had confirmed that the incorporation of an indolizidindione moiety is an effective approach to devise new compounds with potential antitumor activity.¹³⁶ In this work, we report a full account of our efforts towards the synthesis of a new series of diketopiperazine and spirooxindolethiazolidine derivatives and the preliminary results of their biological activity.

5.2 Results and discussion

5.2.1 Chemistry

Our approach to the synthesis of the target spiroindol-2-one[3,30]hexahydro-5,10H-pyrrolo[1,2-a][1,3]thiazolo[3,4-d]pyrazine-5,10-dione derivatives involved the coupling of the spirooxindolethiazolidine scaffold, obtained from isatin derivatives and cysteine, with the N-Boc-Pro residue, followed by N-Boc deprotection and intramolecular cyclization (Scheme 6).

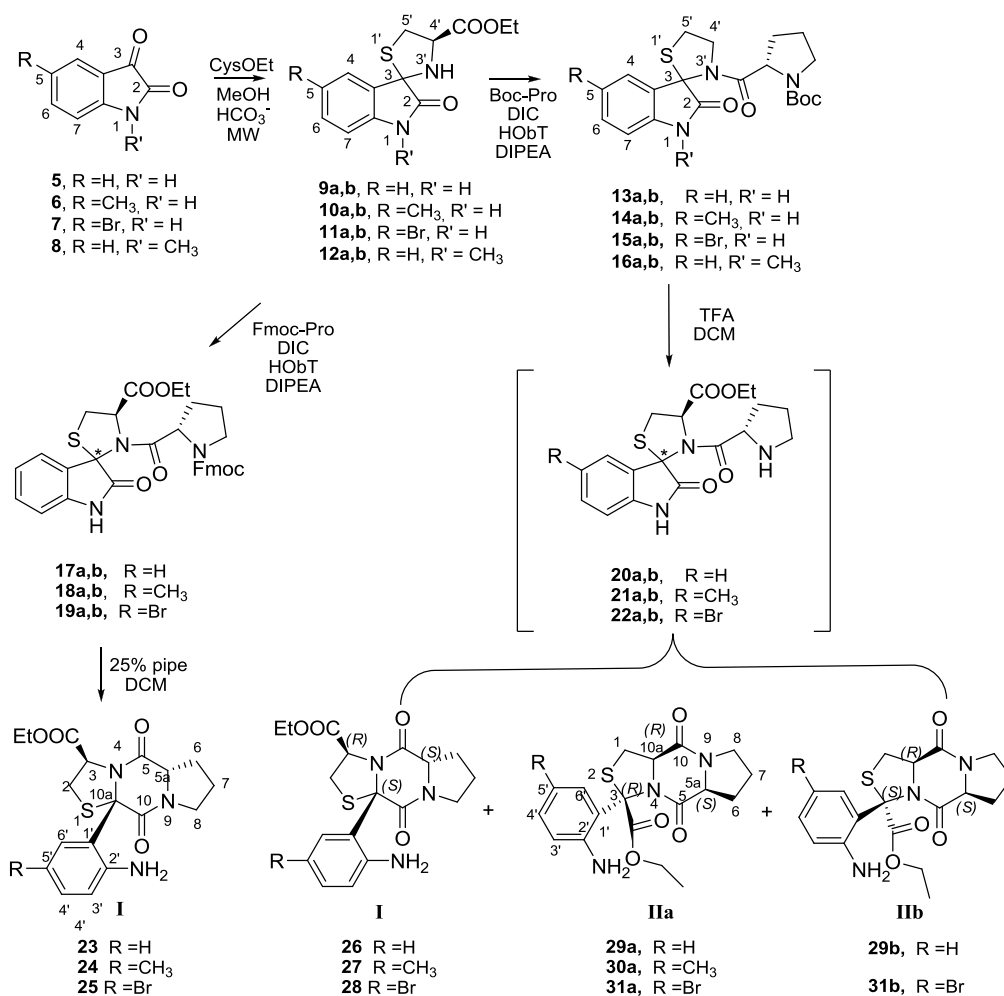


Scheme 6. Retrosynthetic route to spirooxindolethiazolidine derivatives.

The application of this synthetic strategy conducted to the oxindole ring opening and to the formation of two new tricyclic systems: the hexahydropyrrolo[1,2-a][1,3]thiazolo[3,2-d]pyrazine-5,10-dione (structure I) and the hexahydropyrrolo[1,2-a][1,3]thiazolo[3,4-d]pyrazine-5,10-dione (structure II).

As shown in Scheme 7, the spirooxindolethiazolidine skeletons (**9-12**) were constructed through microwave assisted condensation between the isatin derivatives (**4-8**), and cysteine ethyl ester in MeOH under argon.¹³⁶ These derivatives were obtained with 80–90% yields, as (3*R*)/(3*S*) epimeric mixtures ranged from 60/40 to 40/60 ratios. Reaction with Boc-Pro, using DIC as coupling agent led to diastereomeric mixtures **13a,b-15a,b** (75–80%, **a/b**:

3/2–2/3 range) and **16a,b** (31%, a/b: 3/2) which were not separated in this step.



Scheme 7. Synthesis of 3-ethoxycarbonyl-10a-phenyl(substituted)-hexahydropyrrolo[1,2-a][1,3]thiazolo[3,2-d]pyrazine-5,10-dione (structure I) and the 3-ethoxycarbonyl-3-phenyl(substituted)-hexahydropyrrolo[1,2-a][1,3]thiazolo[3,4-d]pyrazine-5,10-dione (structures II) derivatives.

Removal of the N-Boc protecting group of the mixture **13a,b**, or **14a,b**, or **15a,b**, using TFA in DCM, yielded the 3-ethoxycarbonyl-10a-phenyl(substituted)-hexahydropyrrolo[1,2-a][1,3]thiazolo[3,2-d]pyrazine-5,10-dione derivatives (19–21, 23–45% yields) as pure compounds and the 3-ethoxycarbonyl-3-phenyl(substituted)hexahydropyrrolo[1,2-a][1,3]thiazolo[3,4-d]pyrazine-5,10-dione derivatives (**26a,b** and **28a,b** 28–33%) as diastereomeric mixtures (**a/b**: 1:3 ratio), while the derivative **27a** was obtained in 41% yield as pure diastereoisomer (Table 1, entries 1, 2, and 3). Under the same conditions, the derivatives **116a,b** led to a complex and untreatable mixture of reaction (entry 4).

Assignments of the ^1H and ^{13}C NMR resonances and of the stereochemistry in final compounds were made by analysis of 2D NMR data, including COSY, HSQC, HMBC and NOESY. In the case of the regioisomers **23–27(I)**, the stereochemistry was established on the basis of X-ray diffraction studies of compound **25** which indicated $3R,5aS,10aS$ configurations at the three stereogenic centers, as depicted in the ORTEP ¹⁴ diagram (Fig. 14).

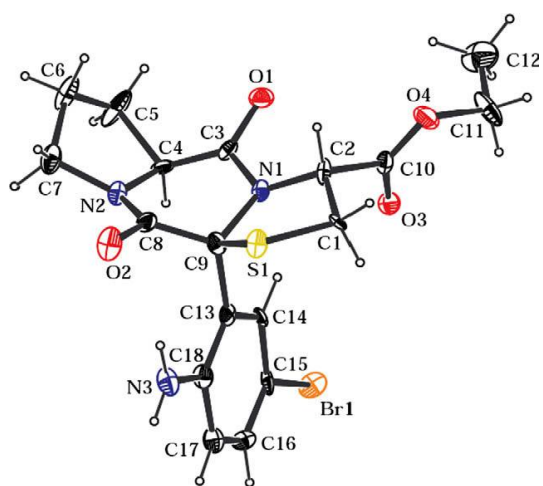


Figure 14. ORTEP representation of the structure of isomer **25**.

This result showed that the stereomutation at the stereogenic centers C-3 and C-5a did not occur during the cyclization process. The stereochemical assignments for compounds **23** and **24**, were established by comparison of their ^1H and ^{13}C NMR spectra with those of **25**. Unfortunately, we could not obtain good crystals for the analysis of any regioisomers **26–28** (**II**). The determination of the configuration at the stereogenic centers was performed by an NMR study of representative derivatives **28a** and **28b**. Considering stereogenic centers C-5a and C-10a, we assumed that they maintain their configuration 5a*S*, 10a*R* after cyclization. NOE enhancement between H-5a and H-10a, indicating their *cis* orientation, is in accordance with this hypothesis since the inversion of both centers seems unlikely (Fig. 15). In the case of the stereogenic center C-3, a NOE enhancement was observed between H-6' and H-10a of **28a**, while the same enhancement was very weak in **28b**. Inspections of molecular models obtained by molecular dynamics (MD) simulations showed that the distance between H-6' and H-10a was about 4.6 Å in the 3*S*, 5a*S*, 10a*R* isomer and about 3.5 Å in the 3*R*, 5a*S*, 10a*R* isomer. Hence, the 3*R* configuration was assigned to the **28a** isomer. The stereochemical assignments for compounds **26a**, **27a**, and **26b** were made by comparison of their ^1H and ^{13}C NMR spectra with those of **28a** and **28b**.

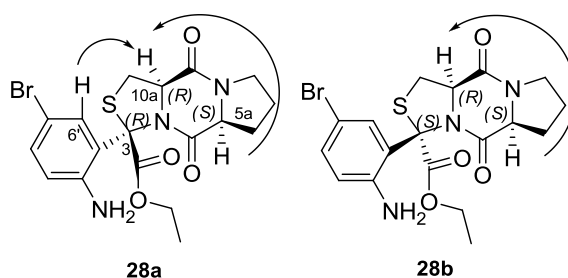


Figure 15. Significant NOEs for derivatives **28**.

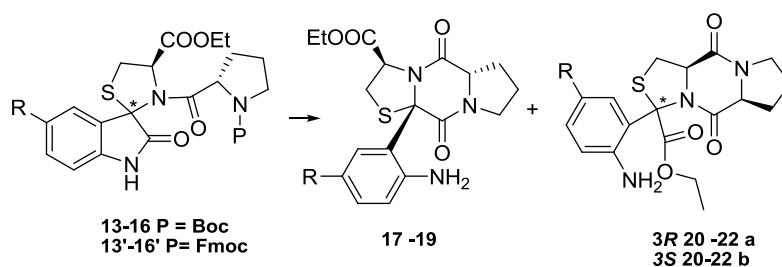
According to these data, the formation of derivatives **I** and **II** implicates an unexpected oxindole ring opening. To the best of our knowledge, no previous examples of this reaction performed under the above described conditions were reported. Dillman and Cardellina¹³⁷ described the isolation and characterization of an unusual sulfur-containing diketopiperazine, from extracts of the Bermudian sponge *Tedania Ignis*, analogue to our hexahydropyrrolo[1,2-a][1,3]thiazolo[3,4-d]pyrazine-5,10-dione (structure **II**). On the contrary, neither the isolation nor the synthesis of the hexahydropyrrolo[1,2-a][1,3]thiazolo[3,2-d]pyrazine-5,10-dione (structure **I**) were reported.

In order to define the factors that could determinate the reaction course we performed studies on the influence of solvent, time, and pH in the formation of these new derivatives and on their Concerning the solvent, the use of CH₃CN (entry 5) led to best results and the corresponding **I** and **II** structures were obtained in an overall yield higher than 85%, while in a less polar aprotic solvent as THF (entry 6) the yield was drastically lower (38%). An increase of reaction time, up to 24 h, produced a decrease in the **I** and **II** yields and a reversion to the starting spirooxindolethiazolidine **5** (entry 7). After 120 h, this reversion was nearly complete (entry 8). The use of 1:3 2N HClaq: MeOH solution for 24 h, led to deprotected derivatives **20**, **21** and **22** (entries 9, 11, 12). An increase of reaction time (entry 10) determined the formation of unidentifiable materials, recovering a 21% of starting isatin **1**. It is interesting to note that an augment of the proportion of 2N HClaq up to 1:1 in MeOH solution favoured, in all cases, the reversion to starting spirooxindolethiazolidine (entry 13).

As alternative route, the Fmoc derivatives **17 a,b**, **18 a,b** and **19 a,b** (Scheme 9) were subjected to the treatment with piperidine (25%) in methylene chloride for 1 h. Under these conditions only the derivates **23**, **24** and **25** were obtained

as simple regioisomers in 80%, 78%, and 81% yields, respectively (entries 14–16).

Table 2. Results of the acid or base promoted intramolecular cyclization of 3-prolylspirooxo indolthiazolidine derivatives



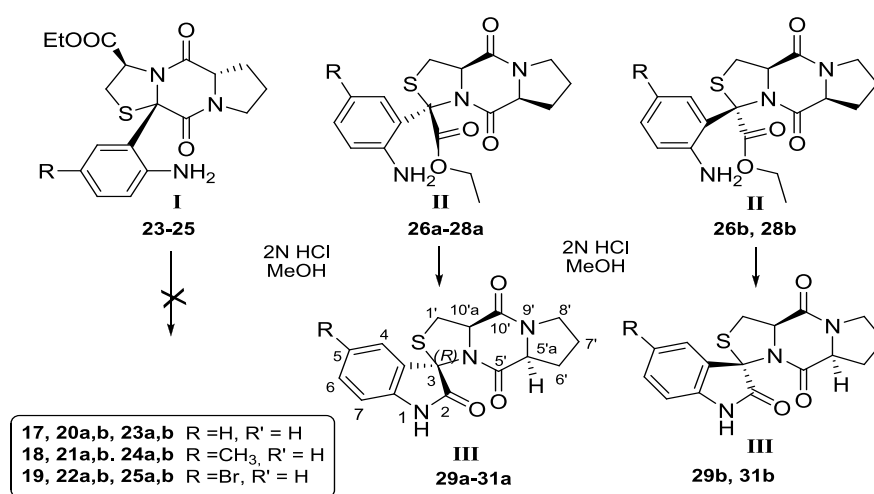
N	Starting	R, R ₁	Solvent	Acid/Base	T (h)	I (%)	IIa (%)	IIb (%)	Other
1	13	H	CH ₂ Cl ₂	TFA	2	23 (40)	26a (9)	26b (24)	
2	14	CH ₃	CH ₂ Cl ₂	TFA	2	24 (41)	27a (23)		
3	15	Br	CH ₂ Cl ₂	TFA	2	25 (45)	28a (8)	28b (20)	
4	16	H,CH ₃	CH ₂ Cl ₂	TFA	2	-		-	-
5	13	H	CH ₃ CN	TFA	2	23 (50)	26a (10)	26b (25) ^a	
6	13	H	THF	TFA	12	23 (20)	26a (5)	26b (12) ^a	
7	13	H	CH ₃ CN	TFA	24	23 (16)	-	26b (22)	9 (20) ^a
8	13	H	CH ₃ CN	TFA	120	-	-	-	9 (80) ^a
9	13	H	MeOH	HCl ^b	24				20 (30) ^a
10	13	H	MeOH	HCl ^b	120				5 (21)
11	14	H	MeOH	HCl ^b	24				21 (37)
12	15	H	MeOH	HCl ^b	24				22 (31)
13	13	H	MeOH	HCl ^c	24				9 (65) ^a
14	17	H	CH ₂ Cl ₂	Piperidine ^d	1	23 (80)			
15	18	CH ₃	CH ₂ Cl ₂	Piperidine ^d	1	24 (78)			
16	19	Br	CH ₂ Cl ₂	Piperidine ^d	1	25 (81)			

^a Similar results were observed from derivatives 10 and 11. ^b 3:1 MeOH/2 N HCl solution.

^c 1:1 MeOH/2 N HCl solution. ^d 25% solution

Regarding the stability, the treatment of derivatives **23–25** with 2N HCl_{aq}/methanol solution for 24 h did not determine structural modifications

and the products were recovered unchanged (Scheme 8). The same acid treatment on the pure derivatives **26a–28a**, **26b**, and **28b**, led to oxoindole ring closing and formation of the corresponding spiro derivatives **23a–25a**, **23b**, and **25b (III)**, that is, the pentacyclic derivatives designed as analogues of spirotryprostatin A, in quantitative yields. This lactamization did not arise when the reaction was carried out in basic media.



Scheme 8. Reactivity of I and II derivatives in acid medium.

The acid treatment on the pure derivatives **20a–22a**, **20b**, and **22b**, led to oxoindole ring closing and formation of the corresponding spiro derivatives **23a–25a**, **123b**, and **25b (III)**, that is, the pentacyclic derivatives designed as analogues of spirotryprostatin A, in quantitative yields. This lactamization did not arise when the reaction was carried out in basic media of triethylamine/methanol at reflux. After 10 h under basic conditions, we observed a partial degradation of all derivatives.

According to these findings, we hypothesized that the formation of the regioisomeric diketopiperazines (**I** and **II**) could be explained by a mechanism

that involved trans (E) and cis (Z) arrangement of the amide bond of deprotected intermediates **20–22**. A theoretical conformational analysis of **13a** (3*R*), and **13b** (3*S*) in their deprotected and deprotonated state (intermediates **20a** and **20b**) was carried out in order to examine possible low-energy structures. Amide bond was considered both in the E and Z configurations thus obtaining four different isomers (3*R*-E, 3*R*-Z, 3*S*-E, 3*S*-Z). Starting from randomly generated structures, minimization and a 2 ns MD simulations at a constant temperature of 500 K were run. The distances between the proline amino group and the carboxyl functions at C-2 (oxoindole carbonyl) and at C-4' (ethoxycarbonyl) were monitored along the complete 2 ns MD trajectory. From these distances, the two possible orientations assumed by the amide bond prompted the system towards two different intramolecular cyclization pathways (Fig. 16).

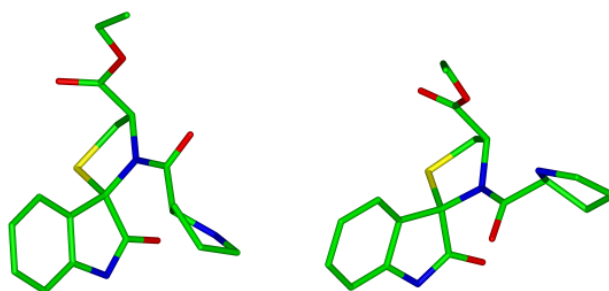


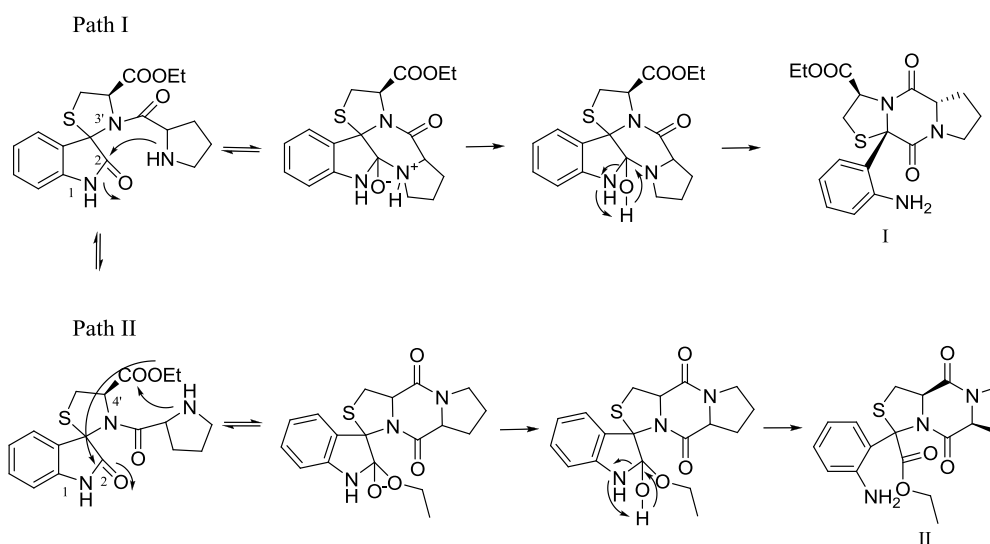
Figure 16. *Lowest-energy conformers of compound 20b containing a trans (left) and cis (right) amide bond.*

E isomers are suitable for the C-2 closure (Scheme 9, path I) while Z isomers are suitable for the C-4' closure (Scheme 11, path II).

Following the hypothesized reaction mechanisms shown in Scheme 4 (path I), the amino group of proline showing an E disposition of the amide bond, attacks at the C-2 carbonyl of the oxoindole giving a pentacyclic intermediate

which evolves to structure I. We calculated the molecular energies of the two intermediates with 3*R* and 3*S* configuration, and found that the 3*S* intermediate energy was about 8 kcal/mol lower than that observed for 3*R*. Evoking the Evans–Polanyi principle,¹³⁸ this means that the reaction of the 3*S* compounds through the path I is kinetically favoured compared to the 3*R* ones. Since starting compounds **13–15** quickly interconvert at the C-3 chiral center, previous result can explain the stereospecific course of the reaction.

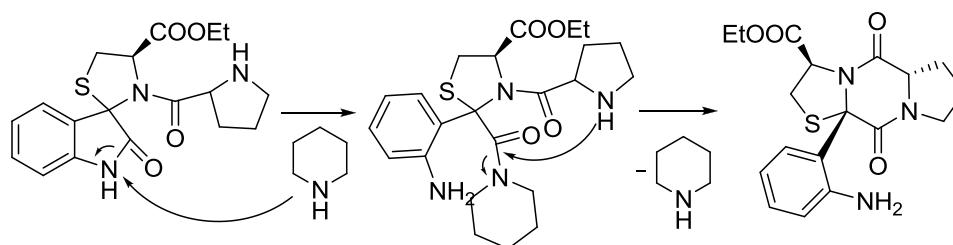
On the other hand, the *Z* geometry of the amide bond allows the attack of the amino group at C-4' carbonyl ester (path II). In the reaction conditions, the oxindole C-2 undergoes a nucleophilic attack from the generated ethoxide residue or from other nucleophilic agents present in solution (data not shown). Again, the tetrahedral C-2 intermediate reverts to a more stable carbonyl form with ring opening and formation of the regioisomers **II**. In this case, stereogenic center C-3 does not influence the intermediates energy.



Scheme 9. Possible reaction pathways for the formation of structures I and II

The C-5 substituent effects are in accordance with reported mechanism. In fact, while the yield ratio of the C-5' unsubstituted derivatives **23** with respect to **26** is 40/33, an electron-donating substituent (CH₃) which should reduce the C-2 reactivity, decreases the yield ratio of compounds **24** versus **27** to 23/41, and an electron-withdrawing substituent (Br) which should enhance the C-2 reactivity, increases the yield ratio of compounds **25** versus **28** to 45/28. In addition, the lack of reactivity observed in the N-methyl derivatives, **16a,b**, may be attributed to the electron-donating effect of the methyl group which prevents the nucleophilic attack at the C-2 carbonyl group. Finally, the higher reactivity of the amino group in weak acid solution could be explained if we considered that an increase of the acidity (HCl vs TFA) should result in a shift toward the unreactive protonated form of the amine group¹⁷.

In basic media, the exclusive and highly efficient formation of structure I implies the oxindole ring opening probably due to nucleophilic attack of piperidine at the C-2 carbonyl and successive transamidation by attack of Pro amino group (Scheme 10).

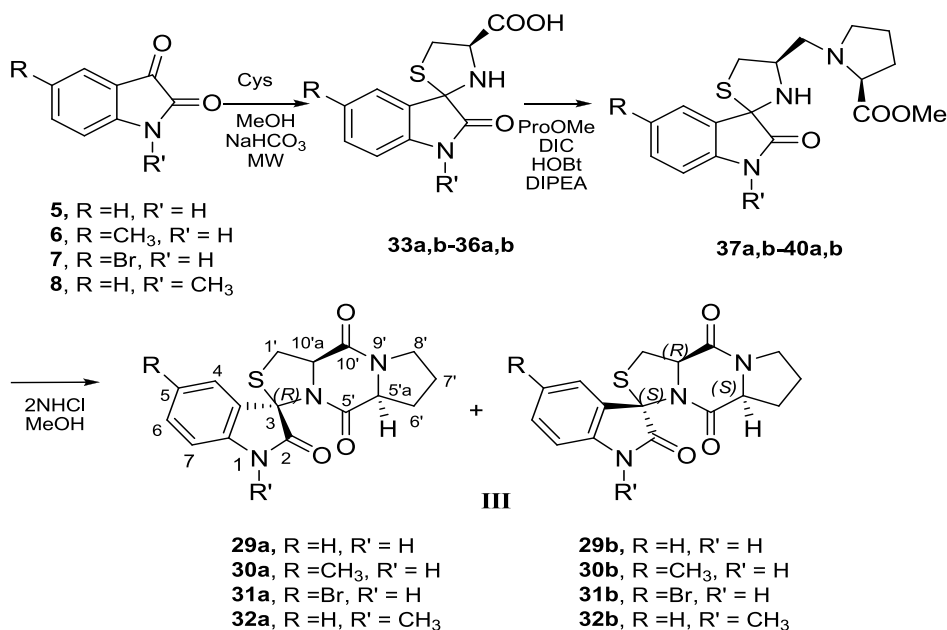


Scheme 10. Hypothesized mechanism for the formation of the structure I in basic media

This unusual but not unexpected oxindole ring opening in piperidine media could be considered analogous to well described aspartimide ring-opening in the peptide chemistry.¹³⁹ In that case, the nucleophilic attack of piperidine at

aspartimide led to ring opening and formation of corresponding a- and b-piperidides.¹⁴⁰

The route indicated in Scheme 11, was applied to the synthesis of the spiroindol-2-one[3,30]hexahydro-5,10H-pyrrolo[1,2-a][1,3]-thiazolo[3,4-d]pyrazine-5,10-dione derivatives (structure **III**). The spirooxindolethiazolidine acid derivatives **9'a,b-12'a,b**, synthesized from condensation between the corresponding isatin derivatives (**5-8**) and cysteine with 60–70% yields, were chosen as starting material. Coupling with Pro-OMe, using DIC as coupling agent, under high dilution condition, led to 1/1 diastereoisomeric mixtures of **23'a,b-26'a,b** (70% yields), which were not separated in this step. The intramolecular lactamization of these compounds using (1/4) 2N HCl_{aq}/MeOH solution gave directly the corresponding spiroindol-2-one[3,30]hexahydro-5,10H-pyrrolo[1,2-a][1,3]thiazolo[3,4-d]pyrazine-5,10-dione derivatives (**23a,b-26a,b**) in ca 90% yields. This synthetic route did not afford any by-products due to the oxindole ring opening.



Scheme 11. Synthesis of spiroindol-2-one[3,30]hexahydro-5,10H-pyrrolo-[1,2-a][1,3]thiazolo [3,4-d]pyrazine-5,10-dione derivatives (29–32, structure III).

NMR analysis of the resulting crude products showed the presence of diastereoisomers **a/b** in 3/2 to 1/1 ratios. The diastereoisomer **29b** was isolated by precipitation. The diastereoisomeric mixtures **30a,b**, and **31a,b** were chromatographically separated while the mixture **32a,b** could not be separated. The physicochemical properties and purity of the final compounds were assessed by TLC, LC-MS, analytical RP-HPLC, and NMR analysis. The determination of the relative configuration at the stereogenic centers was performed by a 2D NMR study of isolate **30a**, **30b**, **31a** and **31b** derivatives. The main difference observed in the 2D NOESY spectra of derivatives “a” compared to “b” was the presence in the first of a NOE enhancement between H-4 and H-10'a (Fig. 17). Again, we hypothesized a configuration retention at

C-5'a and C-10'a. Inspections of molecular models obtained by MD simulations showed that the distance between H-4 and H-10'a was about 2.9 Å in the 3*R*,50a*S*,10'a*R* isomer and about 4.9 Å in the 3*S*, 50a*S*,10a*R* isomer. Hence, the 3*R* configuration was assigned to the 'a' isomers.

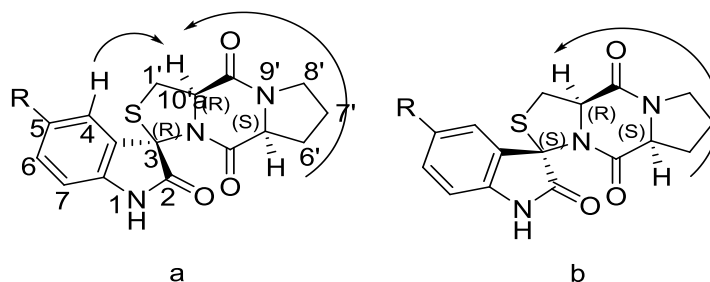


Figure 17. Significant NOEs for derivatives *a* and *b*.

5.2.2 Biological results

All compounds were evaluated as cytotoxic agents in the Biochemistry and Biophysics Department of the Second University of Naples.

The cytotoxic activity of hexahydropyrrolo [1,2-*a*][1,3]thiazolo[3,2-*d*]pyrazine-5,10-dione (series **I**), hexahydropyrrolo [1,2-*a*][1,3]thiazolo [3,4-*d*]pyrazine-5,10-dione (series **II**) and spiroindol-2-one[3,3']hexahydro-5,10H-pyrrolo[1,2-*a*] [1,3]thiazolo[3,4-*d*]pyrazine-5,10-dione (series **III**) derivatives was evaluated against (MCF-7, T47D, and A-431) cell lines.

Interestingly, tricyclic derivatives **23**, **26a**, **27a** and **28a** resulted active against MCF-7 cell growth with IC₅₀ values of 9.1, 14.8, 1.6, and 2.2 μM, respectively. Compound **24** inhibited A431 cell growth at concentration 28.2 μM. None of compounds belonging to series III showed significant cytotoxicity at concentrations below 10⁻⁴ M towards the cell lines. Unfortunately, none of the cytotoxic derivatives showed ability to inhibit the cell cycle of MCF-7 cell line.

CHAPTER 6.
DESIGN OF A POTENTIAL p53 MODULATORS

6. DESIGN OF POTENTIAL p53 MODULATORS

6.1. Background and design

The ability of p53 to respond to stress signals by triggering cell-cycle arrest and cell death by apoptosis is crucial to inhibit tumor development and for the response to anticancer therapy.^{34-118,143} Inactivation of p53 by mutation occurs in about half of all human tumors⁵. Tumors that retain wild-type p53 often acquire an alternative mechanism for its inactivation, largely through deregulation of MDM2 (murin doubleminute-2) protein. Negative regulation of p53 activity and stability is enhanced in many human tumors and effectively impairs the activities of the p53 pathway.¹⁴⁵⁻¹⁴⁸ Therefore, recovery of p53 activity in cancer cells by antagonizing MDM2 has been proposed as a novel approach for treating cancer and validated *in vitro* by macromolecular studies.¹⁴⁹⁻¹⁵¹

More recently, genetic and biochemical analysis of the p53-MDM2 interaction revealed structural features suggesting that it might be targetable by small molecules.¹⁵² The interaction of MDM2 and p53 was shown to be mediated by a deep well-defined hydrophobic cavity on the surface of MDM2.¹⁵³ This cleft is filled only by three side chains of the helical region of p53, making this site an attractive target to design a small molecule able to mimic the contacts and the orientations of these key amino acids, thereby disrupting p53-MDM2 interaction.¹⁵⁴ Several low molecular weight inhibitors, including [2.2.1]bicyclic derivatives¹⁵⁵ sulfonamides¹⁵⁶ and benzodiazepinediones¹⁵⁷ have been identified and reported (Figure 18).

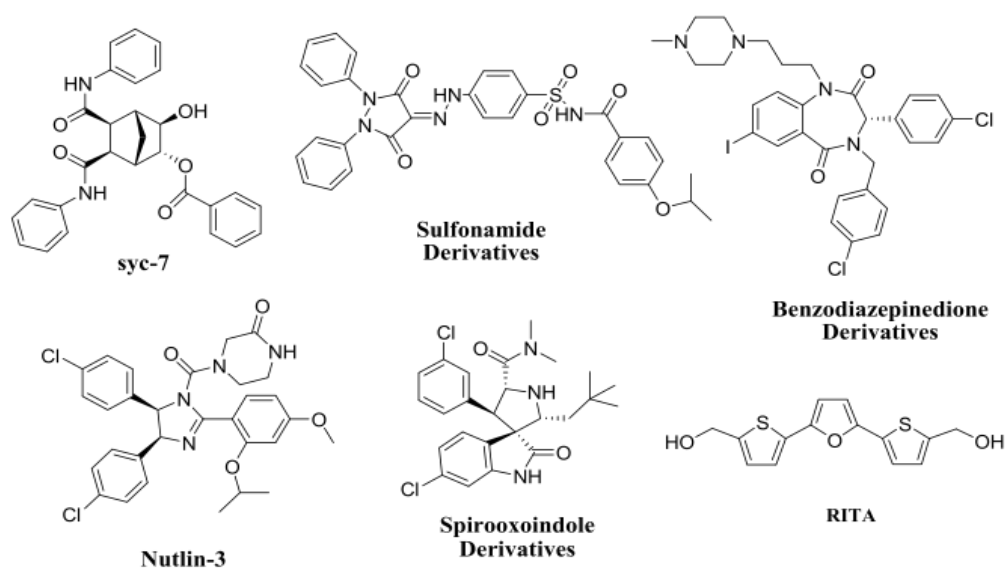
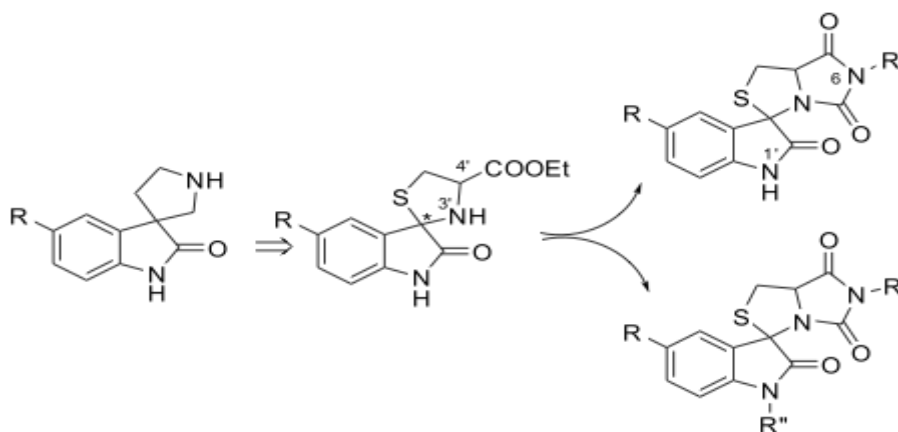


Figure 18. Small-molecule inhibitors of p53-MDM2 interaction

The first potent and selective small molecule identified as an antagonist of the p53-MDM2 interaction, both in vitro and in vivo, were the cis-imidazolidines nutlins. These molecules inhibit xenograft tumor growth with no reported side effects in normal murine tissues.¹⁵⁸ More recently, Wang et al. used structure-based design to develop a new class of small molecule p53-MDM2 antagonists based on a spirooxindole core.¹⁵⁹ All these inhibitors share a common design of a rigid heterocyclic scaffold that can be functionalized with the appropriate side chains. A different type of inhibitor of the p53-MDM2 interactions, termed RITA, activates p53 by a nongenotoxic mechanism involving the disruption of this interaction. However, RITA¹⁶⁰ binds to p53 and not to MDM2. The mechanism by which it interferes with p53-MDM2 binding and its effects on the functionality of p53 are not fully understood yet. On the basis of these findings and on identification of new activators of p53 pathway in tumor cells, we have designed and synthesized two focused libraries of compounds based on the spiro(oxindole-3,3'-thiazolidine) nucleus, a structural

analogue of spirooxindole pyrrolidine template.¹⁶¹ In this context, the 3',4'-hydantoin derived tetracyclic nucleus has turned out to be a very easily derivatizable scaffold. In particular, N-6 and N-10 positions were substituted with aryl and alkyl groups (Scheme 12).



Scheme 12. Design of new derivatives from spiro(oxindole-3,3'-thiazolidine).
R = H, CH₃, Br; *R'* = benzyl derivatives or alkyl; *R''* = H or acyl derivatives.

In our design strategy, oxindole, aryl, and alkyl groups are supposed to mimic the critical p53 residues that binds MDM2, i.e., Trp²³, Phe¹⁹, and Leu²⁶, respectively, while the imidazo-[1,5-c]thiazol nucleus would define the orientation among them. For the construction of the first library, we selected derivatives containing weak releasing (CH₃) and acceptor (Br) electron groups on the oxindole moiety and benzyl substituted or 4,4-dimethylcyclohexyl side chain on the imidazothiazolone scaffold.

On the basis of the “three finger pharmacophore model” described by Domling¹⁶² and according to the preliminary results of cytotoxic activities, we further developed, from the most interesting compounds, a series of derivatives containing a third hydrophobic group. In this case, benzoyl, 4-methylbenzoyl, 4-chlorobenzoyl, and propionyl groups were introduced into our template at the N-1 position (Scheme 12).

The aims of this thesis part were to screen a range of appropriately functionalized spiro[imidazo[1,5-c]thiazole-3,3'-indoline]-2',5,7(6H,7aH)-trione derivatives for cytotoxicity against different cancer cell lines and to explore some of the basic biochemical events correlated to their activity using a range of cell based approaches.

The present thesis read more with the synthesis of this new series of derivatives and with the understanding of their cytotoxic activity, the mechanism of cell cycle perturbation, the p53 expression, and the inhibition of p53-MDM2 interaction.

6.2 Results and discussion

6.2.1 Chemistry

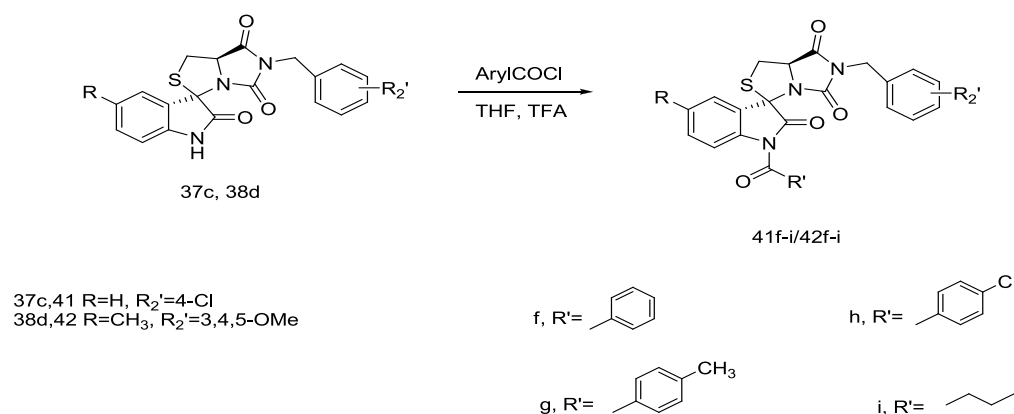
The designed 5',6-disubstituted spiro[imidazo-[1,5-c]-thiazole-3,3'-indoline]-2',5,7(6H,7aH)-trione derivatives (**37a-e/40a-e**, Table 1) were prepared applying the synthetic route shown in Scheme 13.

1-N-carbamoyl derivatives while the reaction performed in THF^a led to the formation of the desired 3'-N intermediate.

The intramolecular cyclization of these derivatives was performed in methanol in the presence of TEA at reflux temperature, and the corresponding spiro[imidazo[1,5-c]-thiazole-3,3'-indoline]-2',5,7(6H,7aH)-trione derivatives (**42a-d/45a-d**) were obtained with 39-56% overall yields as simple isomer. This cyclization was stereospecific toward the 3*R*,7*aR* isomer, as the corresponding C-3 epimer was not detected in the reaction mixture.¹⁶³ The assignment of the relative configuration at the C-3 asymmetric center as 3*R* was determined on the basis of a NOE enhancement between H-40 and H-7*a* observed in the 2D NOESY spectra of all compounds. Absolute configurations were defined hypothesizing configuration retention at C-7*a*.

Finally, the 1'-acylspiro[imidazo[1,5-c]thiazole-3,3'-indoline]-2',5,7(6H,7aH)-trione derivatives (**46f-i/47f-i**) were prepared in 85-89% yields by treatment of starting derivatives 9c and 10d with the corresponding acyl chloride (**f-i**) as depicted in Scheme 14.

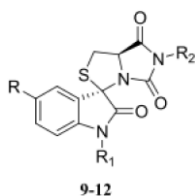
Scheme 14. Synthesis of 1'-acylspiro[imidazo[1,5-c]-thiazole-3,3'-indoline]-2',5,7(6H,7aH)-trione derivatives (**46f-i/47f-i**)



6.4 Biology and Pharmacology

The spiroimidazothiazoloxindole derivatives were examined in the Pharmaceutical Sciences Department of the University of Salerno, at the laboratories of professor B. Maresca, to evaluate antiproliferative activity against three cell lines: the transformed human embryonic kidney HEK, the human melanoma M14, and the human leukemia monocyte lymphoma U937 cell lines. The obtained IC₅₀ values are summarized in Table 3.

Table 3. Cytotoxic activity of spiro[imidazo[1,5-*c*]-thiazole-3,3'-indoline]-2',5,7(6H,7aH)-trione derivatives **42a-e/45a-e**



Comp.	R	R ₁	R ₂	IC ₅₀ (μM) ±SD ^a		
				HEK ^b	M14 ^c	U937 ^d
42a	H	H	-CH ₂ C ₆ H ₅	4.80±0.15	10.64±0.04	3.90±0.01
42b	H	H	-CH ₂ C ₆ H ₄ (4-CH ₃)	4.53±0.15	13.27±0.03	5.91±0.02
42c	H	H	-CH ₂ C ₆ H ₄ (4-Cl)	0.44±0.01	0.53±0.01	0.87±0.01
42d	H	H	-CH ₂ C ₆ H ₂ (3,4,5-OCH ₃)	3.80±0.08	4.73±0.02	2.51±0.05
42e	H	H	4-dimethylcyclohexyl	4.22±0.07	7.07±0.01	2.61±0.05
43a	CH ₃	H	-CH ₂ C ₆ H ₅	3.30±0.07	3.88±0.02	2.09±0.04
43b	CH ₃	H	-CH ₂ C ₆ H ₄ (4-CH ₃)	3.01±0.06	3.39±0.03	2.77±0.02
43c	CH ₃	H	-CH ₂ C ₆ H ₄ (4-Cl)	3.88±0.05	6.65±0.02	3.31±0.04
43d	CH ₃	H	-CH ₂ C ₆ H ₂ (3,4,5-OCH ₃)	2.04±0.03	2.40±0.02	2.06±0.04
43e	CH ₃	H	4-dimethylcyclohexyl	16.01±0.05	19.12±0.07	12.48±0.05
44a	Br	H	-CH ₂ C ₆ H ₅	8.48±0.09	12.04±0.03	7.58±0.05
44b	Br	H	-CH ₂ C ₆ H ₄ (4-CH ₃)	7.61±0.10	10.24±0.10	6.23±0.14

44c	Br	H	-CH ₂ C ₆ H ₄ (4-Cl)	7.13±0.06	7.06±0.05	5.01±0.03
44d	Br	H	-CH ₂ C ₆ H ₂ (3,4,5-OCH ₃)	9.31±0.09	11.04±0.02	5.02±0.03
44e	Br	H	4-dimethylcyclohexyl	>40	>40	>40
45a	H	CH ₃	-CH ₂ C ₆ H ₅	3.98±0.05	6.37±0.04	2.89±0.03
45b	H	CH ₃	-CH ₂ C ₆ H ₄ (4-CH ₃)	10.71±0.10	31.79±0.04	16.75±0.02
45c	H	CH ₃	-CH ₂ C ₆ H ₄ (4-Cl)	2.11±0.05	2.47±0.02	2.91±0.01
45d	H	CH ₃	-CH ₂ C ₆ H ₂ (3,4,5-OCH ₃)	6.01±0.06	7.66±0.23	5.70±0.05
45e	H	CH ₃	4-dimethylcyclohexyl	>40	>40	>40
			Doxorubicin	0.9±0.08	1.0±0.05	0.8±0.01

Doxorubicin was used as reference cytotoxic agent. The most interesting results were obtained with the isatin **42** series. Compound **42c** containing a 4-chlorobenzyl substituent at position N-6 showed an elevated cytotoxic activity with IC₅₀ values of 0.44, 0.53, and 0.87 μM in HEK, M14, and U937 cell lines, respectively. Compounds **42a**, **42b**, and **42d**, with a diverse substituted benzyl group at the N-6 position, retained the cytotoxic activity at micromolar concentration on the HEK and U930 cell lines, while they were less active in the M14 melanoma cell line. The introduction of an electron-releasing group as the -CH₃ group at C-5' position of the indol ring produced different effects: while the derivative **43c** reduced activity in the three cell lines compared to **42c** (8-, 12-, and 3-fold, respectively), compounds **43a**, **43b**, and **43d** increased their biological effect in all cell lines compared to **42a**, **42b**, and **42d**. In particular, these compounds were 2- to 4-fold more potent than the corresponding analogues **42** against M14 cell line.

The introduction at the C-5' position of the isatin moiety of an electron-withdrawing group such as the bromide group caused a reduction of the activity of the corresponding analogues **44a**, **44b**, **44c**, and **11d** in all cell lines. On the other hand, substitution of an aryl group for an alkyl group at the N-6

position was tolerated only in the isatin series **42** (compound **42e**) even with a loss in activity with respect to **42c** (8-, 14-, and 4-fold in the three cell lines, respectively). Compounds **43e**, **44e**, and **45e** showed a dramatic loss of activity. Finally, the derivatives **45a**, **45c**, and **45d**, which incorporate at position N-10 a methyl group, retained cytotoxic levels within the micromolar range. The same substitution was detrimental for the activity of analogues **45b** and **45e**.

The preliminary results on cytotoxicity and morphological cellular differences after treatment with **42c** and **43d** (see below) motivated us to study further the mode of action of these compounds. We have performed a comparative analysis of their effects on growth in immortalized normal thyroid TAD-2 and human papillary thyroid carcinoma TPC1 cell lines to establish a safety profile of these derivatives. Inhibition of proliferation of both cell lines was measured after treatment with 100 nM and 1 μ M of **42c** and **43d** at 48 h.

Figure 1a shows that at 100 nM, **9c** and **10d** caused a net decrease in the total number of cells in the carcinoma TPC1 cell line (70% and 58%, respectively), whereas the percentage of cellular growth inhibition in the TAD-2 cell line was only of 10% for **42c** and void for **43d** (Figure 19b). At 1 μ M, both compounds were cytotoxic for the TAD-2 cell line. These data seem to indicate that at 100 nM, **42c** and **43d** have a good profile of “cell selectivity”.

Furthermore, the introduction into **42c** and/or **43d** of a third hydrophobic group at the N-10 position appeared to have an important effect upon cytotoxicity, particularly in the case of compounds **13**.

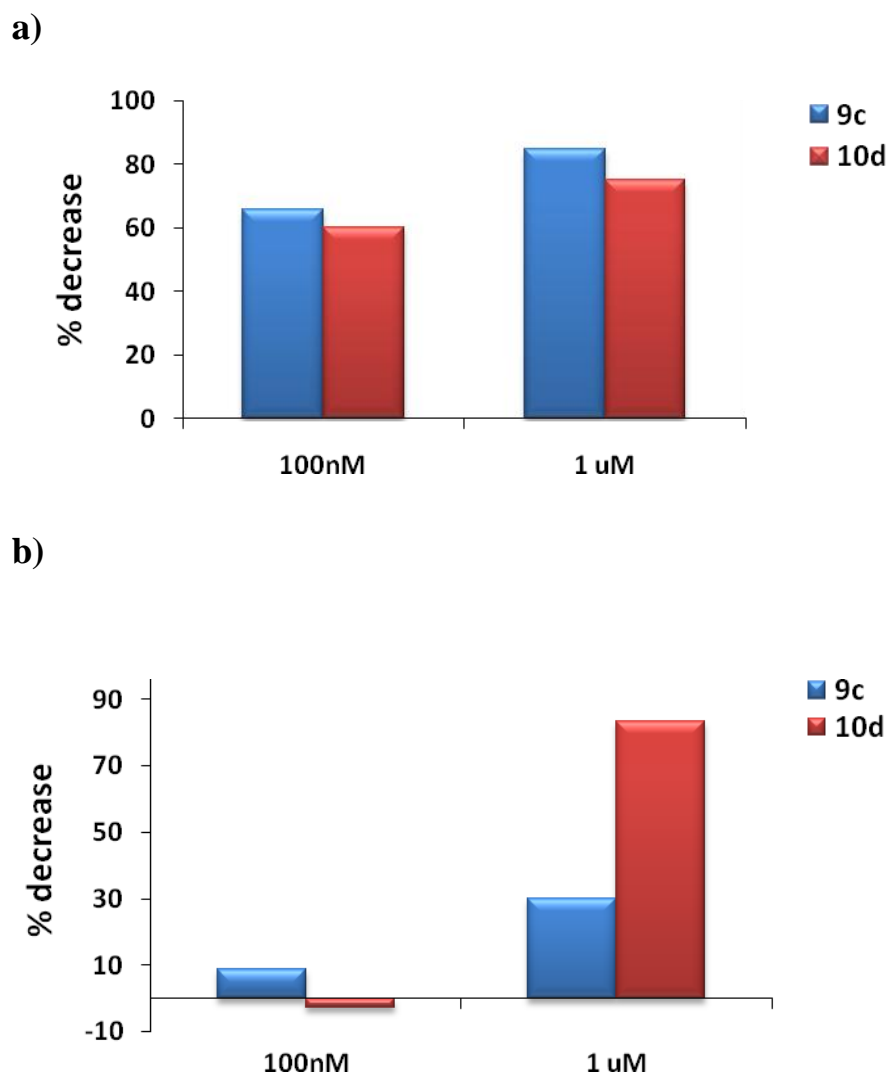
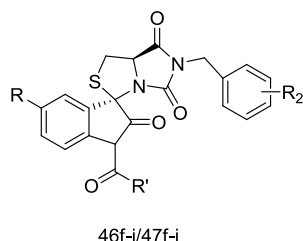


Figure 19. Effect of **42c** and **43d** derivatives on cell growth of (a) human papillary thyroid carcinoma TPC1 and (b) normal thyroid TAD-2 cell lines

Derivatives **46f-i** were 3- to 10-fold less potent than the corresponding analogue **42c**, though they maintain their activity in the micromolar range (IC₅₀ of 2.01-5.01 μ M, Table 3). These results are in agreement with those found for **45c** (IC₅₀ of 2.11-2.91 μ M, Table 1), which has a CH₃ group at the N-10 position, indicating that the introduction of hydrophobic groups in this

position limits the optimal side chain accommodation in the target, independent of their electronic and steric properties. The introduction of acyl side chains in N-10 position of **43d** led to slight or moderate decreases in the cytotoxic activity. Derivatives **47f-i** were only 1.5- to 3-fold less active than their analogue 10d. These findings imply a lower tolerance of compound **42c** to structural modification.

Table 4. Cytotoxic Activity of 1'-Acylspiro[(dihydroimidazo[1,5-c]-thiazolo-5,7-dione)-3,3'-(dehydroindol-2-one)] derivatives **46f-i/47f-i**.



Comp.	R	R ₁ '	R ₂ '	IC ₅₀ (□M) ±SD ^a		
				HEK	M14	U937
42c	H		4-Cl	0.44±0.01	0.53±0.01	0.87±0.01
46f	H	-C ₆ H ₅	4-Cl	3.50±0.02	3.25±0.36	3.12±0.07
46g	H	-C ₆ H ₄ (4-CH ₃)	4-Cl	2.50±0.10	2.08±0.10	2.01±0.15
46h	H	-C ₆ H ₄ (4-Cl)	4-Cl	5.01±0.15	3.37±0.37	2.61±0.05
46i	H	-CH ₂ CH ₂ CH ₃	4-Cl	2.01±0.05	2.04±0.34	2.10 ±0.09
43d	CH ₃		3,4,5-OCH ₃	2.04±0.03	2.40±0.02	2.06±0.04
47f	CH ₃	-C ₆ H ₅	3,4,5-OMe	4.22±0.14	7.84±0.02	4.31±0.02
47g	CH ₃	-C ₆ H ₄ (4-CH ₃)	3,4,5-OMe	3.81±0.05	5.95±0.01	2.42 ±0.04
47h	CH ₃	-C ₆ H ₄ (4-Cl)	3,4,5-OMe	4.71±0.15	8.14±0.02	3.11±0.01
147i	CH ₃	-CH ₂ CH ₂ CH ₃	3,4,5-OMe	4.42±0.16	7.40±0.0126	4.10± 0.02

^a Data represent mean values (SD) of three independent determinations.

6.4.1 Phase-Contrast Microscopic Analysis of Cell Morphology and Apoptosis.

Figure 20 shows that vehicle-treated M14 cells grew normally, while treatment with **42c** and **43d** impaired their morphology as determined by video time lapse microscopy.

A 10 h treatment with these compounds caused the emergence of round and damaged shapes followed by the formation of numerous blebs and a progressive detachment from the plastic well (48 h treatment). Treated cells displayed a lower number of cell division compared to control cells (Figure 2). These modifications were more pronounced and appeared earlier in cell cultures treated with **42c** than with **43d** and were consistent with induction of apoptotic cell death.¹⁶⁴ To confirm this observation, we measured caspase-3 activity. Upon cleavage by upstream proteases in an intracellular cascade, the activation of caspase-3 is considered a hallmark of the apoptotic process.¹⁶⁵

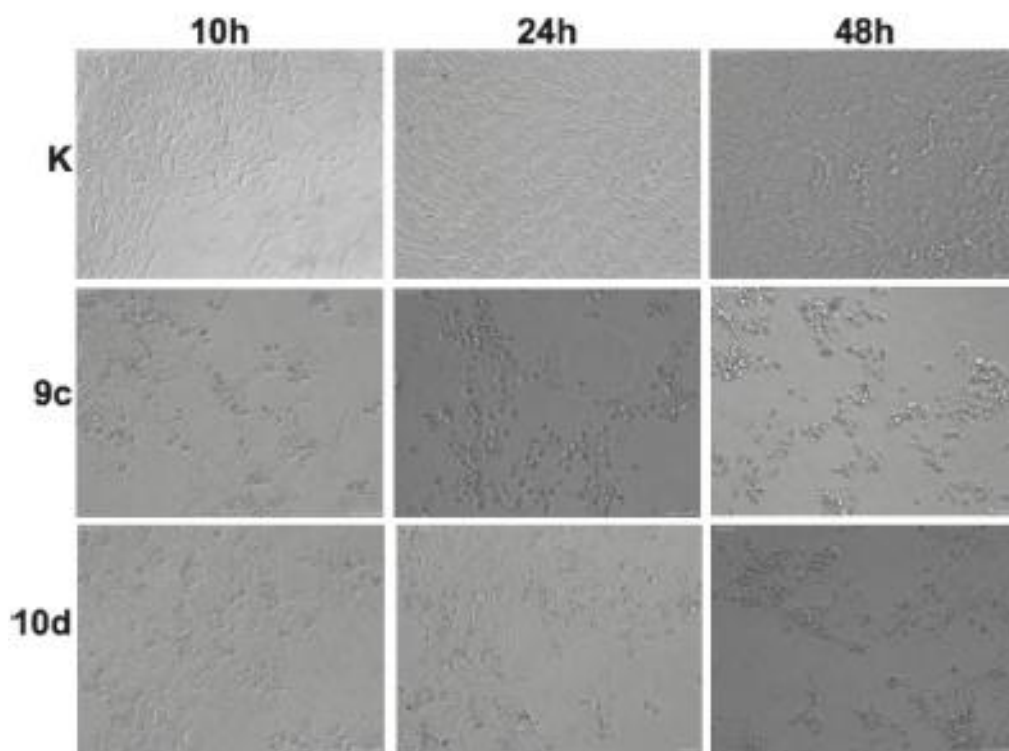


Figure 20. Morphological changes induced by treatment of M14 cell line with **42c** and **43d** after 10, 24, and 48 h at IC50 concentration. Cells had a doubling time of 19 h in culture (confirmed by cell counts, data not shown).

The levels of cleaved active subunits of executioner caspase-3 were evaluated by Western blotting of M14 cell lysates following **42c** (0.1-0.3 μM) and **43d** (1.0-5.0 μM) treatment for 16 and 24 h (Figure 21a). Compound **43d** did not lead to any caspase cleavage even at supra-IC50 concentration. **42c** increased caspase-3 activity after a 16 h exposure. Next, we examined the activation-mediated cleavage of caspase-3 substrate, poly(ADP-ribose) polymerase (PARP), which is a reliable marker of apoptosis (Figure 3b).¹⁶⁶ By use of the cysteine protease activity, caspases separate N-terminal DNA-binding domain of PARP from its C-terminal catalytic domain (85 kDa) showing that **42c** increased caspase-3 activity and PARP cleavage following 16 h of exposure,

suggesting that 9c induced apoptotic cell death in M14 cells. On the contrary, after 24 h and at cytotoxic concentration, compound 10d did not induce apoptotic death

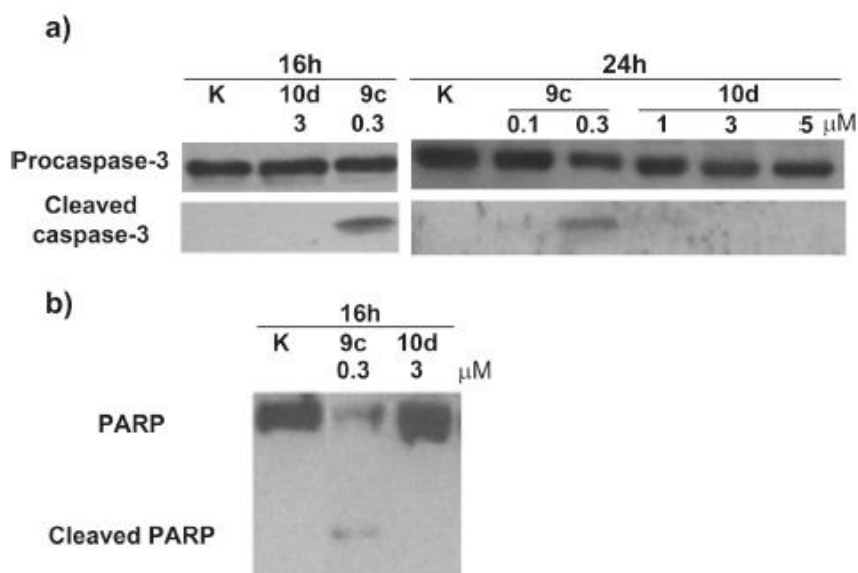


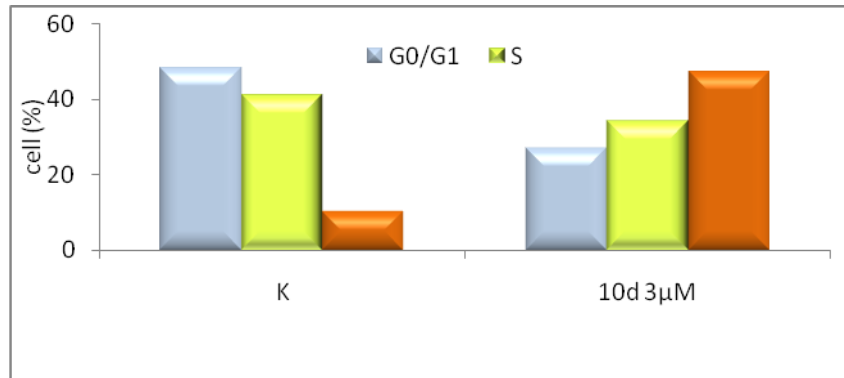
Figure 21. Caspase-3 (a) and PARP (b) cleavages induced for **42c** and **43d**.

6.4.2 Cell Cycle Effects and Expression of p53.

On the basis of previous data, we analyzed the effect of 9c and 10d on cell cycle progression. The cytometric investigation showed a clear arrest at G2/M cell cycle phase of M14 cells treated with **43d** (3 μM) for 24 h compared to control cells (Figure 22a). Accumulation of cells in the G2 phase increased about 47% ($p < 0.001$) with a corresponding decrease of cells in the G0/G1 phase (down to 20%, $p < 0.001$). Under the same conditions, treatment of M14 cells with **42c** (0.3 and 1 μM) did not show any significant effect on the cell cycle progression. The arrest of cell cycle induced by **43d** correlated well with a decreased expression of cyclin B1 compared to the control cells (Figure

22b), indicating that cell cycle progression of cells in the G2/M phase was markedly delayed and cells did not progress into M phase.

a)



b)

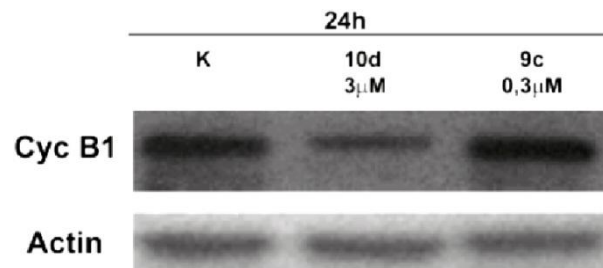
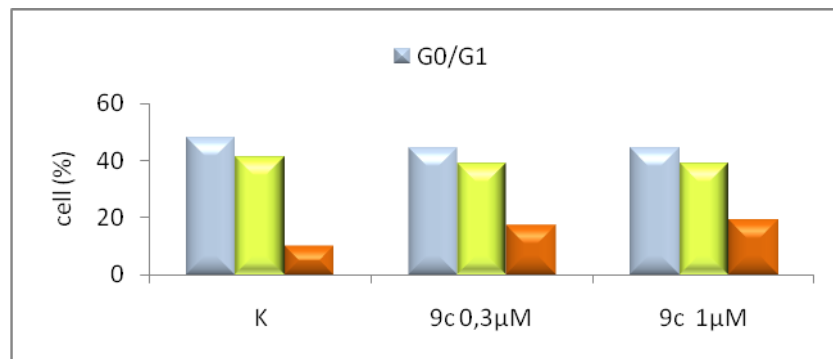


Figure 22. Effects of 42c and 43d on the distribution of cell populations. Data represent the percentage of cells in each cellular cycle phase (a). Shown is the Western blot expression of cyclin B1 in the control and induced by 42c and 43d (b).

Subsequently, we examined expression of the p53 as key regulator of both cell-cycle arrest and cell apoptotic death. Treatment of M14 cells with subcytotoxic concentrations of **42c** and **43c** produced, in both cases, a gradual increase of the p53 levels from 24 to 48 h. As observed in Figure 23, this increase is more significant in the case of **42c** at 24 h compared to control cells.

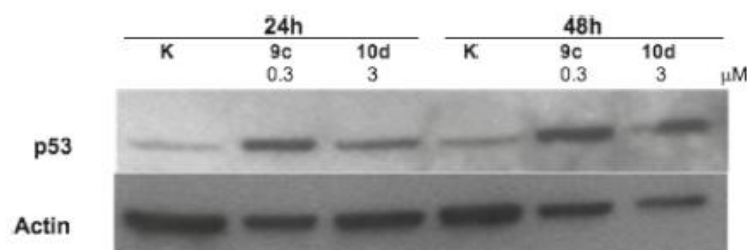


Figure 23. Western blot analysis of cytoplasmic p53 levels in M14 cells untreated (K) and treated with **42c** (0.3 μM) and **10d** (3 μM) after 24 and 48 h.

6.4.3 Inhibition of p53-MDM2 Interaction.

The ability of compounds **9c** and **10d** to block p53-MDM2 interaction was investigated by NMR analysis. Holak et al. have recently described a two-dimensional N-HSQC based NMR assay to determine the effect of antagonists on protein-protein interactions.¹⁶⁷ The method, named AIDA (for antagonist induced dissociation assay), provides information on whether an antagonist of a protein-protein interaction is strong enough to dissociate the complex and whether its mode of action is modulated by denaturation, precipitation, or release of a protein in its functional folded state. AIDA requires the use of a large protein fragment (larger than 30 kDa) to bind to a small reporter protein (less than 20 kDa). In appropriate conditions (flexible residues), 1D proton

NMR spectra may suffice for monitoring the states of proteins in complexes upon treatment with ligands. Because of the highly flexible nature of the N-terminal domain of p53, p53-MDM2 complex is suitable for 1D proton NMR application. In particular, the $^1\text{H}^\epsilon$ side chains of W23 and W53 produce sharp lines in the free p53 1Dproton spectrum. On formation of the complex with MDM2, W23 signal disappears, since W23, together with the p53 residues 17-26, comprises the primary binding site for MDM2.^{167,168} Upon binding, these residues participate in well-defined structures of large p53-MDM2 complexes, whereas W53 is still not structured when p53 is bound to MDM2. The observed $1/T_2$ transverse relaxation rate of the bound W23 in the complexes increases significantly, and the broadening of NMR resonances results in the disappearance of this signal from the spectra. Figure 8a shows the NMR spectrum of the tryptophan residues of the p53-MDM2 complex (only W53 $\text{NH}\epsilon$ side chains signal can be detected). After the addition of **42c** or **43d** to the p53-MDM2 complex, the W23 peak appears (Figure 24b and Figure 6c, respectively). Nutlin-3 was also used as positive control (Figure 24d), causing a complete p53 release.¹⁶⁷ Both compounds **42c** and **43d** released p53-MDM2 complex but were not as efficient as nutlin-3 causing about 80% and 60% p53 release, respectively.

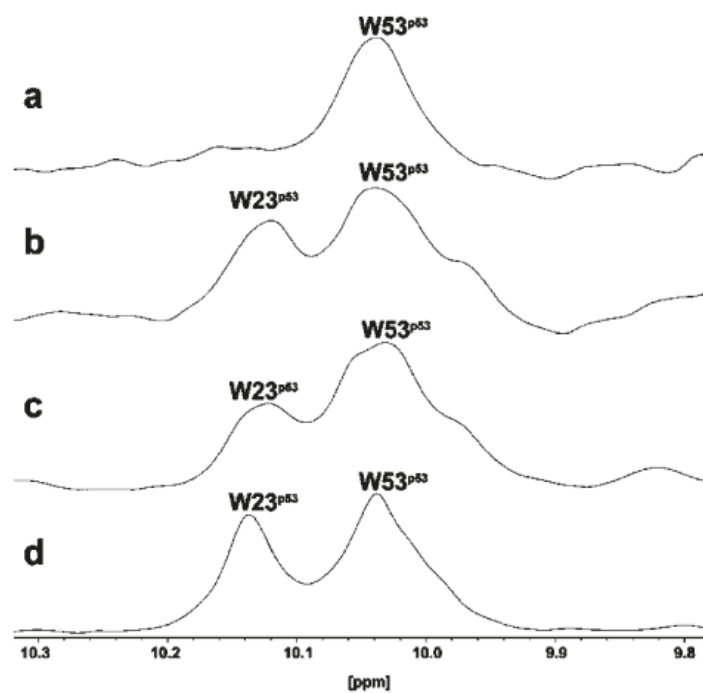


Figure 24. One-dimensional proton spectrum of the side chains of tryptophans (W) of p53-MDM2 complex (a) and after addition of **42c** (b), **43d** (c), and nutlin-3 (d).

CHAPTER 7.
CONCLUSIONS

The p53 tumor suppressor is a sequence-specific transcription factor whose inactivation or loss contributes to carcinogenesis. Several *in vitro* and *in vivo* studies have demonstrated that p53 is involved in growth arrest, genomic stability, cell senescence and differentiation while also activating p53 mediated apoptotic stress responses. Given its role in these fundamental process wild-type p53 is an attractive target for pharmacological intervention. Identification of small molecules able of reactivating specific p53 roles turns into a main aim for an important part of the scientific community .

This PhD thesis work presents the obtained results in the searching for small-molecules able to “reactive” the p53 transcriptional activity. The research was based on the identification of both DNA-damaging agents and compounds that modulate p53-MDM2 interaction, a negative regulator of p53 activity and stability, and included two projects. The first of them was centered in the design and synthesis of carbazole derivatives as DNA- damaging agents. The second, more wide, was based on the valuation of natural product analogues designed as both cellular cycle modulators and p53-MDM2 interaction inhibitors.

The first part of project has taken us to the synthesis of new N-[(9H-carbazol-9-yl)alkyl]-N,N-(diethyl)amine (serie 1) and 2-(9H-carbazol-9-yl)-N-(2-(dimethylamino)ethyl)substituted amide (serie 2) derivatives with cytotoxic activity in the micromolar range. Due to small structural differences in the most active compounds, a rigorous determination of structure-activity relationships is not possible right now. Our research on these compounds will continue by modifying and developing the most promising cytotoxic active compounds.

The results obtained in the second part of project, in this turn divided in two issues, lead to a series of interesting conclusions.

A synthetic level, we show the wide potentiality of the acid and base promoted intramolecular cyclization of 3-propylthiazolidinspirooxindole

derivatives to new tricyclic systems: hexahydropyrrolo[1,2-a][1,3]thiazolo[3,2-d]pyrazine-5,10-dione (structure I) and hexahydropyrrolo[1,2-a][1,3]thiazolo[3,4-d]pyrazine-5,10-dione (structure II). Possible reaction pathways for the formation of these structures imply unusual oxindole ring opening. In contrast, the acid promoted intramolecular cyclization of isomer 30-prolylspirooxindolethiazolidine leads to new spirotryprostatin A-inspired derivatives spiroindol-2-one[3,30]hexahydro-5,10H-pyrrolo[1,2-a][1,3]thiazolo[3,4-d]pyrazine-5,10-dione (structure III). Application of the methodology developed in this work represents a new possibility for molecular diversification of oxindole systems and for the development of other biologically useful members of the diketopiperazine structural class.

Among the hexahydropyrrolo[1,2-a][1,3]thiazolo[3,4-d]pyrazine-5,10-dione derivatives (structure II), the compounds **23a** and **24a** showed remarkable cytotoxic activity against MCF-7 cell lines at micromolar concentration. Moreover, they did not inhibit the cellular cycle, indicating that their mechanism of action did not include an interference with the cell cycle regulation systems. These compounds may become a promising class of cytotoxic agents and further experiments, aimed at defining the target and the mechanisms of the growth-inhibitory effect shown by some of these molecules are currently underway.

The design of N-substituted spiro[imidazo[1,5-c]thiazole-3,30-indoline]-2',5,7-trione derivatives lead to more interest compounds. In particular, compound (3*R*,7*aR*)-6-(4-Chlorobenzyl)-1H-spiro[imidazo[1,5-c]thiazole-3,3'-indoline]-2',5,7(6*H*,7*aH*)-trione (**42c**) showed high efficacy in HEK-293 (kidney), M-14 (melanoma), and U937 (leukemia) human cell lines with IC₅₀ values of 0.44, 0.53, and 0.87 μ M, respectively. The derivative containing a trimethoxybenzyl group at N-6 position, **43d**, was 3- to 5-fold less cytotoxic in all tested cell lines and showed a time-dependent activity different from that

of **42c**. Preliminary studies on the induction of apoptosis and cell cycle progression in M14 cell line confirmed a different behavior of these compounds. Thus, compound **42c** induced apoptotic cell death after 24 h of treatment at cytotoxic concentration, while **43d** did not induce apoptotic death in the same period of time. On the other hand, **43d** markedly prolonged the G2 phase, causing a delay of cell cycle progression in responsive cells, while treatment with **42c** did not alter the normal course of cell cycle. However, both compounds induce a time-dependent increment of p53 expression, indicating that the activity profiles of these derivatives might be regulated by this protein. NMR investigation performed on both compounds demonstrated that the ability of these compounds to block p53-MDM2 interaction caused release of p53. Taken together, that chemical modification at the pyrrolidine moiety of spirooxindole system is an effective approach to study the modulation of p53 activity through p53-MDM2 inhibition.

These preliminary results support the hypothesis of which it is possible the reactivation of p53 by small molecules, validating their potential therapeutic value. In addition, these small molecules will can represent important tools in the identification of pathways and/or factors governing the decision between apoptosis and growth arrest/DNA repair induced by p53.

Further experiments aimed both to identify more potent and selective spirothiazolidin-based derivatives and to better understand the mechanisms of reactivation of p53 are currently underway.

CHAPTER 8
EXPERIMENTAL SECTION

8. EXPERIMENTAL SECTION:

8.1. Materials and methods

Reagents and solvents were purchased from commercial suppliers and used as received. Analytical TLC was performed on plates coated with a 0.25 mm layer of Silica Gel 60 F254 Merck and preparative TLC on 20 × 20 cm glass plates coated with a 0.5 mm layer of silica gel PF254 Merck. Silica Gel 60 (300–400 mesh, Merck) was used for flash chromatography. Melting points are uncorrected. Optical rotations were determined in a 10 cm cell. ¹H and ¹³C NMR spectra were recorded at 400 and 100 MHz, respectively. Chemical shifts are reported in δ values (ppm) relative to internal Me₄Si and J values are reported in hertz. Mass spectra were measured by the ES method. Elemental analyses were carried out with C, H-analyzer. DMEM, fetal bovine serum, glutamine, penicillin, streptomycin, Hepes, sodium pyruvate and PBS were from Bio Whittaker (Caravaggio, BG, Italy). MTT was purchased from SIGMA (Milan, Italy).

8.1.1. NMR spectroscopy

NMR experiments were performed on a Varian Mercury 400 MHz spectrometer at 298 K. NMR samples were prepared by dissolving each compound (about 5 mM) in 0.6 ml of CDCl₃. 2D NOESY spectra of compounds **25a**, **28b**, **30a**, **30b** and **31a**, **31b** were recorded in the phase-sensitive mode, data block sizes were 2048 addresses in t₂ and 512 equidistant t₁ values. Before Fourier transformation, the time domain data matrixes were multiplied by shifted sin² functions in both dimensions. A mixing time of 400 ms was used.

8.1.2. Protein Expression and Purification for NMR Study.

The recombinant human MDM2 (residues 1-118) was overexpressed in *E. coli* BL21(DE3) RIL using the pET-46Ek/LIC vector (Novagen). Cells were grown at 37 °C and induced with 1 mM IPTG at an OD₆₀₀ of 0.7. The protein was purified and renatured from inclusion bodies as described.²⁸ The refolded protein was applied on butyl Sepharose 4 Fast Flow (Amersham) and then purified on a Sephadex G-75. The recombinant human p53 protein (residues 1-312) was overexpressed at 37 °C in *E. coli* BL21 (DE3) RIL using a pET-46Ek/LIC vector (Novagen) modified with N-terminal His-tag. The protein was purified under denaturing conditions using a NiNTA (Qiagen) column, refolded, and further purified using a gel filtration on Sephadex G-75 as previously described.²⁸ Complexes were made by mixing p53 and MDM2 in a molar ratio of 1:2. The excess of MDM2 was then removed by gel filtration on Sephadex G-75.

8.1.3. NMR Study of p53-MDM2 Interaction.

NMR spectra were acquired at 25 °C on a Varian Unity INOVA 700 MHz spectrometer equipped with a cryoprobe. Typically, NMR samples contained up to 0.1 mM protein in 50 mM KH₂PO₄, 50 mM Na₂HPO₄, 150 mM NaCl, pH 7.4, 5 mM DTT, 0.02% NaN₃. Water suppression was carried out by gradient echo.³⁰ NMR data were processed using the Bruker program BioSpin 3.0. For NMR ligand binding experiments, 600 µL of the protein sample containing 10% D₂O, at ~0.1 mM, and a 10 mM stock solution of each compound in DMSO-d₆ were used in all experiments. The final molar ratio protein/inhibitor was 1:1.

8.1.4. Computational data

Molecular modeling and graphics manipulations were performed using the Insight II software package (Accelrys, San Diego, CA). The 3D structures of the compounds were constructed using the module Builder of Insight II program and then optimized using minimization steps (conjugate gradient method), in vacuo, using the CVFF force field²⁰ in Insight II/Discover software packages. MD simulations were performed at 500 K period (time step = 1 fs). MD results were analyzed with the Analysis module of Insight II.

8.1.5. Statistical Analysis.

Data were analyzed using Prism 4.0 (Graph Pad Software, Inc.). Results are expressed as the mean (SEM). All statistical differences were evaluated by a two tailed Student's t test and one way ANOVA. P values less than 0.05 were considered statistically significant.

8.1.6. Crystallographic analysis

A suitable crystal of 21 (0.04 × 0.6 × 0.04 mm) was selected and mounted on a glass fibre. The diffraction data were collected at 100 K with graphite monochromatized Mo K α radiation ($\lambda = 0.71069$ Å, $2\theta_{max} 65.52^\circ$, ω and χ scan mode) on a Rigaku AFC7S diffractometer equipped with a Mercury CCD detector and corrected for Lorentz, polarization and absorption effects. The data collection was performed with a detector to crystal distance $D = 414$ mm using an oscillation angle of $\Delta\omega = 0.5^\circ$ and consisted of 892 images. It covered a resolution range of $d = 26.76$ – 0.80 Å. Intensity data were corrected for absorption.²¹ Lattice constants and crystal orientation were obtained using 1D FFT with DPS algorithm, ²² the number of reflections used was 970 with a refinement of 30 best directions and lengths. The structure was solved by direct methods using SIR92²³ and the refinement, realized by SHELXL97,²⁴ was based on F2 considering all non-hydrogen atoms anisotropically and

hydrogens included on calculated positions, riding on their parent atoms and then refined isotropically. A total of 514 parameters were refined. Maximum and minimum residual density were 0.85 and -0.45 e/A³. Final disagreement indices: R1 = 0.0578 for 3556 reflections with $F_o > 4\sigma(F_o)$ and wR2 = 0.1711 for all 8860 data. ORTEP drawings were prepared by means of the program ORTEP32.25

8.2. *General Procedure for the Synthesis of the N-[(9H-carbazol-9-yl)alkyl]-N,N-(diethyl)amine (1a, 1b, 1c).*

1,2-dibromoethane, or 1,3-dibromopropane, or 1,4-dibromobutane (0.20 mmol) was added to a solution of carbazole (0.10 mmol) in toluene (60 mL). After stirring at room temperature for 10 minutes, a basic solution of NaOH 50% (44mL) containing benzyltriethylammoniumbromide (0.03 mmol) was added. The reaction mixture was then stirred at room temperature for 20 h. Solvent was evaporated and the residue was dissolved into dichloromethane. The organic solution was washed with water (3 x 100 mL), dried over Na₂SO₄, and evaporated in vacuo. The residues were washed with n-hexane to remove the excess of dibromoalkane. The achieved compounds were crystallized with n-hexane to give white solids. The crystallized compounds were dissolved in DMF. and N,N'-diethylamine (0.13 mmol) and Cs₂CO₃ (0.13 mmol) were added. The mixture was stirring at room temperature for 18 h. The mixture was then cooled to ambient temperature and solvent was removed in vacuo. The residue was dissolved in dichloromethane and washed with water (3 x 100 mL). Flash chromatography on silica gel, using ethyl acetate/n-hexane in 1/4 ratio as eluent, yielded the correspondent final derivatives.

N-[(9H-carbazol-9-yl)ethyl]-N,N-(diethyl)amine (1a).

Brown oil. (68%). mp 132°C. ¹H NMR (300 MHz, CDCl₃) δ 1.36 (t, 6H, CH₃); 3.17 (q, 4H, CH₂ ethyl); 3.32 (t, 2H, CH₂ ethyl); 5.02 (t, 2H, CH₂ ethyl); 7.26 (t, 2H, H-2' and H-7'); 7.47 (t, 2H, H-3' and H-6'); 7.61 (d, 2H, J = 8.0 Hz, H-1' e H-8'); 8.06 (d, 2H, H-4' e H-5'). FAB-MS *m/z* calculated for C₁₈H₂₂N₂, 266.18, found, 266.21.

N-[(9H-carbazol-9-yl)propyl]-N,N-(diethyl)amine (1b).

Brown oil. (70%). mp 144 °C. ¹H NMR (300 MHz, CDCl₃) δ 1.26 (t, 6H, CH₃); 1.85-1.91 (m, 2H, CH₂ ethyl); 3.07 (t, 2H, CH₂ ethyl); 3.29 (q, 4H, CH₂ ethyl); 3.78 (t, 2H, CH₂ ethyl); 7.26 (t, 2H, H-2' and H-7'); 7.49 (t, 2H, H-3' e H-6'); 7.64 (d, 2H, J = 8.0 Hz, H-1' e H-8'); 8.08 (d, 2H, H-4' and H-5'). FAB-MS *m/z* calculated for C₁₈H₂₁N₂, 265.18, found, 265.25.

N-[(9H-carbazol-9-yl)butyl]-N,N-(diethyl)amine (1c).

Brown oil. (73%). mp 149 °C. ¹H NMR (300 MHz, CDCl₃) δ 1.26 (t, 6H, CH₃); 1.42-1.48 (m, 2H, CH₂ ethyl); 1.85-1.91 (m, 2H, CH₂ ethyl); 3.07 (t, 2H, CH₂ ethyl); 3.29 (q, 4H, CH₂ ethyl); 3.78 (t, 2H, CH₂ ethyl); 7.26 (t, 2H, H-2' and H-7'); 7.49 (t, 2H, H-3' and H-6'); 7.64 (d, 2H, J = 8.0 Hz, H-1' e H-8'); 8.08 (d, 2H, H-4' and H-5'). FAB-MS *m/z* calculated for C₂₀H₂₇N₂, 295.22, found, 295.26.

8.3. General Procedure for the Synthesis of the N-[(9H-carbazol-9-yl)alkyl]-N,N-(diethyl)amine (2, 3, 4).

Dimethoxytetrahydrofuran (2,5 mmol) in glacial acetic acid (1 mL) was added to a solution in glacial acetic acid (8 mL) of *L*-Phe-OEt, or *L*-Ala-OEt, or *L*-Gly-OEt (1 mmol) and heated to reflux temperature for 4 h, in nitrogen atmosphere. Solvent was evaporated and the residue was dissolved into dichloromethane and precipitate with n-hexane. Flash chromatography on

silica gel, using ethyl acetate/n-hexane in 2/3 ratio as eluent, yielded the correspondent derivatives **2**, **3**, **4**. Compounds **2**, or **3**, or **4** were dissolved in a mixture MeOH/H₂O 1/1 ratio (10 mL) and LiOH (3.0 mmol) was added. The reaction mixture was then stirred at room temperature for 10 h and then the MeOH was removed in vacuo. The water was treated with citric acid and extracted with dichloromethane (3 x 100 mL). The organic solution was dried over Na₂SO₄, and evaporated in vacuo.

8.4. General Procedure for the Synthesis of the 2-(9H-carbazol-9-yl)-N-[2-aminoethyl]substituted-amide derivatives (2a, 2b, 3a, 3b, 4a, 4b).

HOBt (1,3 mmol), HBTU (1,3 mmol) e DIPEA (2,6 mmol) were added to a solution of compound 2', or 3', or 4' (1.0 mmol) in DCM/DMF 10/3 ratio (13 mL). After stirring at room temperature for 10 minutes, a solution in DCM of corresponding amines (N,N'-dimethyl-ethylene-diamine, N-ethyl-morpholine **a-b**) (1,3 mmol) was added. The reaction mixture was then stirred at room temperature for 12 h. Solvent was evaporated and the residue was dissolved into dichloromethane. The organic solution was washed with an aqueous solution of NaHCO₃ (3 x 100 mL), dried over Na₂SO₄, and evaporated in vacuo. Flash chromatography on silica gel, using dichloromethane/methanol in 9/1 ratio as eluent, yielded the correspondent final derivatives. The achieved compounds were crystallized with MeOH to give white solids.

2-(9H-carbazol-9-yl)-N-(2-(dimethylamino)ethyl)acetamide (2a).

White solid. (71%). mp 153 °C. ¹H NMR (300 MHz, CDCl₃) δ 2.81 (s, 6H, CH₃); 3.15 (t, 2H, CH₂ ethyl); 3.67 (t, 2H, CH₂ ethyl); 4.97 (s, 2H, H-2); 7.21 (t, 2H, H-2' and H-7'); 7.39-7.43 (m, 4H, H-1', H-3', H-6' and H-8'); 8.08 (d, 2H, H-4' and H-5'). FAB-MS *m/z*. calculated for C₁₈H₂₁N₃O, 295.17, found, 295.23.

2-(9H-carbazol-9-yl)-N-(2-morpholinoethyl)acetamide (2b).

White solid. (67%). mp 164 °C. ¹H NMR (300 MHz, CDCl₃) δ 1.96 (t, 4H, CH₂ morpholin); 2.11 (t, 2H, CH₂ ethyl); 2.98 (t, 4H, CH₂ morpholin); 3.14 (t, 2H, CH₂ ethyl); 4.95 (s, 2H, H-2); 6.18 (s, 1NH); 7.23 (t, 2H, H-2' and H-7'); 7.31 (t, 2H, H-3' and H-6'); 7.48 (d, 2H, *J* = 8.0 Hz, H-1' and H-8'); 8.17 (d, 2H, H-4' and H-5'). FAB-MS *m/z* calculated for C₂₀H₂₃N₃O₂, 337.18, found, 337.22.

2-(9H-carbazol-9-yl)-N-(2-(dimethylamino)ethyl) propanamide (3a).

White solid. (69%). mp 172 °C. ¹H NMR (300 MHz, CDCl₃) δ 1.77 (d, 3H, *J* = 7.2 Hz, H-3); 1.86 (s, 6H, CH₃); 2.06-2.25 (m, 2H, CH₂ ethyl); 3.17-3.22 (m, 1H, CH₂ ethyl); 3.28-3.38 (m, 1H, CH₂ ethyl); 5.33 (q, 1H, H-2); 6.33 (s, 1NH); 7.26 (t, 2H, H-2' and H-7'); 7.45 (t, 2H, H-3' and H-6'); 7.53 (d, 2H, *J* = 8.0 Hz, H-1' and H-8'); 8.09 (d, 2H, H-4' and H-5'). FAB-MS *m/z* calculated for C₁₉H₂₃N₃O, 309.18, found, 309.26.

2-(9H-carbazol-9-yl)-N-(morpholinoethyl)propanamide (3b).

White solid. (64%). mp 179 °C. ¹H NMR (300 MHz, CDCl₃) δ 1.77 (d, 3H, *J* = 7.2 Hz, H-3); 2.01 (t, 4H, CH₂ morpholin); 2.10 (t, 1H, CH₂ ethyl); 2.19 (t, 1H, CH₂ ethyl); 2.92-3.11 (m, 5H, CH₂ morpholin and CH₂ ethyl); 3.18 (t, 1H, CH₂ ethyl); 5.31-5.34 (m, 1H, H-2); 6.36 (s, 1NH); 7.23 (t, 2H, H-2' and H-7'); 7.34 (t, 2H, H-3' and H-6'); 7.40 (d, 2H, *J* = 8.0 Hz, H-1' and H-8'); 8.09 (d, 2H, H-4' and H-5'). FAB-MS *m/z* calculated for C₂₁H₂₅N₃O₂, 351.19, found, 351.25.

2-(9H-carbazol-9-yl)-N-(2-(dimethylamino)ethyl)-3-phenyl propanamide (4a).

White solid. (73%). mp 203 °C. ¹H NMR (300 MHz, CDCl₃) δ 2.48 (s, 3H, CH₃); 2.69 (s, 3H, CH₃); 2.93-2.98 (m, 2H, CH₂ ethyl); 3.09-3.18 (m, 2H, CH₂

ethyl); 3.45 (t, 1H, Ha-3); 3.67 (dd, 1H, $J' = 4.0$ Hz, $J'' = 14.4$ Hz Hb-3); 4.13 (s, 1NH); 5.66 (dd, 1H, $J' = 4.0$ Hz, $J'' = 8.0$ Hz H-2); 6.81-6.94 (m, 5H, aryl); 7.17-7.36 (m, 6H, H-1', H-2', H-3', H-6', H-7' and H-8'); 8.05 (d, 2H, H-4' e H-5'). FAB-MS m/z calculated for $C_{25}H_{27}N_3O$, 385.22, found, 385.26.

2-(9H-carbazol-9-yl)-N-(2-morpholinoethyl)-3-phenylpropanamide (4b).

White solid. (65%). mp 216 °C. 1H NMR (300 MHz, $CDCl_3$) δ 1.88 (t, 4H, CH_2 morpholin); 2.14 (t, 1H, CH_2 ethyl); 2.23 (t, 1H, CH_2 ethyl); 3.02-3.16 (m, 5H, CH_2 morpholin and CH_2 ethyl); 3.36-3.41 (m, 1H, CH_2 ethyl); 3.50 (t, 1H, Ha-3); 3.91 (dd, 1H, $J' = 4.0$ Hz, $J'' = 14.4$ Hz Hb-3); 5.34 (dd, 1H, $J' = 4.0$ Hz, $J'' = 8.0$ Hz H-2); 6.39 (s, 1NH); 6.76-6.92 (m, 2H, aryl); 8.06 (d, 2H, H-4' and H-5' $J = 8.0$ Hz). FAB-MS m/z calculated for $C_{27}H_{29}N_3O_2$, 427.23, found, 427.27.

8.5. General procedure for the synthesis of spirooxindolethiazolidine ethyl ester derivatives (6a,b–12a,b) and spirooxindolethiazolidine carboxylic acid (29a,b–32a,b) derivatives

The reactions were carried out in a Milestone CombiChem Microwave Synthesizer. All irradiation process, rotation of the rotor, irradiation time, temperature, and power were monitored with the 'easyWAVE' software package. Temperatures were monitored with the aid of an optical fiber inserted into one of the reaction vessels. $NaHCO_3$ (10 mmol) and the corresponding isatin derivatives (**4-8**, 12 mmol) were added to a solution of L-Cys-OEt or L-Cys-OH (10 mmol) in methanol (100 mL) and the suspension was irradiated at 300W until 65 °C was reached. The reaction mixture was held at this temperature for 45 min and then cooled rapidly to room temperature. Then the suspensions were filtered and the filtrates were concentrated. At this step, the

carboxylic acid derivatives (**33-37**) were purified by flash chromatography using EtOAc as eluent system, while the corresponding ethyl ester residues (**9-13**) were dissolved in CH₂Cl₂ and washed with water (3 x 50 mL). The combined organic layer was dried over anhydrous sodium sulfate, filtered, and concentrated. These compounds were used in the next reaction without further purification as diastereomeric mixtures.

(3*R*,4'*R*) and (3*S*,4'*R*) ethyl 2-oxospiro[indoline-3,2'-thiazolidine]-4'-carboxylate (9a,b)

Oil (86%); ¹H NMR (400 MHz, CDCl₃) δ 1.36 (6H, t, CH₃), 3.30–3.33 and 3.35–3.41 (2H, m, H-5'a), 3.62–3.67 and 3.91–3.95 (2H, m, H-5'b), 4.27 (4H, q, CH₂CH₃), 4.48–4.51 and 4.68–4.72 (2H, m, H-40), 6.81 (2H, d, J = 8.0 Hz, H-4), 7.11 (2H, t, H-5), 7.34 (2H, t, H-6), 7.48 (2H, d, J = 8.0, H-7), 8.43 (2H, s, NH). ES-MS m/z: Calculated for C₁₃H₁₄N₂O₃S: 278.07. Found: 278.13.

(3*R*,4'*R*) and (3*S*,4'*R*) ethyl 5-methyl-2-oxospiro[indoline-3,2'-thiazolidine]-4'-carboxylate (10a,b)

Oil (81%); ¹H NMR (400 MHz, CDCl₃) δ 1.36 (6H, t, CH₃), 2.21 (6H, s, CH₃), 3.27–3.31 and 3.38–3.42 (2H, m, H-5'a), 3.65–3.68 and 3.89–3.91 (2H, m, H-5'b), 4.25 (4H, q, CH₂CH₃), 4.43–4.45 and 4.61–4.64 (2H, m, H-40), 6.77 (2H, d, J = 8.0 Hz, H-7), 7.38 (2H, d, J = 8.0 Hz, H-6), 7.45 (2H, s, H-4), 8.70 (2H, s, NH). ES-MS m/z: Calculated for C₁₄H₁₆N₂O₃S: 292.09. Found: 292.13.

(3*R*,4'*R*) and (3*S*,4'*R*) ethyl 5-bromo-2-oxospiro[indoline-3,2'-thiazolidine]-4'-carboxylate (11a,b)

Oil (89%); ¹H NMR (400 MHz, CDCl₃) δ 1.36 (6H, t, CH₃), 3.29–3.34 and 3.41–3.46 (2H, m, H-5'a), 3.70–3.75 and 3.92–3.94 (2H, m, H-5'b), 4.25 (4H, q, CH₂CH₃), 4.46–4.49 and 4.65–4.68 (2H, m, H-40), 6.75 (2H, d, J = 8.0 Hz,

H-7), 7.39 (2H, d, H-6), 7.46 (2H, s, H-4), 7.78 (2H, s, NH). ES-MS *m/z*: Calculated for C₁₃H₁₃BrN₂O₃S: 355.98. Found: 356.03.

(3*R*,4'*R*) and (3*S*,4'*R*) ethyl 1-methyl-2-oxospiro[indoline-3,20-thiazolidine]-4'-carboxylate (12a,b)

Oil (83%); ¹H NMR (400 MHz, CDCl₃) δ 1.36 (6H, t, CH₂CH₃), 3.22 (6H, s, CH₃), 3.39–3.41 and 3.45–3.49 (2H, m, H-5'a), 3.81–3.85 and 3.94–3.97 (2H, m, H-5'b), 4.24 (4H, q, CH₂CH₃), 4.48–4.50 and 4.69–4.72 (2H, m, H-40), 6.82 (2H, d, *J* = 8.0 Hz, H-7), 7.11 (2H, t, H-6), 7.33 (2H, d, *J* = 8.0 Hz, H-4), 7.48 (2H, t, 5H). ES-MS *m/z*: Calculated for C₁₄H₁₆N₂O₃S: 292.09. Found: 292.13.

(3*R*,4'*R*) and (3*S*,4'*R*) 2-oxospiro[indoline-3,20-thiazolidine]-40-carboxylic acid (33a,b)

Oil (68%); ¹H NMR (400 MHz, CDCl₃) δ 3.24–3.28 and 3.37–3.42 (2H, m, H-5'a), 3.63–3.65 and 3.82–3.84 (2H, m, H-5'b), 4.26–4.28 and 4.44–4.47 (2H, m, H-40), 6.81 (1H, d, *J* = 8.0 Hz, H-4), 7.11 (1H, t, H-5), 7.34 (1H, t, H-6), 7.48 (1H, d, *J* = 8.0 Hz, H-7), 8.43 (1H, s, NH). ES-MS *m/z*: Calculated for C₁₁H₁₀N₂O₃S: 250.04. Found: 250.09.

(3*R*,4'*R*) and (3*S*,4'*R*) 5-methyl-2-oxospiro[indoline-3,20-thiazolidine]-4'-carboxylic acid (34a,b)

Oil (61%); ¹H NMR (400 MHz, CD₃OD) δ 2.24 (6H, s, CH₃); 3.26–3.29 and 3.34–3.38 (2H, m, H-5'a), 3.65–3.68 and 3.81–3.85 (2H, m, H-5'b), 4.28–4.30 and 4.45–4.49 (2H, m, H-40), 6.79 (2H, d, *J* = 8.0 Hz, H-7), 7.36 (2H, d, H-6), 7.48 (2H, s, H-4), 8.83 (2H, s, NH). ES-MS *m/z*: Calculated for C₁₂H₁₂N₂O₃S: 264.06. Found: 264.13.

(3R,4'R) and (3S,4'R) 5-bromo-2-oxospiro[indoline-3,20-thiazolidine]-4'-carboxylic acid (35a,b)

Oil (64%); ¹H NMR (400 MHz, CD₃OD) δ 3.23–3.25 and 3.38–3.41 (2H, m, H-5'a), 3.64–3.67 and 3.82–3.85 (2H, m, H-5'b), 4.26–4.28 and 4.48–4.50 (2H, m, H-40), 6.78 (2H, d, J = 8.0 Hz, H-7), 7.15 (2H, d, H-6), 7.33 (2H, s, H-4), 8.49 (2H, s, NH). ES-MS m/z: Calculated for C₁₁H₉BrN₂O₃S: 329.17. Found: 329.26.

(3R,4'R) and (3S,4'R) 1-methyl-2-oxospiro[indoline-3,20-thiazolidine]-4'-carboxylic acid (36a,b)

Oil (66%); ¹H NMR (400 MHz, CD₃OD) δ 3.18 (6H, s, CH₃); 3.26–3.28 and 3.37–3.40 (2H, m, H-5' a), 3.68–3.71 and 3.84–3.86 (2H, m, H-5' b), 4.23–4.26 and 4.45–4.47 (2H, m, H-40), 6.86 (2H, d, J = 8.0 Hz, H-7), 7.18 (2H, t, H-6), 7.41 (2H, d, J = 8.0 Hz, H-4), 7.49 (2H, t, H-5). ES-MS m/z: Calculated for C₁₂H₁₂N₂O₃S: 264.06. Found: 264.14.

8.6. General procedure for the synthesis of 3-ethyl-10a-(substituted) phenyl-5,10-dioxooctahydro-5H-pyrrolo[1,2-a][1,3]thiazolo[3,2-d]pyrazine-3-carboxylate (19–21) and 3-ethyl-3-(substituted)-phenyl-5,10-dioxohexahydro-5H-pyrrolo[1,2-a][1,3]thiazolo[3,4-d]pyrazine-3-carboxylate (26a–b, 27a, 28a–b)

To a solution of the corresponding spirooxindolthiazolidine ethyl esters (**9a,b–12a,b** 3 mmol) in dichloromethane (25 mL), N-Boc-Pro (1.1 equiv), DIC (1.2 equiv), HOBt (1.2 equiv), and DIPEA (2.4 equiv) were successively added. Stirring was continued at room temperature for 4 h. Afterward, the reaction mixture was diluted with dichloromethane (20 mL), and the resulting solution was washed successively with 10% citric acid (2 x 25 mL), 10% NaHCO₃ (2 x

25 mL), and water (2 x 25 mL), dried over Na₂SO₄, and evaporated to dryness. Flash chromatography of the residues, using different eluent systems, yielded, in each case, the correspondent 30-(N-Boc)prolyl derivatives as diastereoisomeric mixture (**13a,b–16a,b**), which were not separated in this step. A solution of derivatives **13a,b** or **14a,b** or **15a,b** or **16a,b** (1 mmol) in CH₂Cl₂ (10 mL), was treated with trifluoroacetic acid (5 mL) and stirred at room temperature. After 2 h, TEA was added until pH 7 and the resulting mixtures were washed with water (3 x 25 mL), dried over Na₂SO₄, evaporated to dryness, and purified and separated by flash column chromatography using different eluent systems to yield the title compounds.

(3*R*,5*aS*,10*aS*) 3-Ethyloxycarbonyl-10a-(2'-amino)-phenyl-5,10-dioxooctahydro-5H-pyrrolo [1,2-*a*][1,3] thiazolo[3,2-*d*]pyrazine (23)

FC in ethyl acetate/n-hexane 3/2. White solid (40%); mp 140–141 °C; α_{D}^{25} -30.1 (c 0.1 in CHCl₃); ¹H NMR (400 MHz, CDCl₃) δ 1.33 (3H, t, CH₂CH₃), 1.81–1.86 (1H, m, H-7a), 1.96–2.04 (1H, m, H-7b), 2.21–2.29 (2H, m, H-6), 2.96 (1H, t, H-2a), 3.24 (1H, dd, J = 6.4 and 12.4 Hz, H-2b), 3.42–3.47 (1H, m, H-8a), 3.59–3.66 (1H, m, H-8b), 4.12 (1H, t, H-5a), 4.27 (1H, q, CH₂CH₃), 4.31 (1H, q, CH₂CH₃), 4.83 (1H, dd, J = 6.0 and 10.4 Hz, H-3), 6.70 (1H, d, J = 7.2 Hz, H-30), 6.75 (1H, t, H-50), 7.16 (1H, t, H-40), 8.02 (1H, d, J = 7.2 Hz, H-60); ¹³C NMR (100 MHz, CDCl₃) δ 14.3 (CH₃), 23.4 (C-6), 27.6 (C-7), 31.8 (C-2), 46.9 (C-8), 59.3 (C-5a), 62.2 (CH₂), 65.4 (C-3), 82.5 (C-10a), 117.1 (C-40), 118.0 (C-60), 127.7 (C-50), 128.5 (C-10), 130.4 (C-30), 145.7 (C-20), 164.3, 166.7, 168.8 (C=O). Anal. Calculated for C₁₈H₂₁N₃O₄S: C, 57.58; H, 5.64; N, 11.19; S, 8.54. Found: C, 57.41; H, 5.59; N, 11.22; S, 8.61.

(3*R*,5*aS*,10*aS*) 3-Ethylloxycarbonyl-10*a*-(2'-amino-5,10 methyl)- phenyl-5,10-dioxooctahydro-5*H*-pyrrole[1,2-*a*][1,3]thiazole[3,2-*d*]-pyrazine (24)

FC in ethyl acetate/n-hexane 3/2. White solid (41%); mp 159–161 °C; α^{25}_{D} -24.9 (c 0.12 in CHCl₃); ¹HNMR (400 MHz, CDCl₃) δ 1.32 (3H, t, CH₂CH₃), 1.78–1.85 (1H, m, H-7*a*), 1.95–2.01 (1H, m, H-7*b*), 2.23–2.28 (2H, m, H-6), 2.27 (3H, s, CH₃-50), 2.97 (1H, t, H-2*a*), 3.24 (1H, dd, J = 6.4 and 12.4 Hz, H-2*b*), 3.42–3.48 (1H, m, H-8*a*), 3.60–3.67 (1H, m, H-8*b*), 4.08 (1H, t, H-5*a*), 4.25 (1H, q, CH₂ CH₃), 4.33 (1H, q, CH₂ CH₃), 4.82 (1H, dd, J = 6.0 and 10.4 Hz, H-3), 6.63 (1H, d, J = 8.0 Hz, H-30), 6.98 (1H, d, H-40), 7.84 (1H, s, H-60); ¹³C NMR (100 MHz, CDCl₃) δ 14.3 (CH₃), 23.6 (C-6), 25.3(CH₃), 27.9 (C-7), 31.5 (C-2), 46.7 (C-8), 59.5 (C-5*a*), 62.4 (CH₂), 65.8 (C-3), 81.8 (C-10*a*), 120.2 (C-30), 122.4 (C-10), 125.6 (C-40), 128.3 (C-50), 131.1 (C-60), 144.1 (C-20), 164.2, 166.5, 168.9 (C=O). Anal. Calculated for C₁₉H₂₃N₃O₄S: C, 58.59; H, 5.95; N, 10.79; S, 8.23. Found C, 58.32; H, 5.51; N, 10.90; S, 8.35.

(3*R*,5*aS*,10*aS*) 3-Ethylloxycarbonyl-10*a*-(2'-amino-5'-bromo)-phenyl-5,10-dioxooctahydro-5*H*-pyrrole[1,2-*a*][1,3]thiazole[3,2-*d*]-pyrazine (25)

FC in dichloromethane/acetone 95/5. White solid (45%); mp 195–196 °C; α^{25}_{D} -27.1 (c 0.1 in CHCl₃); ¹HNMR (400 MHz, CDCl₃) δ 1.34 (t, 3H, CH₂CH₃), 1.81–1.88 (1H, m, H-7*a*), 1.98–2.04 (1H, m, H-7*b*), 2.26–2.30 (2H, m, H-6), 2.97 (1H, t, H-2*a*), 3.26 (1H, dd, J = 6.0 and 11.6 Hz, H-2*b*), 3.45–3.49 (1H, m, H-8*a*), 3.59–3.66 (1H, m, H-8*b*), 4.14 (1H, t, H-5*a*), 4.22 (1H, q, CH₂ CH₃); 4.33 (1H, q, CH₂ CH₃), 4.83 (1H, dd, J = 6.0 and 10.8 Hz, H-3), 6.58 (1H, d, J = 8.4 Hz, H-30), 7.24 (1H, d, H-40), 8.16 (1H, s, H-60); ¹³C NMR (100 MHz, CDCl₃) δ 14.4 (CH₃), 23.3 (C-6), 27.6 (C-7), 31.7 (C-2), 46.9 (C-

8), 59.4 (C-5a), 62.4 (CH₂), 65.6 (C-3), 81.9 (C-10a), 116.1 (C-50), 119.5 (C-30), 122.7 (C-10), 129.8 (C-40), 133.1 (C-60), 145.1 (C-20), 164.1, 166.6, 168.5(C=O). Anal. Calculated for C₁₈H₂₀BrN₃O₄S: C, 47.58; H, 4.44; Br, 17.59; N, 9.25; S, 7.06. Found: C, 47.41; H, 4.2; Br, 17.71; N, 9.12; S, 7.24.

(3R,5aS,10aR) 3-Ethylloxycarbonyl-3-(2'-amino)phenyl-5, 10-dioxooctahydro-5H-pyrrolo[1,2-a][1,3]thiazolo[3,4-d]pyrazine (26a)

FC in ethyl acetate/n-hexane 3/2. Oil (9%); $[\alpha]_D^{25}$ -71.2 (c 0.1 in CHCl₃); ¹H NMR (400 MHz, CDCl₃) δ 1.24 (3H, t, CH₂CH₃), 1.53–1.61 (1H, m, H-7a), 1.85–1.93 (1H, m, H-7b), 2.38–2.41 (2H, m, H-6), 3.03–3.09 (2H, m, H-1), 3.46–3.52 (1H, m, H-8a), 3.62–3.68 (1H, m, H-8b), 3.96–4.02 (1H, m, H-5a), 4.22–4.28 (2H, m, CH₂ CH₃), 5.13 (1H, d, J = 5.1 Hz, H-10a), 6.70 (1H, t, J = 8.0 Hz, H-50), 6.79 (1H, d, J = 8.0 Hz, H-30), 6.85 (1H, d, H-60), 7.12 (1H, t, H-40); ¹³C NMR (100 MHz, CDCl₃) δ 13.7 (CH₃), 21.0 (C-7), 28.5 (C-6), 31.7 (C-1), 46.1 (C-8), 60.1 (C-5a), 61.2 (CH₂), 62.0 (C-10a), 63.9 (C-3), 118.0 (C-30), 119.5 (C-50), 122.6 (C-10), 128.4 (C-40), 130.9 (C-60), 149.8 (C-20), 164.8, 166.7, 169.6 (C=O). Anal. Calculated for C₁₈H₂₁N₃O₄S: C, 57.58; H, 5.64; N, 11.19; S, 8.54. Found: C, 57.42; H, 5.49; N, 11.27; S, 8.59.

(3S,5aS,10aR) 3-Ethylloxycarbonyl-3-(2'-amino)phenyl-5,10-dioxooctahydro-5H-pyrrolo[1,2-a][1,3]thiazolo[3,4-d] pyrazine (26b)

FC in ethyl acetate/n-hexane 3/2. Oil (24%); $[\alpha]_D^{25}$ -152.5 (c 0.11 in CHCl₃); ¹H NMR (400 MHz, CDCl₃) δ 1.32 (3H, t, CH₂CH₃), 1.63–1.71 (1H, m, H-7a), 1.87–1.92 (1H, m, H-6b), 2.31–2.35 (2H, m, H-7), 3.02–3.11 (2H, m, H-1), 3.28–3.33 (1H, m, H-8a), 3.77–3.82 (1H, m, H-8b), 4.20–4.28 (3H, m, H-5a, CH₂CH₃), 4.83 (1H, d, J = 5.2 Hz, H-10a), 6.66 (1H, t, H-50), 6.71 (1H, d, J = 8.0 Hz, H-30); 6.78 (1H, d, J = 8.0 Hz, H-60), 7.12 (1H, t, H-40); ¹³C NMR (100 MHz, CDCl₃) δ 14.1 (CH₃), 20.3 (C-7), 28.8 (C-6), 32.6 (C-1),

45.7 (C-8), 61.9 (C-5a), 62.1 (CH₂), 62.8 (C-10a), 63.7 (C-3), 118.0 (C-30), 119.5 (C-50), 123.4 (C-10), 127.4 (C-40), 131.6 (C-60), 150.6 (C-20), 163.9, 166.9, 168.7 (C=O). Anal. Calculated for C₁₈H₂₁N₃O₄S: C, 57.58; H, 5.64; N, 11.19; S, 8.54. Found: C, 57.47; H, 5.53; N, 11.29; S, 8.63.

(3*R*,5*aS*,10*aR*) 3-Ethylloxycarbonyl-3-(2'-amino-5'-methyl)-phenyl-5,10-dioxoctahydro-5H-pyrrole[1,2-*a*][1,3]thiazole[3,4-*d*]pyrazine-3-carboxylate (27a)

FC in ethyl acetate/n-hexane 3/2. Oil (23%); $|\alpha_{\text{D}}^{25} - 66.7$ (c 0.12 in CHCl₃); ¹HNMR (400 MHz, CDCl₃) δ 1.29 (3H, t, CH₂CH₃), 1.78–1.82 (1H, m, 7a-H), 1.92–2.01 (1H, m, 7b-H), 2.22 (3H, s, CH₃), 2.27–2.30 (2H, m, H-6), 3.12–3.18 (2H, m, H-1), 3.42–3.46 (1H, m, H-8a), 3.69–3.74 (1H, m, H-8b), 4.00 (1H, t, H-5a), 4.21 (2H, q, CH₂CH₃), 5.12 (1H, d, J = 5.2 Hz, H-10a), 6.62 (1H, d, H-30), 6.64 (1H, s, H-60), 6.98 (1H, d, J = 8.0 Hz, H-40); ¹³C NMR (100 MHz, CDCl₃) δ 14.5 (CH₃), 20.8 (C-7), 23.9 (CH₃), 28.3 (C-6), 32.9 (C-2), 45.9 (C-8), 61.0 (C-5a), 62.5 (CH₂), 63.6 (C-10a), 64.8 (C-3), 119.8 (C-30), 126.7 (C-40), 129.4 (C-60), 130.1 (C-50), 146.3 (C-20), 163.8, 166.4, 168.1 (C=O). Anal. Calculated for C₁₉H₂₃N₃O₄S: C, 58.59; H, 5.95; N, 10.79; S, 8.23. Found: C, 58.41; H, 5.57; N, 10.88; S, 8.41.

(3*R*,5*aS*,10*aR*) 3-Ethylloxycarbonyl-3-(2'-amino-5'-bromo)-phenyl-5,10-dioxoctahydro-5H-pyrrole[1,2-*a*][1,3]thiazole[3,4-*d*]pyrazine (28a)

FC in dichloromethane/acetone 95/5. Oil (8%); $|\alpha_{\text{D}}^{25} - 69.2$ (c 0.2 in CHCl₃); ¹HNMR (400 MHz, CDCl₃) δ 1.30 (3H, t, CH₂CH₃), 1.79–1.83 (1H, m, H-7a), 1.90–1.99 (1H, m, H-7b), 2.29–2.34 (2H, m, H-6), 3.11–3.20 (2H, m, H-1), 3.46–3.49 (1H, m, H-8a), 3.62–3.68 (1H, m, H-8b), 3.99 (1H, t, H-5a), 4.23 (2H, m, CH₂CH₃), 5.14 (1H, d, J = 5.2 Hz, H-10a), 6.60 (1H, d, J = 8.0 Hz, H-30), 7.01 (1H, s, H-60), 7.21 (1H, d, H-40); ¹³C NMR (100 MHz, CDCl₃)

δ 14.4 (CH₃), 23.4 (C-7), 28.3 (C-6), 32.4 (C-2), 46.9 (C-8), 60.0 (C-5a), 61.0 (CH₂), 62.1 (C-10a), 63.9 (C-3), 118.2 (C-50), 119.7 (C-30), 127.3 (C-40), 133.1 (C-60), 149.1(C-20), 163.9, 167.1, 168.1 (C=O). Anal. Calculated for C₁₈H₂₀BrN₃O₄S: C, 47.58; H, 4.44; Br, 17.59; N, 9.25; S, 7.06. Found: C, 47.49; H, 4.27; Br, 17.72; N, 9.09; S, 7.25.

(3S,5aS,10aR) 3-Ethylloxycarbonyl-3-(2'-amino-5'-bromo)-phenyl-5,10-dioxooctahydro-5H-pyrrole[1,2-a][1,3]thiazole[3,4-d]pyrazine (28b)

FC in dichloromethane/acetone 95/5. Oil (20%); α_D^{25} -176.2 (c 0.12 in CHCl₃); ¹HNMR (400 MHz, CDCl₃) δ 1.32 (3H, t, CH₂CH₃), 1.58–1.63 (1H, m, H-7a), 1.93–1.95 (1H, m, H-7b), 2.37–2.41 (2H, m, H-6), 3.05–3.10 (2H, m, H-1), 3.28–3.35 (1H, m, H-8a), 3.77– 3.84 (1H, m, H-8b), 4.21–4.25 (1H, m, H-5a), 4.30–4.32 (2-H, q, CH₂CH₃), 4.86 (1H, d, J = 5.8 Hz, H-10a), 6.59 (1H, d, J = 8.8 Hz, H-30), 6.92 (1H, s, H-60), 7.20 (1H, d, H-40); ¹³C NMR (100 MHz, CDCl₃) δ 14.3 (CH₃), 22.4 (C-7), 28.4 (C-6), 32.7 (C-2), 45.3 (C-8), 61.9 (C-5a), 62.3 (CH₂), 62.5 (C-10a), 68.3(C-3), 109.2 (C-50), 121.1 (C-30), 123.6 (C-10), 128.8 (C-40), 133.2 (C-60), 145.2 (C-20), 162.8, 164.9, 168.3 (C=O). Anal. Calculated for C₁₈H₂₀BrN₃O₄S: C, 47.58; H, 4.44; Br, 17.59; N, 9.25; S, 7.06. Found: C, 47.51; H, 4.38; Br, 17.80; N, 9.07; S, 7.19.

8.7. General procedure for the synthesis of spiro-indol-2-one[3,30]-hexahydro-5,10H-pyrrolo[1,2-a][1,3]thiazolo[3,4-d]pyrazine-5,10-dione derivatives (29a,b–32a,b)

To a solution of the corresponding spirooxoindolethiazolidine carboxylic acids (**33a,b–36a,b**, 3 mmol) in 29/1 dichloromethane/DMF (300 mL), L-Pro-OMe (1.1 equiv), DIC (1.2 equiv), HOBT (1.2 equiv), and DIPEA (2.4 equiv) were successively added. Stirring was continued at room temperature for 6 h.

Afterward, the reaction mixture was diluted with dichloromethane (20 mL), and the resulting solution was washed successively with 10% NaHCO₃ (2 x 50 mL) and water (2 x 50 mL), dried over Na₂SO₄, and evaporated to dryness. Flash chromatography of the residues, using different eluent systems, yielded, in each case, the correspondent 40- (carbonyl-propyl-OMe) spirooxindole thiazolidine derivatives as diastereoisomeric mixture (**37a,b–40a,b**) which were not separated in this step.

A solution of derivatives **37a,b** or **37a,b** or **39a,b** or **40a,b** (1 mmol) was treated with 1/4: 2 N HClaq/MeOH solution (10 mL) and stirred at room temperature. After 2 h, the mixtures were concentrated and dissolved in DCM. 10% NaHCO₃ solution was added until pH 7 and the resulting mixtures were washed with water (3 x 25 mL), dried over Na₂SO₄, evaporated to dryness, and purified and separated by flash column chromatography using different eluent systems to yield the title compounds.

(3*R*,5'*a*S,10'*a*R) Spiro[[indol-2-one[3,30]-hexahydro-5,10Hpyrrolo[1,2-*a*][1,3]thiazolo[3,4-*d*]pyrazine]]-5,10-dione (29a)

FC in ethyl acetate. White solid (31%); mp 175–176 °C; α_{D}^{25} -76.3 (c 0.13 in CHCl₃); ¹H NMR (400 MHz, CDCl₃) δ 1.90–2.02 (3H, m, H-60 , H-7' a), 2.17–2.25 (1H, m, H-7' b), 3.51–3.58 (3H, m, H-80 , H-1' a), 3.78–3.83 (1H, m, H-1' b), 4.22 (1H, t, H-5' a); 5.01 (1H, dd, J = 6.0 and 10.0 Hz, H-10' a), 6.79 (1H, d, J = 8.0 Hz, H-7), 7.01 (1H, t, H-5), 7.18 (1H, d, J = 8.0 Hz, H-4), 7.24 (1H, t, H-6), 8.03 (1H, s, NH); ¹³C NMR (100 MHz, CDCl₃) δ 23.6 (C-60), 27.4 (C-70), 33.9 (C-10), 45.8 (C-80), 60.1 (C-50a), 66.3 (C-100a), 70.2 (C-3), 114.2 (C-7), 123.8 (C-4), 125.1 (C-5), 127.2 (C-3a), 131.5 (C-6), 140.7 (C-7a), 163.8, 164.6, 175.2 (C=O). Anal. Calculated for C₁₆H₁₅N₃O₃S: C, 58.34; H, 4.59; N, 12.76; S, 9.74. Found: C, 58.21; H, 4.48; N, 12.63; S, 9.89.

**(3*S*,5'*aS*,10'*aR*) Spiro[[indol-2-one[3,30]hexahydro-5,10Hpyrrolo
[1,2-*a*][1,3]thiazolo[3,4-*d*]pyrazine]]-5,10-dione (29b)**

FC in ethyl acetate. White solid (37%); mp 190–191 °C; α_D^{25} - 104.1 (c 0.11 in CHCl₃); ¹H NMR (400 MHz, CDCl₃) δ 1.92–2.06 (3H, m, H-60 , H-7' a), 2.23–2.30 (1H, m, H-7' b), 3.58–3.69 (3H, m, H-80 , H-1' a); 3.81 (1H, t, H-1' b); 4.27 (1H, t, H-5' a); 5.04 (1H, dd, J = 6.0 and 10.0 Hz, H-10' a), 6.81 (1H, d, J = 8.0 Hz, H-7), 7.02 (1H, t, H-5), 7.21 (1H, d, J = 8.0 Hz, H-4), 7.26 (1H, t, H-6), 7.83 (1H, s, NH); ¹³C NMR (100 MHz, CDCl₃) δ 23.2 (C-60), 28.0 (C-70), 33.5 (C-10), 45.6 (C-80), 60.8 (C-50a), 66.1 (C-100a), 70.4 (C-3), 114.5 (C-7), 123.3 (C-4), 124.2 (C-5), 126.8 (C-3a), 130.6 (C-6), 140.9 (C-7a), 163.7, 164.5, 175.9 (C=O). Anal. Calculated for C₁₆H₁₅N₃O₃S: C, 58.34; H, 4.59; N, 12.76; S, 9.74. Found: C, 58.20; H, 4.50; N, 12.59; S, 9.91.

**(3*R*,5'*aS*,10'*aR*) 5-Methyl spiro[[indol-2-one[3,30]-hexahydro-5,10H-
pyrrolo[1,2-*a*][1,3]thiazolo[3,4-*d*] pyrazine]]-5,10-dione (30a)**

FC in ethyl acetate. White solid (29%); mp 181–183 °C; α_D^{25} - 40.3 (c 0.12 in CHCl₃); ¹H NMR (400 MHz, CDCl₃) δ 1.93–1.97 (1H, m, H-6' a), 2.05–2.11 (2H, m, H-6' b, H-7' a), 2.22–2.26 (1H, m, H-7' b), 2.30 (3H, s, CH₃), 3.51–3.69 (3H, m, H-80 , H-1' a), 3.83 (1H, t, H-1' b), 4.28 (1H, t, H-5' a), 5.02 (1H, dd, J = 6.0 and 10.0 Hz, H-10' a), 6.74 (1H, d, J = 8.0 Hz, H-7), 7.38 (1H, d, H-6), 7.41 (1H, s, H-4), 7.92 (1H, s, NH); ¹³C NMR (100 MHz, CDCl₃) δ 23.2 (C-60), 24.6 (CH₃), 27.9 (C-70), 33.5 (C-10), 45.6 (C-80), 60.4 (C-50a), 66.1 (C-100a), 69.9 (C-3), 112.1 (C-7), 124.5 (C-3a), 127.5 (C-4), 133.0 (C-6), 134.7 (C-5), 138.2 (C-7a), 163.6, 164.9, 175.4 (C=O). Anal. Calculated for C₁₇H₁₇N₃O₃S: C, 59.46; H, 4.99; N, 12.24; S, 9.34. Found: C, 59.49; H, 5.12; N, 12.09; S, 9.41.

(3S,5'aS,10'aR) 5-Methyl spiro[[indol-2-one[3,30]-hexahydro-5,10H-pyrrolo[1,2-a][1,3]thiazolo[3,4-d] pyrazine]]-5,10-dione (30b)

FC in ethyl acetate. White solid (35%); mp 190–191 °C; α_D^{25} - 130.8 (c 0.2 in CHCl₃); ¹H NMR (400 MHz, CDCl₃) δ 1.95–2.03(3H, m, H-6' a, H-70), 2.24–2.30 (1H, m, H-6' b), 2.33 (3H, s, CH₃), 3.57–3.64 (3H, m, H-80, H-1' a); 3.82 (1H, t, H-1' b); 4.35 (1H, t, H-5' a); 5.04 (1H, dd, J = 5.6 and 10.8 Hz, H-100a), 6.74 (1H, d, J = 8.0 Hz, H-7), 7.39 (1H, d, J = 8.0 Hz, H-6), 7.42 (1H, s, H-4), 8.59 (1H, s, NH); ¹³C NMR (100 MHz, CDCl₃) δ 23.5 (C-60), 24.8 (CH₃), 28.0 (C-70), 32.5 (C-10), 45.5 (C-80), 61.0 (C-5' a), 65.8 (C-10' a), 71.1 (C-3), 112.3 (C-7), 122.7 (C-3a), 125.8 (C-4), 132.3 (C-5), 132.9 (C-6), 136.2 (C-7a), 164.2, 166.5, 174.3 (C=O). Anal. Calculated for C₁₇H₁₇N₃O₃S: C, 59.46; H, 4.99; N, 12.24; S, 9.34. Found C, 59.51; H, 5.08; N, 12.17; S, 9.52.

(3R,50aS,100aR) 5-Bromo Spiro[[indol-2-one[3,30]-hexahydro-5,10H-pyrrolo[1,2-a][1,3] thiazolo[3,4-d] pyrazine]]-5,10-dione (31a)

FC in ethyl acetate. White solid (28%); mp 178–179 °C; α_D^{25} -68.0 (c 0.12 in CHCl₃); ¹H NMR (400 MHz, CDCl₃) δ 1.89–1.96 (1H, m, H-6' a), 2.04–2.09 (2H, m, H-6' b, H-7' a), 2.19–2.23 (1H, m, H-7' b), 3.49–3.65 (3H, m, H-80, H-1' a), 3.82 (1H, t, H-1' b); 4.26 (1H, t, H-5' a), 5.00 (1H, dd, J = 6.0 and 10.0 Hz, H-100a), 6.73 (1H, d, J = 8.0 Hz, H-7), 7.38 (1H, d, H-6), 7.41 (1H, s, H-4) 7.75 (1H, s, NH); ¹H NMR (400 MHz, CD₃OD) δ 1.93–2.03 (3H, m, H-6' a, H-70), 2.16–2.19 (1H, m, H-6' b), 3.54–3.64 (2H, m, H-80), 3.65–3.68 (1H, m, H-1' a), 3.65 (1H, t, J 10.0 Hz, H-1' b), 4.43 (1H, m, H-5' a), 5.27 (1H, dd, J = 6.4 and 9.6 Hz, H-10' a), 6.81 (1H, d, J = 8.0 Hz, H-7), 7.42 (1H, d, H-6), 7.55 (1H, s, H-4); ¹³C NMR (100 MHz, CDCl₃) δ 23.6 (C-60), 27.8 (C-70), 33.9 (C-10), 46.5 (C-80), 61.9 (C-5'a), 66.0(C-10'a),

71.1 (C-3), 107.8 (C-5), 112.1 (C-7), 123.4 (C-6), 128.8 (C-3a), 130.7 (C-4), 138.9 (C-7a), 167.1, 169.2, 174.8 (C=O). Anal. Calculated for C₁₆H₁₄BrN₃O₃S: C, 47.07; H, 3.46; Br, 13.57; N, 10.29; S, 7.85. Found C, 46.91; H, 3.48; Br, 13.71; N, 10.40; S, 7.97.

(3S,5'aS,10'aR) 5-Bromo spiro[[indol-2-one[3,30]-hexahydro-5,10H-pyrrolo[1,2-a][1,3]thiazolo[3,4-d] pyrazine]]-5,10-dione (31b)

FC in ethyl acetate. White solid (33%), mp 187–189 °C; α_D^{25} -128.6 (c 0.14 in CHCl₃); ¹H NMR (400 MHz, CDCl₃) δ 1.94–2.05 (3H, m, H-6' a, H-70), 2.25–2.30 (1H, m, H-6' b), 3.60–3.67 (3H, m, H-80, H-1' a), 3.82 (1H, t, H-1' b), 4.32 (1H, t, H-5' a), 5.06 (1H, dd, J = 5.6 and 10.8 Hz, H-10' a), 6.81 (1H, d, J = 8.0 Hz, H-7), 7.39 (1H, d, H-6), 7.42 (1H, s, H-4), 8.33 (s, NH); ¹H NMR (400 MHz, CD₃OD) δ 1.88–2.02 (3H, m, H-6a', H-7'), 2.20–2.21 (1H, m, H-6' b), 3.54–3.64 (2H, m, H-8'), 3.65–3.68 (1H, m, H-1' a), 3.84 (1H, t, J = 10.4 Hz, H-1' b), 4.43 (1H, m, H-5' a); 5.14 (1H, dd, J = 6.8 and 9.6 Hz, H-10'a), 6.81 (1H, d, J = 8.0 Hz, H-7), 7.38 (1H, d, H-6); 7.42 (1H, s, H-4); ¹³C NMR (100 MHz, CDCl₃) δ 23.7 (C-60), 28.2 (C-70), 32.4 (C-10), 45.8 (C-80), 61.4 (C-50a), 65.9 (C-100a), 70.8 (C-3), 109.9 (C-5), 111.6 (C-7), 130.4 (C-6), 136.5 (C-4), 139.8 (C-7a), 164.6, 166.0, 174.6 (C=O). Anal. Calculated for C₁₆H₁₄BrN₃O₃S: C, 47.07; H, 3.46; Br, 13.57; N, 10.29; S, 7.85. Found C, 46.96; H, 3.39; Br, 13.68; N, 10.42; S, 7.96.

(3R and 3S,50aS,100aR) 1-Methyl spiro[[indol-2-one[3,30]-hexahydro-5,10H-pyrrolo[1,2-a][1,3]thiazolo[3,4-d]pyrazine]]-5,10-dione (32a,b)

FC in ethyl acetate. White solid (72%) ¹H NMR (400 MHz, CDCl₃) δ 1.83–2.04 (3H, m, H-60, H-7' a), 2.11–2.23 (1H, m, H-7' b), 3.21 (3H, s, CH₃); 3.42–3.61 (3H, m, H-80, H-1' a), 3.78 (1H, t, H-1' b), 4.19 (1H, m, H-5' a), 4.24 (1H, m, H-5' a); 5.00 (1H, m, H-10' a), 5.03 (1H, m, H-10' a),

6.81 (1H, d, J= 8.0 Hz, H-7), 7.02 (1H, t, H-6), 7.22 (1H, d, J = 8.0 Hz, H-4), 7.33 (1H, t, H-5). ¹³C NMR (100 MHz, CDCl₃) δ 23.6, 24.9 (C-6'), 26.5 (C-7'), 29.1 and 29.8 (CH₃), 39.0 and 42.1 (C-1'), 46.9 and 52.9 (C-8'), 59.1 (C-5' a), 62.9 and 66.7 (C-10' a), 73.2 (C-3), 108.7, 109.0 (C-7), 123.5 (C-4), 124.3 (C-5), 129.2 and 130.7 (C-6), 130.1 (C-5), 142.1 (C-7a), 168.1, 169.2, 172.4, 176.7 (C=O). Anal. Calculated for C₁₇H₁₇N₃O₃S: C, 59.46; H, 4.99; N, 12.24; S, 9.34. Found: C, 59.63; H, 4.89; N, 12.59; S, 9.29.

8.8. General Procedure for the Synthesis of the (3R,7aR)-6-(Alkyl or benzylsubstituted)-spiro[imidazo[1,5-c]thiazole-3,30-indoline]-20,5,7(6H,7aH)-trione Derivatives (42a-e/45a-e).

Triphosgene (0.3 mmol) and TEA (0.9 mmol) were added to a solution of (20R,4'R)- and (20S,4'R)-ethyl 2-oxospiro[indoline-3,20-thiazolidine]-4'-carboxylate derivatives (5-8, 200 mg, 0.7 mmol) in dry THF (15 mL). After the mixture was stirred at room temperature for 10 min, a solution in dry THF of corresponding amines (benzylamine, 4-methylbenzylamine, 4-chlorobenzylamine, 3,4,5-trimethoxybenzylamine, or 4,4 dimethyl cyclohexylamine, **a-e**) (0.75 mmol) was added. The reaction mixture was then stirred at room temperature for 3 h. Solvent was evaporated, and the residue was dissolved in dichloromethane. The organic solution was washed with water (3 x 100 mL), dried over Na₂SO₄, and evaporated in vacuo. The residues were dissolved in MeOH and TEA until pH 8.0 was obtained, and the mixture was heated to reflux temperature for 2 h. The mixture was then cooled to ambient temperature, and solvent was removed in vacuo. The residue was dissolved in dichloromethane and washed with water (3 x 100 mL). Flash chromatography on silica gel, using ethyl acetate/n-hexane in 3/2 ratio as eluent, yielded the correspondent final derivatives. The achieved compounds were crystallized with MeOH to give white solids.

(3*R*,7*aR*)-6-Benzyl-1*H*-spiro[imidazo[1,5-*c*]thiazole-3,3'-indoline]-2',5,7(6*H*,7*aH*)-trione (42a).

Yield 44%, mp 181-182 °C, $[\alpha]_D^{25}$ -6.9° (*c* 0.11, MeOH). ¹H NMR (400 MHz, CDCl₃) δ 3.35 (dd, 1H, *J*=5.6 and 11.6Hz, Ha-1); 3.72 (t, 1H, Hb-1); 4.56 (d, 1H, *J*=14.8 Hz, CH₂); 4.71 (d, 1H, CH₂); 5.00 (dd, 1H, *J*=5.6 and 11.2 Hz, H-7a); 6.83 (d, 1H, *J*=7.6Hz, H-7'); 7.07 (t, 1H, H-6'); 7.26-7.34 (m, 6H, H-5' and aryl); 7.39 (d, 1H, H-4'); 7.81 (s, 1H, NH). ¹³C NMR (100 MHz, CDCl₃) δ 32.4 (C-1), 43.0 (CH₂), 68.9 (C-7a), 70.1 (C-3), 110.3, 123.4, 125.3, 125.8, 129.1, 130.2, 131.5, 133.4, 135.4, 138.2 (aryl), 156.3, 169.9, 176.0 (C=O). ESIMS *m/z* calculated for C₁₉H₁₅N₃O₃S, 365.08; found, 365.13.

(3*R*,7*aR*)-6-(4-Methylbenzyl)-1*H*-spiro[imidazo[1,5-*c*]thiazole-3,3'-indoline]-2',5,7(6*H*,7*aH*)-trione (42b).

1.1.1. Yield 48%, mp 212-213 °C, $[\alpha]_D^{25}$ -7.1° (*c* 0.1, MeOH). ¹H NMR (400 MHz, CDCl₃) δ 2.29 (s, 3H, CH₃); 3.33 (dd, 1H, *J* = 5.6 and 11.2 Hz, Ha-1); 3.71 (t, 1H, Hb-1); 4.51 (d, 1H, *J* = 14.4 Hz, CH₂); 4.67 (d, 1H, CH₂); 4.97 (dd, 1H, *J*=5.6 and 10.8 Hz, H-7a); 6.81 (d, 1H, *J*=7.6 Hz, H-7'); 7.04-7.11 (m, 6H, H-6' and aryl); 7.28 (t, 1H, H-5'); 7.37 (d, 1H, *J* = 7.6 Hz, H-4'); 8.06 (s, 1H, NH). ¹³C NMR (100 MHz, CDCl₃) δ 21.2 (CH₃), 32.5 (C-1), 43.1 (CH₂), 68.9 (C-7a), 70.2 (C-3), 110.9, 123.6, 125.3, 125.9, 128.1, 128.4, 128.9, 131.7, 133.4, 135.2, 138.0 (aryl), 156.4, 169.6, 176.2 (C=O). ESIMS *m/z* calculated for C₂₀H₁₇N₃O₃S, 379.10; found, 379.18.

(3*R*,7*aR*)-6-(4-Chlorobenzyl)-1*H*-spiro[imidazo[1,5-*c*]thiazole-3,3'-indoline]-2',5,7(6*H*,7*aH*)-trione (42c).

Yield 48%, mp 205-206 °C, $[\alpha]_D^{25}$ -8.8° (*c* 0.12, MeOH). ¹H NMR (400 MHz, CDCl₃) δ 3.35 (dd, 1H, *J*=5.6 and 11.2 Hz, Ha-1); 3.71 (t, 1H, Hb-1); 4.53 (d, 1H, *J*=15.2 Hz, CH₂); 4.67 (d, 1H, CH₂); 5.00 (dd, 1H, *J* = 5.6 and 10.8 Hz, H-7a); 6.78 (d, 1H, *J* = 8.0 Hz, H-70); 7.06 (t, 1H, H-6'); 7.25-7.30 (m, 5H, H-5' and aryl); 7.39 (d, 1H, H-4');

8.43 (s, 1H, NH). ¹³C NMR (100 MHz, CDCl₃) δ 32.4 (C-1), 42.5 (CH₂), 68.9 (C-7a), 70.1 (C-3), 111.2, 123.7, 125.3, 125.4, 129.2, 130.1, 131.2, 133.8, 134.2, 140.8 (aryl), 156.4, 169.9, 176.1 (C=O). ESIMS m/z calculated for C₁₉H₁₄ClN₃O₃S, 399.04; found, 399.13.

(3*R*,7*aR*)-6-(3,4,5-Trimethoxybenzyl)-1*H*-spiro[imidazo[1,5-*c*]-thiazole-3,3'-indoline]-2',5,7(6*H*,7*aH*)-trione (42*d*).

Yield 47%, mp 219-220 °C, [α]²⁵_D -8.2° (c 0.12, MeOH). ¹H NMR (400 MHz, CDCl₃) δ 3.34 (dd, 1H, J₀ =5.6 and 11.6 Hz, Ha-1); 3.66 (t, 1H, Hb-1); 3.72 (s, 3H, OCH₃); 3.81 (s, 6H, OCH₃); 4.46 (d, 1H, J=14.4 Hz, CH₂); 4.64 (d, 1H, CH₂); 5.00 (dd, 1H, J=5.2 and 10.6 Hz, H-7a); 6.56 (s, 2H, aryl); 6.83 (d, 1H, J =7.2 Hz, H-7o); 7.09 (t, 1H, H-6'); 7.25 (t, 1H, H-5'); 7.38 (d, 1H, H-4'); 8.22 (s, 1H, NH). ¹³C NMR (100 MHz, CDCl₃) δ 32.5 (C-1), 43.3 (CH₂), 56.4 (OCH₃), 68.9 (C-7a), 70.6 (C-3), 105.4, 110.8, 125.4, 126.0, 130.9, 131.2, 133.5, 137.2, 138.4, 154.9 (aryl), 156.3, 169.4, 175.7 (C=O). ESIMS m/z calculated for C₂₂H₂₁N₃O₆S, 455.12; found, 455.25.

(3*R*,7*aR*)-6-(4,4-Dimethylcyclohexyl)-1*H*-spiro[imidazo[1,5-*c*]-thiazole-3,3'-indoline]-2',5,7(6*H*,7*aH*)-trione (42*e*).

Yield 52%, mp 180-181 °C, [α]²⁵_D -8.1° (c 0.1, MeOH). ¹H NMR (400 MHz, CDCl₃) δ 0.89 (s, 3H, CH₃); 0.93 (s, 3H, CH₃); 1.19-1.25 (m, 2H, CH₂); 1.41-1.49 (m, 4H, CH₂); 2.21-2.33 (m, 2H, CH₂); 3.32 (dd, 1H, J=5.2 and 10.8 Hz, Ha-1); 3.71 (t, 1H, Hb-1); 3.78-3.82 (m, 1H, CH); 4.93 (dd, 1H, J = 5.6 and 10.8 Hz, H-7a); 6.85 (d, 1H, J = 7.6 Hz, H-7'); 7.08 (t, 1H, H-6'); 7.27 (t, 1H, H-5'); 7.41 (d, 1H, H-4'); 8.06 (s, 1H, NH). ¹³C NMR (100 MHz, CDCl₃) δ 24.8 (CH₂); 25.4 (CH₂); 26.7 (CH₃); 29.9 (CH₃); 32.3 (C-1), 38.7 (CH), 52.8 (C), 68.7 (C-7a), 70.6 (C-3), 109.6, 123.6, 125.0, 125.3, 131.1, 143.6 (aryl), 156.6, 170.5, 174.6 (C=O). ESIMS m/z calculated for C₂₀H₂₃N₃O₃S, 385.15; found, 385.21.

(3*R*,7*aR*)-6-Benzyl-5'-methyl-1*H*-spiro[imidazo[1,5-*c*]thiazole-3,3'-indoline]-2',5,7(6*H*,7*aH*)-trione (43a).

Yield 45%, mp 193-194 °C, $[\alpha]_D^{25}$ -12.4° (c 0.11, MeOH). ¹H NMR (400 MHz, CDCl₃) δ 2.30 (s, 3H, CH₃); 3.33 (dd, 1H, J=5.2 and 11.2 Hz, Ha-1); 3.73 (t, 1H, Hb-1); 4.56 (d, 1H, J=14.8 Hz, CH₂); 4.71 (d, 1H, CH₂); 5.00 (dd, 1H, J = 5.6 and 10.8 Hz, H-7a); 6.70 (d, 1H, J=8.0 Hz, H-7'); 7.05 (d, 1H, H-6'); 7.23 (s, 1H, H-4'); 7.26-7.36 (m, 5H, aryl); 8.11 (s, 1H, NH). ¹³CNMR (100 MHz, CDCl₃) δ 21.2 (CH₃); 32.4 (C-1), 43.2 (CH₂), 68.9 (C-7a), 70.3 (C-3), 110.9, 125.3, 126.0, 128.3, 128.7, 128.9, 131.6, 133.4, 135.4, 138.2 (aryl), 156.4, 169.9, 176.0 (C=O). ESIMS m/z calculated for C₂₀H₁₇N₃O₃S, 379.10; found, 379.23.

(3*R*,7*aR*)-5'-Methyl-6-(4-methylbenzyl)-1*H*-spiro[imidazo-[1,5-*c*]thiazole-3,3'-indoline]-2',5,7(6*H*,7*aH*)-trione (43b).

Yield 45%, mp 234-235 °C, $[\alpha]_D^{25}$ -12.5° (c 0.11, MeOH). ¹H NMR (400 MHz, CDCl₃) δ 2.30 (s, 6H, CH₃); 3.31 (dd, 1H, J=5.6 and 11.6 Hz, Ha-1); 3.71 (t, 1H, Hb-1); 4.51 (d, 1H, J= 14.8 Hz, CH₂); 4.67 (d, 1H, CH₂); 4.97 (dd, 1H, J=5.2 and 10.8 Hz, H-7a); 6.72 (d, 1H, J = 8.0 Hz, H-7'); 7.07-7.26 (m, 6H, H-4', H-6', and aryl); 7.72 (s, 1H, NH). ¹³CNMR (100 MHz, CDCl₃) δ 21.2 (CH₃); 21.3 (CH₃); 32.5 (C-1), 42.9 (CH₂), 68.9 (C-7a), 70.2 (C-3), 110.7, 125.3, 126.1, 128.7, 129.5, 131.5, 133.6, 135.8, 138.0 (aryl), 156.5, 169.6, 176.1 (C=O). ESIMS m/z calculated for C₂₁H₁₉N₃O₃S, 393.11; found, 393.24.

(3*R*,7*aR*)-6-(4-Chlorobenzyl)-5'-methyl-1*H*-spiro[imidazo-[1,5-*c*]thiazole-3,3'-indoline]-2',5,7(6*H*,7*aH*)-trione (43c).

Yield 39%, mp 208-209 °C, $[\alpha]_D^{25}$ -14.5° (c 0.13, MeOH). ¹H NMR (400 MHz, CDCl₃) δ 2.29 (s, 3H, CH₃); 3.30 (dd, 1H, J = 5.6 and 11.6 Hz, Ha-1); 3.69 (t, 1H, Hb-1); 4.50 (d, 1H, J = 15.2 Hz, CH₂); 4.63 (d, 1H, CH₂); 4.99

(dd, 1H, J = 4.8 and 10.4 Hz, H-7a); 6.72 (d, 1H, J=8.0 Hz, H-7'); 7.05 (d, 1H, H-6'); 7.20-7.26 (m, 5H, H-4' and aryl); 8.54 (s, 1H, NH). ¹³C NMR (100 MHz, CDCl₃) δ 21.2 (CH₃); 32.3 (C-1), 42.4 (CH₂), 68.9 (C-7a), 70.3 (C-3), 110.9, 125.3, 126.0, 129.1, 130.1, 131.6, 133.3, 133.9, 134.2, 138.4 (aryl), 156.3, 169.9, 176.1 (C=O). ESIMS m/z calculated for C₂₀H₁₆ClN₃O₃S, 413.06; found, 413.17.

(3*R*,7*aR*)-5'-Methyl-6-(3,4,5-trimethoxybenzyl)-1*H*-spiro-[imidazo[1,5-*c*]thiazole-3,3'-indoline]-2',5,7(6*H*,7*aH*)-trione (43d).

Yield 47%, mp 241-242 °C, [α]_D²⁵ -13.9° (c 0.11, MeOH). ¹H NMR (400 MHz, CDCl₃) δ 2.31 (s, 3H, CH₃); 3.28 (dd, 1H, J = 5.6 and 11.6 Hz, Ha-1); 3.64 (t, 1H, Hb-1); 3.73 (s 3H, OCH₃); 3.76 (s 6H, OCH₃); 4.39 (d, 1H, J=14.8Hz, CH₂); 4.59 (d, 1H, CH₂); 4.94 (dd, 1H, J = 5.6 and 10.8 Hz, H-7a); 6.50 (s, 2H, aryl); 6.45 (d, 1H, J=8.0Hz, H-7'); 6.99 (d, 1H, H-6'); 7.16 (s, 1H, H-4'); 8.04 (s, 1H, NH). ¹³C NMR (100 MHz, CDCl₃) δ 21.2 (CH₃); 32.5 (C-1), 43.4 (CH₂), 56.4 (OCH₃); 68.9 (C-7a), 70.6 (C-3), 105.5, 110.9, 125.3, 126.0, 131.1, 131.6, 133.4, 137.9, 138.2, 153.6 (aryl), 156.4, 169.9, 175.8 (C=O). ESIMS m/z calculated for C₂₃H₂₃N₃O₆S, 469.13; found, 469.32.

(3*R*,7*aR*)-6-(4,4-Dimethylcyclohexyl)-5'-methyl-1*H*-spiro-[imidazo[1,5-*c*]thiazole-3,3'-indoline]-2',5,7(6*H*,7*aH*)-trione (43e).

Yield 54%, mp 183-184 °C, [α]_D²⁵ -13.6° (c 0.12, MeOH). ¹H NMR (400 MHz, CDCl₃) δ 0.89 (s, 3H, CH₃); 0.93 (s, 3H, CH₃); 1.18-1.30 (m, 2H, CH₂); 1.41-1.48 (m, 4H, CH₂); 2.21-2.29 (m, 2H, CH₂); 2.31 (s, 3H, CH₃); 3.32 (dd, 1H, J = 5.2 and 11.2 Hz, Ha-1); 3.71 (t, 1H, Hb-1); 3.73-3.82 (m, 1H, CH); 4.91 (dd, 1H, J=5.6 and 10.8 Hz, H-7a); 6.75 (d, 1H, J= 8.0 Hz, H-7'); 7.08 (d, 1H, H-6'); 7.24 (s, 1H, H-4'); 7.90 (s, 1H, NH). ¹³C NMR (100 MHz, CDCl₃) δ 22.4 (CH₃); 24.1 (CH₂); 24.9 (CH₂); 25.0 (CH₃); 29.7 (CH₃), 32.5 (C-1), 38.6 (CH), 52.5 (C), 68.4 (C-7a), 70.8 (C-3), 109.2, 125.0, 125.3, 131.1, 143.6

(aryl), 156.6, 170.5, 174.6 (C=O). ESIMS m/z calculated for C₂₁H₂₅N₃O₃S, 399.16; found, 399.21.

(3*R*,7*aR*)-6-(Benzyl)-5'-bromo-1*H*-spiro[imidazo[1,5-*c*]thiazole-3,3'-indoline]-2',5,7(6*H*,7*aH*)-trione (44a).

Yield 40%, mp 209-210 °C, [α]_D²⁵ -11.8° (c 0.1, MeOH). ¹H NMR (400 MHz, CDCl₃) δ 3.35 (dd, 1H, J=5.3 and 11.3 Hz, Ha-1); 3.72 (t, 1H, Hb-1); 4.56 (d, 1H, J=14.8 Hz, CH₂); 4.71 (d, 1H, CH₂); 5.00 (dd, 1H, J = 5.6 and 11.1 Hz, H-7a); 6.77 (d, 1H, J = 7.2 Hz, H-7'); 7.26-7.32 (m, 5H, aryl); 7.43 (d, 1H, H-6'); 7.54 (s, 1H, H-4'); 8.01 (s, 1H, NH). ¹³C NMR (100 MHz, CDCl₃) δ 32.3 (C-1), 43.9 (CH₂), 69.1 (C-7a), 72.2 (C-3), 113.3, 123.4, 125.8, 128.3, 130.2, 131.5, 133.6, 136.2, 139.1 (aryl), 156.1, 169.8, 175.8 (C=O). ESIMS m/z calculated for C₁₉H₁₄BrN₃O₃S, 442.99; found, 443.16.

(3*R*,7*aR*)-5'-Bromo-6-(4-methylbenzyl)-1*H*-spiro-[imidazo[1,5-*c*]thiazole-3,3'-indoline]-2',5,7(6*H*,7*aH*)-trione (44b).

Yield 39%, mp 233-234 °C, [α]_D²⁵ -10.3° (c 0.1, MeOH). ¹H NMR (400 MHz, CDCl₃) δ 2.29 (s, 3H, CH₃); 3.33 (dd, 1H, J=5.3 and 11.0 Hz, Ha-1); 3.71 (t, 1H, Hb-1); 4.51 (d, 1H, J= 14.5 Hz, CH₂); 4.67 (d, 1H, CH₂); 4.97 (dd, 1H, J = 5.6 and 10.8 Hz, H-7a); 6.79 (d, 1H, J=7.5Hz, H-7'); 7.04-7.11 (m, 4H, aryl); 7.41 (d, 1H, H-6'); 7.51 (s, 1H, H-4'); 8.00 (s, 1H, NH). ¹³C NMR (100 MHz, CDCl₃) δ 21.5 (CH₃), 32.4 (C-1), 43.0 (CH₂), 68.9 (C-7a), 71.9 (C-3), 115.2, 125.3, 128.1, 129.4, 129.9, 132.9, 133.7, 136.2, 139.0 (aryl), 156.2, 169.6, 176.2 (C=O). ESIMS m/z calculated for C₂₀H₁₆BrN₃O₃S, 457.01; found, 457.11.

(3*R*,7*aR*)-5'-Bromo-6-(4-chlorobenzyl)-1H-spiro[imidazo[1,5-*c*]-thiazole-3,3'-indoline]-2',5,7(6*H*,7*aH*)-trione (44c).

Yield 38%, mp 202-203 °C, $[\alpha]_D^{25}$ -11.9° (c 0.11, MeOH). ¹H NMR (400 MHz, CDCl₃) δ 3.30 (dd, 1H, J = 5.5 and 11.1 Hz, Ha-1); 3.69 (t, 1H, Hb-1); 4.50 (d, 1H, J = 15.2 Hz, CH₂); 4.63 (d, 1H, CH₂); 4.98 (dd, 1H, J=4.8 and 10.4 Hz, H-7a); 6.75 (d, 1H, J=7.1 Hz, H-7'); 7.20-7.26 (m, 4H, aryl); 7.43 (d, 1H, H-6'); 7.55 (s, 1H, H-4'); 8.11 (s, 1H, NH). ¹³C NMR (100 MHz, CDCl₃) δ 32.3 (C-1), 42.4 (CH₂), 69.0 (C-7a), 72.0 (C-3), 115.2, 125.3, 126.0, 129.1, 130.1, 132.1, 133.9, 134.2, 140.7 (aryl), 156.4, 168.9, 176.0 (C=O). ESIMS m/z calculated for C₁₉H₁₃BrClN₃O₃S, 476.95; found, 476.89

(3*R*,7*aR*)-5'-Bromo-6-(3,4,5-trimethoxybenzyl)-1H-spiro-[imidazo[1,5-*c*]thiazole-3,3'-indoline]-2',5,7(6*H*,7*aH*)-trione (44d).

Yield 40%, mp 255-256 °C, $[\alpha]_D^{25}$ -12.3° (c 0.13, MeOH). ¹H NMR (400 MHz, CDCl₃) δ 3.38 (dd, 1H, J = 5.6 and 11.6 Hz, Ha-1); 3.72 (t, 1H, Hb-1); 3.79 (s 3H, OCH₃); 3.82 (s, 6H, OCH₃); 4.47 (d, 1H, J = 14.4 Hz, CH₂); 4.64 (d, 1H, CH₂); 5.02 (dd, 1H, J=5.2 and 10.4 Hz, H-7a); 6.51 (s, 2H, aryl); 6.77 (d, 1H, J = 7.2 Hz, H-7'); 7.45 (d, 1H, H-6'); 7.56 (s, 1H, H-4'); 8.02 (s, 1H, NH). ¹³C NMR (100 MHz, CDCl₃) δ 32.5 (C-1), 43.3 (CH₂), 56.2 (OCH₃); 69.1 (C-7a), 71.9 (C-3), 105.3, 115.9, 125.6, 131.1, 131.6, 133.4, 137.9, 139.1, 153.6 (aryl), 156.4, 169.9, 175.8 (C=O). ESIMS m/z calculated for C₂₂H₂₀BrN₃O₆S, 533.03; found, 533.21.

(3*R*,7*aR*)-5'-Bromo-6-(4,4-dimethylcyclohexyl)-1H-spiro-[imidazo[1,5-*c*]thiazole-3,3'-indoline]-2',5,7(6*H*,7*aH*)-trione (44e).

Yield 42%, mp 200-201 °C, $[\alpha]_D^{25}$ -13.1° (c 0.12, MeOH). ¹H NMR (400 MHz, CDCl₃) δ 0.88 (s, 3H, CH₃); 0.92 (s, 3H, CH₃); 1.18-1.26 (m, 2H, CH₂); 1.41-1.49 (m, 4H, CH₂); 2.23-2.33 (m, 2H, CH₂); 3.32 (dd, 1H, J = 5.3 and 11.0 Hz, Ha-1); 3.71 (t, 1H, Hb-1); 3.78-3.82 (m, 1H, CH); 4.93 (dd, 1H,

J=5.3 and 10.8 Hz, H-7a); 6.73 (d, 1H, J=7.01 Hz, H-7'); 7.46 (d, 1H, H-6'); 7.56 (s, 1H, H-4'); 8.00 (s, 1H, NH). ¹³C NMR (100 MHz, CDCl₃) δ 24.9 (CH₂), 25.2 (CH₂), 27.9 (CH₃), 29.3 (CH₃), 32.4 (C-1), 38.9 (CH), 52.7 (C), 69.0 (C-7a), 71.6 (C-3), 116.1, 125.3, 131.1, 133.9, 140.1 (aryl), 156.6, 170.5, 174.6 (C=O). ESIMS m/z calculated for C₂₀H₂₂BrN₃O₃S, 463.06; found, 463.19.

(3*R*,7*aR*)-6-Benzyl-10-methyl-1*H*-spiro[imidazo[1,5-*c*]thiazole-3,3'-indoline]-2',5,7(6*H*,7*aH*)-trione (45a).

Yield 46%, mp 177-178 °C, [α]_D²⁵ -16.2° (c 0.11, MeOH). ¹H NMR (400 MHz, CDCl₃) δ 3.27 (s, 3H, CH₃); 3.35 (dd, 1H, J=5.2 and 11.2 Hz, Ha-1); 3.76 (t, 1H, Hb-1); 4.54 (d, 1H, J=14.4 Hz, CH₂); 4.71 (d, 1H, CH₂); 4.98 (dd, 1H, J=5.6 and 11.2 Hz, H-7a); 6.86 (d, 1H, J=8.0 Hz, H-7'); 7.10 (t, 1H, H-6'); 7.26-7.38 (m, 6H, H-5' and aryl); 7.41 (d, 1H, H-4'). ¹³C NMR (100 MHz, CDCl₃) δ 26.8 (CH₃), 32.4 (C-1), 42.9 (CH₂), 68.7 (C-7a), 70.3 (C-3), 110.0, 123.6, 125.4, 128.7, 129.9, 131.3, 132.6, 138.1, 143.8 (aryl), 156.2, 169.8, 174.5 (C=O). ESIMS m/z calculated for C₂₀H₁₇N₃O₃S, 379.10; found, 379.19.

(3*R*,7*aR*)-10-Methyl-6-(4-methylbenzyl)-1*H*-spiro[imidazo-[1,5-*c*]thiazole-3,3'-indoline]-2',5,7(6*H*,7*aH*)-trione (45b).

Yield 48%, mp 185-186 °C, [α]_D²⁵ -15.3° (c 0.1, MeOH). ¹H NMR (400 MHz, CDCl₃) δ 2.29 (s, 3H, CH₃); 3.28 (s, 3H, CH₃); 3.33 (dd, 1H, J=5.2 and 10.8 Hz, Ha-1); 3.74 (t, 1H, Hb-1); 4.48 (d, 1H, J=14.4 Hz, CH₂); 4.67 (d, 1H, CH₂); 4.96 (dd, 1H, J=5.6 and 11.2 Hz, H-7a); 6.85 (d, 1H, J = 7.6 Hz, H-7'); 7.09-7.26 (m, 5H, H-6' and aryl); 7.33-7.41 (m, 2H, H-5' and H-4'). ¹³C NMR (100 MHz, CDCl₃) δ 21.8 (CH₃), 26.9 (CH₃), 32.5 (C-1), 42.8 (CH₂), 68.9 (C-7a), 70.2 (C-3), 109.2, 123.7, 125.1, 128.8, 129.6, 131.2, 132.5, 138.0, 143.6 (aryl), 156.2, 169.8, 174.5 (C=O). ESIMS m/z calculated for C₂₁H₁₉N₃O₃S, 393.11; found, 393.25.

(3*R*,7*aR*)-6-(4-Chlorobenzyl)-10-methyl-1*H*-spiro[imidazo-[1,5-*c*]thiazole-3,3'-indoline]-2',5,7(6*H*,7*aH*)-trione (45c).

Yield 41%, mp 182-183 °C, $[\alpha]_{\text{D}}^{25}$ -17.1° (c 0.13, MeOH). ¹H NMR (400 MHz, CDCl₃) δ 3.30 (s, 3H, CH₃); 3.33 (dd, 1H, J=5.2 and 10.8 Hz, Ha-1); 3.74 (t, 1H, Hb-1); 4.49 (d, 1H, J= 14.4 Hz, CH₂); 4.67 (d, 1H, CH₂); 4.96 (dd, 1H, J=5.6 and 11.2 Hz, H-7a); 6.85 (d, 1H, J = 8.0 Hz, H-7'); 7.09-7.26 (m, 5H, H-6' and aryl); 7.33-7.41 (m, 2H, H-5' and H-4'); ¹³C NMR (100 MHz, CDCl₃) δ 26.4 (CH₃); 32.7 (C-1), 42.8 (CH₂), 68.9 (C-7a), 70.4 (C-3), 110.9, 125.6, 126.2, 129.3, 130.4, 131.7, 133.5, 133.8, 134.1, 138.2 (aryl), 156.3, 169.9, 176.3 (C=O). ESIMS m/z calculated for C₂₀H₁₆ClN₃O₃S, 413.06; found, 413.12.

(3*R*,7*aR*)-10-Methyl-6-(3,4,5-trimethoxybenzyl)-1*H*-spiro-[imidazo[1,5-*c*]thiazole-3,3'-indoline]-2',5,7(6*H*,7*aH*)-trione (45d).

Yield 53%, mp 197-198 °C, $[\alpha]_{\text{D}}^{25}$ -16.1° (c 0.1, MeOH). ¹H NMR (400 MHz, CDCl₃) δ 3.18 (s, 3H, CH₃,); 3.33 (dd, 1H, J = 5.6 and 11.6 Hz, Ha-1); 3.64 (t, 1H, Hb-1); 3.71 (s 3H, OCH₃,); 3.79 (s, 6H, OCH₃,); 4.48 (d, 1H, J = 14.4 Hz, CH₂); 4.62 (d, 1H, CH₂); 5.04 (dd, 1H, J=5.2 and 10.4Hz, H-7a); 6.48 (s 2H, benzyl); 6.81 (d, 1H, J=7.2 Hz, H-7'); 7.12 (t, 1H, H-6'); 7.26 (t, 1H, H-5'); 7.35 (d, 1H, H-4'). ¹³C NMR (100MHz,CDCl₃) δ, 26.2 (CH₃); 32.6 (C-1), 43.8 (CH₂), 56.7 (OCH₃); 68.9 (C-7a), 70.3 (C-3), 105.7, 110.6, 125.3, 126.1, 129.8, 133.4, 138.2, 153.6 (aryl), 156.5, 169.8, 175.6 (C=O). ESIMS m/z calculated for C₂₃H₂₃N₃O₆S, 469.13; found, 469.29.

(3*R*,7*aR*)-6-(4,4-Dimethylcyclohexyl)-10-methyl-1*H*-spiro-[imidazo[1,5-*c*]thiazole-3,3'-indoline]-2',5,7(6*H*,7*aH*)-trione (45e).

Yield 56%, mp 174-175 °C, $[\alpha]_{\text{D}}^{25}$ -16.8° (c 0.1, MeOH). ¹H NMR (400 MHz, CDCl₃) δ 0.89 (s, 3H, CH₃); 0.94 (s, 3H, CH₃); 1.19-1.25 (m, 2H, CH₂); 1.41-1.50 (m, 4H, CH₂); 2.18-2.31 (m, 2H, CH₂); 3.26 (s, 3H, CH₃); 3.32 (dd,

1H, J = 5.2 and 10.8 Hz, Ha-1); 3.72 (t, 1H, Hb-1); 3.70-3.76 (m, 1H, CH); 4.90 (dd, 1H, J=5.6 and 11.2 Hz, H-7a); 6.85 (d, 1H, J= 7.6 Hz, H-7'); 7.11 (t, 1H, H-6'); 7.34 (t, 1H, H-5'); 7.43 (d, 1H, H-4'). ¹³C NMR (100 MHz, CDCl₃) δ 24.1 (CH₂); 24.9 (CH₂); 25.0 (CH₃); 26.9 (CH₃); 29.7 (CH₃); 32.5 (C-1), 38.6 (CH), 52.5 (C), 68.3 (C-7a), 70.7 (C-3), 109.2, 123.6, 125.3, 131.0, 143.5 (aryl), 156.5, 170.5, 174.6 (C=O). ESIMS m/z calculated for C₂₁H₂₅N₃O₃S, 399.16; found, 399.27.

8.9 General Procedure for the Synthesis of the (3*R*,7*aR*)-10-Acyl-6-(benzylsubstituted)-1*H*-spiro[imidazo[1,5-*c*]thiazole-3,3'-indoline]-2',5,7(6*H*,7*aH*)-trione Derivatives (46*f*-i/47*f*-i).

42c or **43d** (100 mg, 0.2 mmol) was dissolved in dichloromethane (10 mL), and the appropriate acyl chloride (benzoyl chloride, 4-methylbenzoyl chloride, 4-chlorobenzoyl chloride or butyryl chloride, **f-i**) (0.22 mmol) and TEA (0.30 mmol) were added. The mixture was stirred at room temperature for 2 h. Then the organic solution was washed with 10% NaHCO₃ and water, dried over Na₂SO₄, and evaporated to dryness. Flash chromatography was performed on silica gel, using as eluent a mixture ethyl acetate/*n*-hexane, 1/3, to obtain the corresponding N-substituted derivatives as white solids.

(3*R*,7*aR*)-10-Benzoyl-6-(4-chlorobenzyl)-1*H*-spiro[imidazo-[1,5-*c*]thiazole-3,3'-indoline]-2',5,7(6*H*,7*aH*)-trione (46*f*).

Yield 85%, mp 245-246 °C, [α]_D²⁵ -9.3° (c 0.1, MeOH). ¹H NMR (400 MHz, CDCl₃) δ 3.36 (dd, 1H, J=6.0 and 12.0 Hz, Ha-1); 3.60 (t, 1H, Hb-1); 4.45 (d, 1H, J=14.4 Hz, CH₂); 4.63 (d, 1H, CH₂); 5.03 (dd, 1H, J = 5.6 and 10.8 Hz, H-7a); 7.29 (t, 1H, H-6'); 7.42-7.48 (m, 3H, H-5' and aryl); 7.55 (d, 1H, H-4'); 7.61 (t, 1H, aryl); 7.77-7.80 (m, 2H, aryl); 7.83 (d, 1H, H-7'). ¹³C NMR (100 MHz, CDCl₃) δ 32.8 (C-1), 42.4 (CH₂), 68.9 (C-7a), 71.5 (C-3), 115.2, 124.4,

125.5, 126.0, 128.7, 129.4, 130.1, 130.3, 131.7, 133.3, 137.6, 144.5 (aryl), 156.2, 167.8, 169.1, 174.3 (C=O). ESIMS m/z calculated for C₂₆H₁₈ClN₃O₄S, 503.07; found, 503.16.

(3*R*,7*aR*)-6-(4-Chlorobenzyl)-10-(4-methylbenzoyl)-1H-spiro-[imidazo[1,5-*c*]thiazole-3,3'-indoline]-2',5,7(6H,7aH)-trione (46g).

Yield 87%, mp 261-262 °C, $[\alpha]_D^{25}$ -8.1° (c 0.1, MeOH). ¹H NMR (400 MHz, CDCl₃) δ 2.40 (s, 3H, CH₃); 3.35 (dd, 1H, J = 5.6 and 11.6 Hz, Ha-1); 3.62 (t, 1H, Hb-1); 4.46 (d, 1H, J = 14.8 Hz, CH₂); 4.61 (d, 1H, CH₂); 5.02 (dd, 1H, J = 5.2 and 10.8 Hz, H-7a); 7.24 (t, 1H, H-6'); 7.42 (t, 1H, H-5'); 7.56 (d, 1H, J = 8.0 Hz, H-4'); 7.78 (d, 2H, J = 8.0 Hz, aryl); 7.81 (d, 1H, H-7'); 7.59 (d, 2H, aryl); ¹³C NMR (100 MHz, CDCl₃) δ 21.8 (CH₃), 32.7 (C-1), 42.5 (CH₂), 68.9 (C-7a), 70.7 (C-3), 115.7, 124.8, 125.2, 125.9, 128.9, 129.2, 129.9, 130.1, 130.2, 131.6, 133.7, 137.1, 144.6 (aryl), 156.6, 167.8, 169.5, 174.3 (C=O). ESIMS m/z calculated for C₂₇H₂₀ClN₃O₄S, 517.09; found, 517.19.

(3*R*,7*aR*)-10-(4-Chlorobenzoyl)-6-(4-chlorobenzyl)-1H-spiro-[imidazo[1,5-*c*]thiazole-3,3'-indoline]-2',5,7(6H,7aH)-trione (46h).

Yield 90%, mp 258-259 °C, $[\alpha]_D^{25}$ -7.8° (c 0.12, MeOH). ¹H NMR (400 MHz, CDCl₃) δ 3.34 (dd, 1H, J = 5.6 and 11.6 Hz, Ha-1); 3.59 (t, 1H, Hb-1); 4.52 (d, 1H, J = 14.8 Hz, CH₂); 4.62 (d, 1H, CH₂); 5.02 (dd, 1H, J = 5.2 and 10.8 Hz, H-7a); 7.31 (t, 1H, H-6'); 7.43 (d, 2H, J = 8.0 Hz, aryl); 7.48 (t, 1H, H-5'); 7.53 (d, 1H, J = 8.0 Hz, H-4'); 7.78 (d, 2H, aryl); 7.87 (d, 1H, H-7'); ¹³C NMR (100 MHz, CDCl₃) δ 32.5 (C-1), 43.6 (CH₂), 68.9 (C-7a), 70.9 (C-3), 115.8, 124.4, 125.3, 126.2, 128.8, 129.2, 130.0, 131.4, 131.7, 137.7, 137.9, 138.1, 139.0, 141.5 (aryl), 156.8, 167.6, 169.4, 174.1 (C=O). ESIMS m/z calculated for C₂₆H₁₇Cl₂N₃O₄S, 537.03; found, 537.12.

(3*R*,7*aR*)-10-Butyryl-6-(4-chlorobenzyl)-1*H*-spiro[imidazo-[1,5-*c*]thiazole-3,3'-indoline]-2',5,7(6*H*,7*aH*)-trione (46i).

Yield 89%, mp 231-232 °C, $[\alpha]_D^{25}$ -7.3° (c 0.1, MeOH). ¹H NMR (400 MHz, CDCl₃) δ 1.04 (t, 3H, CH₃); 1.72-1.82 (m, 2H, CH₂); 2.96-3.08 (m, 2H, CH₂); 3.37 (dd, 1H, J = 5.6 and 11.6 Hz, Ha-1); 3.67 (t, 1H, Hb-1); 4.52 (d, 1H, J=14.4 Hz, CH₂); 4.64 (d, 1H, CH₂); 5.01 (dd, 1H, J = 5.2 and 10.8 Hz, H-7a); 7.24 (t, 1H, H-6'); 7.41 (t, 1H, H-5'); 7.47 (d, 1H, J = 8.0 Hz, H-4'); 8.25 (d, 1H, H-7'); ¹³C NMR (100 MHz, CDCl₃) δ 13.9 (CH₃), 17.9 (CH₂), 32.8 (C-1), 40.4 (CH₂), 42.6 (CH₂), 68.9 (C-7a), 71.3 (C-3), 117.5, 124.3, 124.9, 126.1, 129.2, 130.2, 131.7, 133.7, 134.4, 140.1 (aryl), 157.3, 169.5, 173.7, 175.2 (C=O). ESIMS m/z calculated for C₂₃H₂₀ClN₃O₄S, 469.09; found, 469.18.

(3*R*,7*aR*)-10-Benzoyl-5'-methyl-6-(3,4,5-trimethoxybenzyl)-1*H*-spiro[imidazo[1,5-*c*]thiazole-3,3'-indoline]-2',5,7(6*H*,7*aH*)-trione (47f).

Yield 87%, mp 271-273 °C, $[\alpha]_D^{25}$ -11.8° (c 0.11, MeOH). ¹H NMR (400 MHz, CDCl₃) δ 2.39 (s, 3H, CH₃); 3.34 (dd, 1H, J = 6.0 and 12.0 Hz, Ha-1); 3.59 (t, 1H, Hb-1); 3.66 (s, 3H, OCH₃); 3.78 (s, 6H, OCH₃); 4.43 (d, 1H, J = 14.4 Hz, CH₂); 4.62 (d, 1H, CH₂); 5.02 (dd, 1H, J = 5.6 and 10.8 Hz, H-7a); 6.47 (s, 2H, aryl); 7.23-7.26 (m, 2H, H-6' and H-7'); 7.36 (s, 1H, H-4'); 7.41-7.45 (m, 2H, aryl); 7.58 (t, 1H, aryl); 7.80-7.83 (m, 2H, aryl). ¹³C NMR (100 MHz, CDCl₃) δ 21.5 (CH₃); 32.4 (C-1), 42.8 (CH₂), 56.9 (OCH₃), 68.9 (C-7a), 71.2 (C-3), 105.5, 115.9, 124.6, 125.8, 126.9, 128.7, 129.3, 130.2, 131.8, 131.3, 132.0, 133.6, 153.5 (aryl), 156.6, 167.2, 169.4, 174.1 (C=O). ESIMS m/z calculated for C₃₀H₂₇N₃O₇S, 573.16; found, 573.21.

(3*R*,7*aR*)-5'-Methyl-10-(4-methylbenzoyl)-6-(3,4,5-trimethoxybenzyl)-1*H*-spiro[imidazo[1,5-*c*]thiazole-3,3'-indoline]-2',5,7-(6*H*,7*aH*)-trione (47g).

Yield 89%, mp 293-294 °C, $[\alpha]_D^{25}$ -12.7° (c 0.11, MeOH). ¹H NMR (400 MHz, CDCl₃) δ 2.38 (s, 3H, CH₃); 2.42 (s, 3H, CH₃); 3.33 (dd, 1H, J = 5.6 and

11.6 Hz, Ha-1); 3.60 (t, 1H, Hb-1); 3.67 (s 3H, OCH₃); 3.76 (s, 6H, OCH₃); 4.42 (d, 1H, J=14.8 Hz, CH₂); 4.62 (d, 1H, CH₂); 5.01 (dd, 1H, J=5.2 and 10.8 Hz, H-7a); 6.49 (s 2H, aryl); 7.23-7.26 (m, 3H, H-6', H-7' and aryl); 7.35 (s, 1H, H-4'); 7.71-7.77 (m, 3H, aryl). ¹³C NMR (100 MHz, CDCl₃) δ: 21.2 (CH₃); 21.8 (CH₃), 32.6 (C-1), 42.7 (CH₂), 56.5 (OCH₃), 68.8 (C-7a), 70.9 (C-3), 105.4, 115.8, 124.7, 125.5, 128.9, 129.6, 130.4, 131.5, 131.6, 132.9, 133.6, 137.3, 154.0 (aryl), 156.8, 167.3, 169.1, 174.3 (C=O). ESIMS m/z calculated for C₃₁H₂₉N₃O₇S, 587.17; found, 587.29.

(3R,7aR)-10-(4-Chlorobenzoyl)-5'-methyl-6-(3,4,5-trimethoxybenzyl)-1H-spiro[imidazo[1,5-c]thiazole-3,3'-indoline]-2',5,7-(6H,7aH)-trione (47h).

Yield 91%, mp 280-281 °C, [α]²⁵_D -13.5° (c 0.13, MeOH). ¹H NMR (400 MHz, CDCl₃) δ 2.39 (s, 3H, CH₃); 3.32 (dd, 1H, J₀ = 5.6 and 11.6 Hz, Ha-1); 3.61 (t, 1H, Hb-1); 3.69 (s, 3H, OCH₃); 3.77 (s, 6H, OCH₃); 4.43 (d, 1H, J=14.8 Hz, CH₂); 4.64 (d, 1H, CH₂); 5.03 (dd, 1H, J= 5.2 and 10.8 Hz, H-7a); 6.49 (s, 2H, aryl); 7.26 (d, 1H, J = 8.0 Hz, H-7'); 7.36 (s, 1H, H-4'); 7.41-7.44 (m, 2H, H-6', and aryl); 7.72-7.83 (m, 3H, aryl). ¹³C NMR (100 MHz, CDCl₃) δ 21.4 (CH₃); 32.9 (C-1), 43.5 (CH₂), 56.3 (OCH₃), 68.9 (C-7a), 71.3 (C-3), 105.1, 115.8, 124.4, 125.6, 128.8, 129.1, 130.8, 131.2, 131.8, 132.2, 136.3, 137.4, 137.9, 139.7, 153.6 (aryl), 156.7, 167.7, 169.5, 174.4 (C=O). ESIMS m/z calculated for C₃₀H₂₆ClN₃O₇S, 607.12; found, 607.22.

(3R,7aR)-10-Butyryl-5'-methyl-6-(3,4,5-trimethoxybenzyl)-1H-spiro[imidazo[1,5-c]thiazole-3,3'-indoline]-2',5,7(6H,7aH)-trione (47i).

Yield 91%, mp 258-259 °C, [α]²⁵_D -14.2° (c 0.15, MeOH). ¹H NMR (400 MHz, CDCl₃) δ 1.00 (t, 3H, CH₃); 1.73-1.80 (m, 2H, CH₂); 2.32 (s, 3H, CH₃); 3.00 (t, 2H, CH₂); 3.37 (dd, 1H, J=5.6 and 11.6 Hz, Ha-1); 3.65 (t, 1H, Hb-1); 3.81 (s, 3H, OCH₃); 3.85 (s, 6H, OCH₃); 4.45 (d, 1H, J = 14.4 Hz, CH₂); 4.62 (d, 1H, CH₂); 5.03 (dd, 1H, J = 5.2 and 10.8 Hz, H-7a); 6.56 (s, 2H, aryl); 7.21

(d, 1H, J = 8.0 Hz, H-7'); 7.28 (s, 1H, H-4'); 8.12 (d, 1H, H-6'). ¹³C NMR(100 MHz, CDCl₃) δ: 13.5 (CH₃), 17.6 (CH₂), 21.5 (CH₃), 32.7 (C-1), 40.6 (CH₂), 42.9 (CH₂), 56.6 (OCH₃), 68.9 (C-7a), 71.5 (C-3), 105.6, 117.2, 124.6, 125.8, 129.1, 130.4, 131.3, 137.7, 139.5, 152.1 (aryl), 157.1, 169.7, 173.2, 175.7 (C=O). ESIMS m/z calculated for C₂₇H₂₉N₃O₇S, 539.17; found, 539.28.

8.10. Biology.

modified Eagle's medium (DMEM), fetal bovine serum (FBS), trypsin-EDTA solution (1₁), penicillin and streptomycin, phosphate-buffered saline (PBS) were from Cambrex Biosciences. 3-(4,5-Dimethylthiazol-2-yl)-2,5-diphenyltetrazolium bromide (MTT), propidium iodide (PI), Triton X-100, sodium citrate, formamide, mouse monoclonal anti-tubulin were purchased from Sigma (Milan, Italy). Rabbit polyclonal anti-caspase-3, mouse monoclonal anti-PARP-1, mouse monoclonal anti-actin, mouse monoclonal anti-p53, and horseradish peroxidase (HRP) conjugated anti-mouse and anti-rabbit secondary antibodies were purchased from Santa Cruz Biotechnology (DBA; Milan, Italy). Rabbit polyclonal anti-cyclin B1 primary antibody were from Cell Signaling Technology (Celbio; Milan, Italy). ECL reagent was obtained from Amersham Pharmacia Biotech, U.K.

8.10.1. Cell Culture.

Human embryonic kidney HEK 293, human melanoma M14, human monocytic leukemia U937, human normal thyroid TAD-2, and human papillary thyroid carcinoma TPC1 cell lines cell lines were grown at 37 °C in Dulbecco's modified Eagle's medium containing 10 mM glucose (DMEMHG) supplemented with 10% fetal calf serum and 100 units/mL each of penicillin and streptomycin and 2 mmol/L glutamine. In each experiment, cells were

placed in fresh medium, cultured in the presence of synthesized compounds (from 0.1 to 25 mM), and followed for further analyses.

8.10.2. Cell Viability Assay.

Cell viability for M14, HEK, U937, TPC1n, and TAD-2 cell lines was determined using the 3-[4,5-dimethylthiazol-2,5-diphenyl-2H-tetrazolium bromide (MTT)

8.10.3. Cytotoxic activity assay

The human breast adenocarcinoma MCF-7, human ductal breast carcinoma T47D, and human epidermoid carcinoma A431 cells were cultured at 37 °C in humidified 5%CO₂/95% air in Dulbecco's Modified Eagle's Medium (DMEM) containing 10% fetal bovine serum, 2 mM glutamine, 100 U/ml penicillin, 100 g/ml streptomycin, 25 mM HEPES and 5 mM sodium pyruvate. The cells were plated in 24 culture wells at a density of 2.5 × 10⁵ cells/ml per well or 10 cm diameter culture dishes at a density of 3 × 10⁶ cells/ml per dish and allowed to adhere for 2 h. Thereafter the medium was replaced with fresh medium and cells were incubated with isatins (10⁻⁷, 10⁻⁶, 10⁻⁵ M) added to the cells for 48 h. Stocks of antitumoral compounds were dissolved in saline or saline and 1% DMSO, sterilized by 30 min of UV irradiation and stored at 20 °C. The cell viability was determined by using 3-(4,5-dimethylthiazol-2-yl)-2,5-diphenyl-2H-tetrazolium dimethylthiazol-2-yl)-2,5-diphenyl-2H-tetrazolium bromide (MTT) conversion assay as previously described.²⁶ Briefly, 100 µl MTT (5 mg/ml in complete DMEM) was added and the cells were incubated for an additional 3 h. After this time point the cells were lysed and the dark blue crystals solubilized with 500 µl of a solution containing 50% (v:v) N,N-dimethylformamide, 20% (w:v) SDS with an adjusted pH of

4.5. The optical density (OD) of each well was measured with a microplate spectrophotometer equipped with a 620 nm filter. The cell viability in response to treatment with test compounds was calculated as % dead cells = $100 \times (\text{OD treated} / \text{OD control}) \times 100$.

CHAPTER 9.
REFERENCES

REFERENCES

1. Hanahan D, Weinberg RA. The hallmarks of cancer. *Cell* 2000; 100:57–70.
2. Oller AR, Rastogi P, Morgenthaler S, Thilly, WG. A statistical model to estimate variance in long term-low dose mutation assays: testing of the model in a human lymphoblastoid mutation assay. *Mutat. Res.* 1989; 216:149–161.
3. Evan G, Littlewood, T. A matter of life and cell death. *Science* 1998; 281: 1317–1322.
4. Reddy L, Odhav B, Bhoola KD. Natural products for cancer prevention: a global perspective. *Pharmacol. Ther.* 2003; 99:1-13 and references therein
5. Schwartz GK, Manish AS. Targeting the Cell Cycle: A New Approach to Cancer Therapy *J. Clin. Oncol.* 2005; 10:23.
6. Heichman KA, Roberts JM, Rules to replicate by. *Cell* 1994; 79: 557-562 (b) Wuarin J, Nurse P. Regulating S phase: CDKs, licensing and proteolysis. *Cell* 1996; 85: 785-787.
7. (a) Hunter T, Pines J. Cyclins and cancer. II: Cyclin D and CDK inhibitors come of age *Cell* 1994; 79: 573-582. (b) Hall M, Peters G. Genetic alterations of cyclins, cyclin-dependent kinases, and Cdk inhibitors in human cancer. *Adv. Cancer Res.* 1996; 68: 67-108
8. (a) Pardee AB. G1 events and regulation of cell proliferation *Science* 1989; 246: 603-608. (b) Sherr CJ. G1 phase progression: cycling on cue. *Cell* 1994; 79: 551-552
9. Sherr CJ, Roberts JM. CDK inhibitors: Positive and negative regulators of G1-phase progression. *Genes Dev* 1999; 13:1501-1512.
10. Grana X, Reddy EP. Cell cycle control in mammalian cells: Role of cyclins, cyclin dependent kinases (CDKs), growth suppressor genes

- and cyclin-dependent kinase inhibitors (CKIs). *Oncogene* 1995; 11:211-219. (b) Johnson DG, Walker CL. Cyclins and cell cycle checkpoints. *Annu. Rev. Pharmacol. Toxicol.* 1999; 39:295-312,
11. Kaldis P, Russo AA, Chou HS, et al: Human and yeast cdk-activating kinases (CAKs) display distinct substrate specificities. *Mol. Biol. Cell* 1998; 9:2545-2560.
 12. Hunter T. Signaling—2000 and beyond. *Cell* 2000; 100:113–127.
 13. Harbour JW, Dean DC. The Rb/E2F pathway: expanding roles and emerging paradigms. *Genes Dev.* 2000; 14:2393–2409.
 14. Sherr C J. Cancer cell cycles. *Science* 1996; 274:1672–1677.
 15. Baudino TA, Cleveland JL. The Max network gone mad. *Mol. Cell. Biol.* 2001; 21, 691–702
 16. (a) Tocker H, Hafen E. Genetic control of cell size. *Curr. Opin. Genet. Dev.* 2000; 10, 529–535. (b) Johnston LA, Prober, DA, Edgar BA, Eisenman, RN, Gallant P. Drosophila myc regulates cellular growth during development. *Cell* 1999; 98: 779–790. (c) Iritani BM, Eisenman RN. c-Myc enhances protein synthesis and cell size during B lymphocyte development. *Proc. Natl Acad. Sci. USA* 1999; 96: 13180–13185.
 17. Elend M, Eilers M. Cell growth: downstream of Myc—to grow or to cycle? *Curr. Biol.* 1999; 9: R936–R938. (b) Dang CV, et al. Function of the c-Myc oncogenic transcription factor. *Exp. Cell Res.* 1999; 253: 63–77.
 18. Gu W. et al. Interaction of myogenic factors and the retinoblastoma protein mediates muscle cell commitment and differentiation. *Cell* 1993;72, 309–324.
 19. Lasorella A, Nosedà M, Beyna M, Iavarone, A. Id2 is a retinoblastoma protein target and mediates signalling by Myc oncoproteins. *Nature* 2000; 407, 592–598.

20. Dash P. Apoptosis [www. Sgul.ac.uk/depts/immunology/-dash](http://www.Sgul.ac.uk/depts/immunology/-dash) and reference therein
21. Walczak H, Krammer PH. The CD95 (APO-1/Fas) and the TRAIL (APO-2L) apoptosis systems. *Exp. Cell Res.* 2000; 256, 58–66.
22. Vander Heiden MG, *et al.* Outer mitochondrial membrane permeability can regulate coupled respiration and cell survival. *Proc. Natl Acad. Sci. USA* 2000; 97: 4666–4671
23. Hengartner MO. The biochemistry of apoptosis. *Nature* 2000; 407, 770–776.
24. Soengas MS. *et al.* Inactivation of the apoptosis effector Apaf-1 in malignant melanoma. *Nature* 2001; 409: 207–211.
25. Evan G, *et al.* Induction of apoptosis in fibroblasts by c-myc protein. *Cell* 1992; 63: 119–125 (b) Askew D, Ashmun R, Simmons B, Cleveland J. Constitutive c-myc expression in IL-3-dependent myeloid cell line suppresses cycle arrest and accelerates apoptosis. *Oncogene* 1991; 6: 1915–1922
26. Sherr, CJ, Weber JD. The ARF/p53 pathway. *Curr. Opin. Genet. Dev.* 2000; 10: 94–99.
27. Woods DB, Vousden KH. Regulation of p53 function. *Exp. Cell Res.* 2001; 264: 56–66.
28. Gibbs JB. Mechanism-based target identification and drug discovery in cancer research. *Science* 2000; 287, 1969–1973.
29. Felsher DW, Bishop JM. Reversible tumorigenesis by myc in hematopoietic lineages. *Mol. Cell* 1999; 4 : 199–207.
30. Woods D B , Vousden K H. Regulation of p53 function. *Exp. Cell Res.* 2001; 264, 56–66.
31. Giaccia, AJ, Kastan, MB. The complexity of p53 modulation: emerging patterns from divergent signals. *Genes Dev.* 1998; 12: 2973-298.

32. Lohrum MA, Vousden KH. Regulation and activation of p53 and its family members. *Cell Death Differ.* 1999; 6, 1162-1168. (b) Jin S, Levine AJ. The p53 functional circuit. *J. Cell Sci.* 2001; 114: 4139-4120.
33. Royds JA, Iacopetta B. p53 and disease: when the guardian angel fails. *Cell Death Differ.* 2006, 13, 1017–102. (b) Kirsch DG, Kastan MB. Tumor-suppressor p53: Implications for tumor development and prognosis. *J. Clin.Oncol.* 1998; 16:3158–3168.
34. Vogelstein B, Lane D, Levine AJ. Surfing the p53 network. *Nature* 2000; 408, 307-10.
35. Donehower LA. The p53-deficient mouse: a model for basic and applied cancer studies. *Sem. Cancer Biol.* 1996; 7: 269–278.
36. Pietsch C, Humbey O, Murphey ME. Polymorphisms in the p53 pathway. *Oncogene* 2006; 25: 1602–1611.
37. Lapenko O, Prives C. Transcriptional regulation by p53: one protein, many possibilities. *Cell Death Differ.* 2006; 13: 951–961.
38. Matoba S, et al. p53 regulates mitochondrial respiration. *Science* 2006; 312:1650–1653
39. Bensaad, K. TIGAR, a p53-inducible regulator of glycolysis and apoptosis. *Cell* 2006; 126: 107–120.
40. Crighton D, et al. DRAM, a p53-induced modulator of autophagy, is critical for apoptosis. *Cell* 2006, 14, 121–134.
41. Gatz SA, Wiesmuller L. p53 in recombination and repair. *Cell Death Differ.* 2006; 13: 1003–1016.
42. Bensaad K, Vousden KH. Savior and slayer: the two faces of p53. *Nature Med.* 2005; 11: 1278–1279 .
43. Roger L, Gadea G, Roux P. Control of cell migration: a tumour suppressor function for p53? *Biol. Cell* 2006; 98:141–152.

44. Kortleverm RM, Higgi PJ, Bernards R. Plasminogen activator inhibitor-1 is a critical downstream target of p53 in the induction of replicative senescence. *Nature Cell Biol.* 2006; 8: 877–884.
45. Toeodoro JG., Parker AE, Zhu X, Green MR. p53-mediated inhibition of angiogenesis through upregulation of a collagen prolyl hydroxylase. *Science* 2006; 313: 968–971.
46. Murray-Zmijewski F, Lane DP, Bourdon JC. p53/p63/p73 isoforms: an orchestra of isoforms to harmonise cell differentiation and response to stress. *Cell Death Differ.* 2006; 13: 962–972.
47. Wang X, et al. p53 functions as a negative regulator of osteoblastogenesis, steoblast-dependent osteoclastogenesis, and bone remodeling. *J. Cell Biol.* 2006; 172: 115–125.
48. Lane DP. Cancer. p53, guardian of the genome. *Nature* 1992; 358:15-16.
49. Siliciano JD, Canman CE, Taya Y, Sakaguchi K, Appella E, Kastan MB. DNA damage induces phosphorylation of the amino terminus of p53. *Genes Dev* 1997; 11: 3471-81
50. Kurz EU, Lees-Miller SP. DNA damage-induced activation of ATM and ATM-dependent signaling pathways. *DNA Repair (Amst)* 2004; 3: 889-900
51. (a) Bartkova J, Horejsi Z, Koed K, Kramer A, Tort F, Zieger K, Guldberg P, Sehested M, Nesland JM, Lukas C, Orntoft T, Lukas J, Bartek J. DNA damage response as a candidate anti-cancer barrier in early human tumorigenesis. *Nature* 2005; 434: 864-70. (b) Gorgoulis VG, Vassiliou LV, Karakaidos P, Zacharatos P, Kotsinas A, Liloglou T, Venere M, Ditullio Jr RA, Kastriakis NG, Levy B, Kletsas D, Yoneta A, Herlyn M, Kittas C, Halazonetis TD. Activation of the DNA damage checkpoint and genomic instability in human precancerous lesions. *Nature* 2005; 434: 907-13

52. Jackson AL, Loeb LA. The contribution of endogenous sources of DNA damage to the multiple mutations in cancer. *Mutat Res* 2001; 477: 7-21
53. (a) Bartkova J, Rezaei N, Liontos M, Karakaidos P, Kletsas D, Issaeva N, Vassiliou LV, Kolettas E, Niforou K, Zoumpourlis VC, Takaoka M, Nakagawa H, Tort F, Fugger K, Johansson F, Sehested M, Andersen CL, Dyrskjot L, Orntoft T, Lukas J, Kittas C, Helleday T, Halazonetis TD, Bartek J, Gorgoulis VG. Oncogene-induced senescence is part of the tumorigenesis barrier imposed by DNA damage checkpoints. *Nature* 2006; 444: 633-7. (b) Di Micco R, Fumagalli M, Cicalese A, Piccinin S, Gasparini P, Luise C, Schurra C, Garre M, Nuciforo PG, Bensimon A, Maestro R, Pelicci PG, d'Adda di Fagagna F. Oncogene-induced senescence is a DNA damage response triggered by DNA hyper-replication. *Nature* 2006; 444: 638-42.
54. Chao C, Herr D, Chun J, Xu Y. Ser18 and 23 phosphorylation is required for p53-dependent apoptosis and tumor suppression. *Embo J*. 2006; 25:2615-22
55. (b) Donehower LA. The p53-deficient mouse: a model for basic and applied cancer studies. *Sem. Cancer Biol.* 1996; 7: 269–278. (c) Jacks T, Remington L, Williams BO, Schmitt EM, Halachmi S, Bronson RT, Weinberg RA. Tumor spectrum analysis in p53-mutant mice. *Curr. Biol.* 1994; 4:1-7.
56. (a) Milne DM, Campbell LE, Campbell DG, Meek DW. p53 is phosphorylated in vitro and in vivo by an ultraviolet radiation-induced protein kinase characteristic of the c-Jun kinase, JNK1. *J Biol Chem* 1995; 270:5511-8. (b) Buschmann T, Potapova O, Bar-Shira A, Ivanov VN, Fuchs SY, Henderson S, Fried VA, Minamoto T, Alarcon-Vargas D, Pincus MR, Gaarde WA, Holbrook NJ, Shiloh Y,

- Ronai Z. Jun NH2-terminal kinase phosphorylation of p53 on Thr-81 is important for p53 stabilization and transcriptional activities in response to stress. *Mol. Cell Biol.* 2001; 21:2743-54. (b) Harris SL, Levine AJ. The p53 pathway: Positive and negative feedback loops. *Oncogene* 2005; 24:2899-908.
57. Feng J, Yan J, Chen J, Schlake G, Jiang Z, Buzin CH, Sommer SS, Dritschilo M. Absence of somatic ATM missense mutations in 58 mammary carcinomas. *Cancer Genet. Cytogenet.* 2003; 145: 179-82. (b) Ingvarsson S, Sigbjornsdottir BI, Huiping C, Hafsteinsdottir SH, Ragnarsson G, Barkardottir RB, Arason A, Egilsson V, Bergthorsson JT. Mutation analysis of the CHK2 gene in breast carcinoma and other cancers. *Breast Cancer Res* 2002; 4:R4
58. Gumy-Pause F, Wacker P, Sappino AP. ATM gene and lymphoid malignancies. *Leukemia* 2004; 18:238-42.
59. Greenman C, Stephens P, Smith R, Dalgliesh GL, Hunter C, Bignell G, Davies H, Teague J, Butler A, Stevens C, Edkins S, et al. Patterns of somatic mutation in human cancer genomes. *Nature* 2007; 446:153-8.
60. Serrano M, Lin AW, McCurrach ME, Beach D, Lowe SW. Oncogenic ras provokes premature cell senescence associated with accumulation of p53 and p16INK4a. *Cell* 1997; 88: 593-602.
61. Francoz S, Froment P, Bogaerts S, De Clercq S, Maetens M, Doumont G, Bellefroid E, Marine GC. Mdm4 and Mdm2 cooperate to inhibit p53 activity in proliferating and quiescent cells in vivo. *Proc. Natl. Acad. Sci. USA* 2006;. 9: 3232-3237.
62. (a) Palmero I, Pantoja C, Serrano M. p19ARF links the tumour suppressor p53 to Ras. *Nature* 1998; 395: 125-6. (b) Zindy F, Eischen CM, Randle DH, Kamijo T, Cleveland JL, Sherr CJ, Roussel MF. Myc signaling via the ARF tumor suppressor regulates p53-

- dependent apoptosis and immortalization. *Genes Dev* 1998; 12: 2424-29
63. Gil J, Peters G. Regulation of the INK4b-ARF-INK4a tumour suppressor locus: All for one or one for all. *Nat. Rev. Mol. Cell Biol.* 2006; 7: 667-77.
64. Inoue K, Wen R, Rehg JE, Adachi M, Cleveland JL, Roussel MF, Sherr CJ. Disruption of the ARF transcriptional activator DMP1 facilitates cell immortalization, Ras transformation, and tumorigenesis. *Genes Dev.* 2000; 14:1797-809.
65. Kamijo T, Bodner S, van de Kamp E, Randle DH, Sherr CJ. Tumor spectrum in ARF-deficient mice. *Cancer Res* 1999; 59:2217-22.
66. Jacks T, Remington L, Williams BO, Schmitt EM, Halachmi S, Bronson RT, Weinberg RA. Tumor spectrum analysis in p53-mutant mice. *Curr, Biol.* 1994; 4:1-7.
67. Moore L, Venkatachalam S, Vogel H, Watt JC, Wu CL, Steinman H, Jones SN, Donehower LA. Cooperativity of p19ARF, Mdm2, and p53 in murine tumorigenesis. *Oncogene* 2003; 22:7831-7.
68. Sharpless NE. INK4a/ARF: A multifunctional tumor suppressor locus. *Mutant Res* 2005; 576:22-38.
69. Rizos H, Puig S, Badenas C, Malveyh J, Darmanian AP, Jimenez L, Mila M, Kefford RF. A melanoma-associated germline mutation in exon 1beta inactivates p14ARF. *Oncogene* 2001; 20:5543-7
70. Kim WY, Sharpless NE. The regulation of INK4/ARF in cancer and aging. *Cell* 2006; 127: 265-75.
71. Rozenfeld-Granot G, Krishnamurthy, J, Kannan K, Toren A, Amariglio N, Givol D., Rechavi G. A positive feedback mechanism in the transcriptional activation of Apaf-1 by p53 and the coactivator Zac-1. *Oncogene* 2002; 21:1469-1476.

72. Sheen JH, Dickson RB. Overexpression of c-Myc alters G(1)/S arrest following ionizing radiation. *Mol. Cell. Biol.* 2002; 22: 1819-1833.
73. Vafa O, Wade M., Kern S, Beeche M, Pandita T K, Hampton GM, Wahl GM. c-Myc can induce DNA damage, increase reactive oxygen species, and mitigate p53 function: a mechanism for oncogene induced genetic instability. *Mol. Cell* 2002; 9: 1031-1044.
74. Herold S, Wanzel M, Beuger V, Frohme C, Beul D, Hillukkala T, Syvaioja J, Saluz H P, Haenel F, Eilers M. Negative regulation of the mammalian UV response by Myc through association with Miz-1. *Mol. Cell* 2002; 10: 509-521. (b) Seoane J, Le H V, Massague J. Myc suppression of the p21(Cip1) Cdk inhibitor influences the outcome of the p53 response to DNA damage. *Nature* 2002; 419: 729-734
75. Strasser A, Harris AW, Jacks T, Cory S. DNA damage can induce apoptosis in proliferating lymphoid cells via p53-independent mechanisms inhibitable by Bcl-2. *Cell* 1994; 79, 329-339. (b) Samuels-Lev Y, O'Connor, D J, Bergamaschi D, Trigiante G., Hsieh JK, Zhong S, Campargue I, Naumovski L, Crook T, Lu, X. ASPP proteins specifically stimulate the apoptotic function of p53. *Mol. Cell* 2001; 8: 781-794.
76. Flores ER, Tsai, KY, Crowley D, Sengupta S, Yang A, McKeon F, Jacks T. p63 and p73 are required for p53-dependent apoptosis in response to DNA damage. *Nature* 2002; 416, 560-564.
77. Urist M, Prives C. p53 leans on its siblings. *Cancer Cell* 2002; 1: 311-313
78. Shaul Y. c-Abl: activation and nuclear targets. *Cell Death Differ.* 2000; 7: 10-16.
79. Bourdon JC, V. Deguin-Chambon, J.C. Lelong, P. Dessen, P. May, B. Debuire, E. May, Further characterisation of the p53 responsive

- element identification of new candidate genes for trans-activation by p53. *Oncogene* 1997; 14: 85–94.
80. Hoh J, Jin S, Parrado T, Edington J, Levine AJ, Ott J, The p53MH algorithm and its application in detecting p53-responsive genes. *Proc. Natl. Acad. Sci. USA* 2002; 99: 8467–8472
81. Kim YT, Zhao M. Aberrant cell cycle regulation in cervical carcinoma, *Med. J.* 2005; 46 597–613. (b) Makoto N, Yoko K., Hitoshi M., Kyoji I. Direct interaction of p21 cyclindependent kinase inhibitor with the retinoblastoma tumor suppressor protein, *Biochem. Biophys. Res. Commun.* 1999; 263, 35–40.
82. Hollstein M, Sidransky D, Vogelstein B, Harris CC. p53 mutations in human cancers. *Science* 1991; 253: 49–53.
83. Levine AJ. p53, the cellular gatekeeper for growth and division. *Cell* 1997; 88:323–331.
84. Wang X, Ohnishi K, Takahashi A and Ohnishi T. Poly(ADPribose)ation is required for p53-dependent signal transduction induced by radiation. *Oncogene* 1998; 17: 2819–2825. (b) Vaziri H, West MD, Allsopp RC, Davison TS, Wu YS, Arrowsmith CH, Poirier GG and Benchimol S. ATM-dependent telomere loss in aging human diploid fibroblasts and DNA damage lead to the posttranslational activation of p53 protein involving poly(ADP-ribose) polymerase. *EMBO J.* 1997; 16: 6018–6033.
85. Reed M, Woelker B, Wang P, Wang Y, Anderson ME and Tegtmeier P. The C-terminal domain of p53 recognizes DNA damaged by ionizing radiation. *Proc. Natl. Acad. Sci. USA* 1995; 92: 9455–9459. (b) Lee S, Elenbaas B, Levine A, Griffith J. p53 and its 14 kDa Cterminal domain recognize primary DNA damage in the form of insertion/deletion mismatches. *Cell* 1995; 81: 1013–1020.

86. Jean D, Gendron D, Delbecchi L and Bourgaux P. p53-mediated DNA renaturation can mimic strand exchange. *Nucleic Acids Res.* 1997; 25: 4004–4012
87. Dudenhoffer C, Kurth M, Janus F, Deppert W and Wiesmuller L. Dissociation of the recombination control and the sequence-specific transactivation function of p53. *Mol. Cell. Biol.* 1998; 18: 5332–5342.
- (b) Janz C, Susse S, Wiesmuller L. p53 and recombination intermediates: role of tetramerization at DNA junctions in complex formation and exonucleolytic degradation. *Oncogene* 2002; 21: 2130–2140.
88. Bakhanashvili M. Exonucleolytic proofreading by p53 protein. *Eur. J. Biochem.* 2001; 268: 2047–2054.
89. Mummenbrauer T, Janus F, Muller B, Wiesmuller L, Deppert W and Grosse F. P53 exhibits 30- to 50-exonuclease activity. *Cell* 1996; 85: 1089–1099. (b) Janus F, Albrechtsen N, Knippschild U, Wiesmuller L, Grosse F and Deppert W. Different regulation of the core domain activities 30 to 50 exonuclease and sequence-specific DNA binding. *Mol. Cell. Biol.* 1999; 19: 2155–2168.
90. (a) Albrechtsen N, Dornreiter I, Grosse F, Kim E, Wiesmuller L and Deppert W. Maintenance of genomic integrity by p53: complementary roles for activated and non-activated p53. *Oncogene* 1999; 18: 7706–7717. (b) Bertrand P, Saintigny Y, Lopez BS, p53's double life: transactivation independent repression of homologous recombination, *Trends Genet.* 2004; 20: 235–243.
91. Fridman JS, Lowe SW. Control of apoptosis by p53. *Oncogene* 2003; 22: 9030–9040. (b) Vousden KH, Lu X. Live or let die: the cell's response to p53. *Nat. Rev. Cancer* 2002; 2: 594–604.

92. Moll UM, Wolff S, Speidel D, Wolfgang Deppert W. Transcription-independent pro-apoptotic functions of p53. *Current Opinion in Cell Biology* 2005, 17:1–6.
93. Lee JH, Kang Y, Kharel V, Jin ZY, Kang MY, Yoon Y, Hyun JW, Chung M-H, Cho S-I, Jun J Y, Chang IY, You H. The p53-inducible gene 3 (*PIG3*) contributes to early cellular response to DNA damage *Oncogene* (2010) 29, 1431–50
94. Yin Y, Liu YX, Yan J, Jin J, Hall EJ, Barrett C. PAC1 phosphatase is a transcription target of p53 in signalling apoptosis and growth suppression *Nature* 2003; 422: 527-531
95. Scott CI, Schuler M, Vanessa S. Marsden VS, Egle A, Pellegrini M, Nesic D, Gerondakis S, Nutt SL, Green DR, Strasser A. Apaf-1 and caspase-9 do not act as tumor suppressors in *myc*-induced lymphomagenesis or mouse embryofibroblast transformation. *J. Cell Biol.* 2004; 164: 89–96
96. Haupt S, Berger M, Zehavit Goldberg Z, Haupt Y. Apoptosis - the p53 network *J. Cell Sc.* 2003; 116: 4077-4085
97. (a) Yonish-Rouach E, Resnitzky D, Lotem J, Sachs L, Kimchi A, Oren M. Wildtype p53 induces apoptosis of myeloid leukaemic cells that is inhibited by interleukin-6. *Nature* 1991; 352: 345-7. (b) Selvakumaran M, Lin HK, Miyashita T, Wang HG, Krajewski S, Reed JC, Hoffman B, Liebermann D. Immediate early up-regulation of bax expression by p53 but not TGF β 1: A paradigm for distinct apoptotic pathways. *Oncogene* 1994; 9:1791-8.
98. Miyashita T, Krajewski S, Krajewski M, Wang HG, Lin HK, Liebermann DA, Hoffman B, Reed JC. Tumor suppressor p53 is a regulator of bcl-2 and bax gene expression in vitro and in vivo. *Oncogene* 1994; 9:1799-805.

99. Vesely DB, Hoffman B, Liebermann DA. Phosphatidylinositol 3-kinase/Akt signaling mediates interleukin-6 protection against p53-induced apoptosis in M1 myeloid leukemic cells. *Oncogene* 2006; 13:1-10.
100. Bennett M, Macdonald K, Chan SW, Luzio JP, Simari R, Weissberg P. Cell surface trafficking of Fas: A rapid mechanism of p53-mediated apoptosis. *Science* 1998; 282:290-293.
101. Buckbinder L, Talbott R, Velascomiguel S, Takenaka I, Faha B, Seizinger BR, Kley N. Induction of the growth inhibitor IGF-binding protein 3 by p53. *Nature* 1995; 377: 646-649.
102. Baserga R. Oncogenes and the strategy of growth factors. *Cell* 1994; 79:927-30.
103. Wu GS, Saftig P, Peters C, El-Deiry WS. Potential role for cathepsin D in p53-dependent tumor suppression and chemosensitivity. *Oncogene* 1998; 16:2177-83
104. Israeli D, Tessler E, Haupt Y, Elkeles A, Wilder S, Amson R, Telerman A, Oren M. A novel p53-inducible gene, PAG608, encodes a nuclear zinc finger protein whose overexpression promotes apoptosis. *EMBO J.* 1997; 16:4384-439.
105. Nemani M, Linares-Cruz G, Bruzzoni-Giovanelli H, Roperch JP, Tuynder M, Bougueleret L, Cherif D, Medhioub M, Pasturaud P, Alvaro V, der Sarkissan H, Cazes L, Le Paslier D, Le G, Israeli D, Dausset J, SigauxF, Chumakov I, Oren M, Calvo F, Amson RB, Cohen D, Telerman A. Activation of the human homologue of the *Drosophila sina* gene in apoptosis and tumor suppression. *Proc Natl Acad Sci USA* 1996; 93:9039-42.
106. Polyak, K., Xia, Y., Zweier, J. L., Kinzler, K. W., Vogelstein, B. A model for p53-induced apoptosis. *Nature* 1997; 389: 300–305.

107. Faraonio R, Vergara P, Di Marzo D, Pierantoni MG, Napolitano M, Russo T, Cimino F. p53 suppresses the Nrf2-dependent transcription of antioxidant response genes. *J Biol Chem* 2006; 31, 219-224,
108. Moll UM, Marchenko N, Zhang XK. p53 and Nur77/TR3 – Transcription factors that directly target mitochondria for cell death induction. *Oncogene* 2006; 25: 4725-43
109. Shibue T, Suzuki S, Okamoto H, Yoshida H, Ohba Y, Takaoka A, Taniguchi T. Differential contribution of Puma and Noxa in dualregulation of p53-mediated apoptotic pathways. *EMBO J*. 2006; 25: 4952-62
110. Chen X, Ko LJ, Jayaraman L, Prives C. p53 levels, functional domains, and DNA damage determine the extent of the apoptotic response of tumor cells. *Genes Dev* 1996; 10: 2438-51
111. Haupt Y, Rowan S, Shaulian E, Vousden KH, Oren M. Induction of apoptosis in HeLa cells by trans-activation-deficient p53. *Genes Dev*. 1995; 9: 2170- 83.
112. Caelles C, Helmborg A, Karin M. p53-dependent apoptosis in the absence of transcriptional activation of p53-target genes. *Nature* 1994; 370: 220-3.
113. Koumenis C, Alarcon R, Hammond E, Sutphin P, Hoffman W, Murphy M, Derr J, Taya Y, Lowe SW, Kastan M, Giaccia A. Regulation of p53 by hypoxia: dissociation of transcriptional repression and apoptosis from p53-dependent transactivation. *Mol. Cell Biol*. 2001; 21: 1297-310.
114. Marchenko ND, Zaika A, Moll UM. Death signal-induced localization of p53 protein to mitochondria. A potential role in apoptotic signaling. *J Biol Chem*. 2000; 275, 16202-12

115. Dumont P, Leu JI, Della Pietra AC, George DL, Murphy M. The codon 72 polymorphic variants of p53 have markedly different apoptotic potential. *Nat Genet.* 2003; 33: 357-65.
116. (a) Griffiths GJ, Dubrez L, Morgan CP, Jones NA, Whitehouse J, Corfe BM, Dive C, Hickman JA. Cell damage-induced conformational changes of the pro-apoptotic protein Bak in vivo precede the onset of apoptosis. *J. Cell Biol.* 1999; 144: 903-14. (b) Wei MC, Lindsten T, Mootha VK, Weiler S, Gross A, Ashiya M, Thompson CB, Korsmeyer SJ. tBID, a membrane-targeted death ligand, oligomerizes BAK to release cytochrome c. *Genes Dev.* 2000; 14: 2060-71.
117. (a) Mihara M, S. Erster, A. Zaika, O. Petrenko, T. Chittenden, P. Pancoska, U.M. p53 has a direct apoptogenic role at the mitochondria. *Mol. Cell* 2003; 11: 577–590. (b) Chipuk JE, Kuwana T, Bouchier-Hayes L, Droin NM, Newmeyer DD, Schuler M, Green DR. Direct activation of Bax by p53 mediates mitochondrial membrane permeabilization and apoptosis. *Science.* 2004; 303:1010-4.
118. Hainaut P, Hollstein M. p53 and human cancer: the first ten thousand mutations. *Adv. Cancer Res.* 2000; 77: 81-137 .
119. Issaeva N, Bozko P, Enge M, Protopopova M., Verhoef LG, Masucci M, Pramanik A, Selivanova G. Small molecule RITA binds to p53, blocks p53-HDM-2 interaction and activates p53 function in tumors. *Nat. Med.* 2004; 10: 1321–1328
120. Fakharzadeh SS, Trusko SP, George DL. Tumorigenic potential associated with enhanced expression of a gene that is amplified in a mouse tumor cell line. *EMBO J.* 1991, 10: 1565-1569. (b) Oliner JD, Kinzler KW, Meltzer PS, George DL, Vogelstein, B.

- Amplification of a gene encoding a p53-associated protein in human sarcomas. *Nature* 1992, 358, 80-83.
121. Corde DGA. Biological and pharmacological activity of carbazole alkaloids in *The Alkaloids: Chemistry and Biology*. Academic Press, Elsevier. 2008
122. (a) Asche C, Demeunynck Martine. Antitumor Carbazoles. *Anti-Cancer Agents in Medicinal Chemistry* 2007; 7: 247-267 and references therein. (b) Itoigawa M, Kashiwada Y, Ito C, Furukawa H, Tachibana Y, Kenneth F. Bastow KF, Lee KH. Antitumor Agents. Carbazole Alkaloid Murrayquinone A and Related Synthetic Carbazolequinones as Cytotoxic Agents *J. Nat. Prod.* 2000; 63: 893–897. (c) Stiborová M, Sejbal J, Bořek-Dohalská L, Aimová D, Poljaková J, Forsterová K, Rupertová M, Wiesner J, Hudeček J, Wiessler M, Frei E. The anticancer drug Ellipticine forms covalent DNA adducts, mediated by human cytochromes P450, through metabolism to 13-Hydroxyellipticine and Ellipticine N²-Oxide. *Cancer Res* 2004; 64:8374
123. Belmont P, Bosson J, Godet T, Tiano M. Acridine and Acridone Derivatives, Anticancer Properties and Synthetic Methods: Where Are We Now? *Anti-Cancer Agents in Medicinal Chemistry* 2007; 7: 139-169
124. Adams A, Guss JM, Collyer CA. Data Crystal structure of the topoisomerase II poison 9-Amino-[N-(2-dimethylamino)ethyl]acridine-4-carboxamide bound to the DNA hexanucleotide d(CGTACG)₂. *Biochemistry* 1999; 38 : 9221–9233
125. Horstmann MA, Hassenpflug WA, zur Stadt U, Escherich G, Janka G, Kabisch H. Amsacrine combined with etoposide and high-dose methylprednisolone as salvage therapy in acute lymphoblastic leukemia in children. *Haematologica*. 2005; 12:1701-3.

126. Wong W, Ho WC, Dicker DT, Mackinnon C, Winkler JD, Marmorstein R, El-Deiry WS. Acridine derivatives activate p53 and induce tumor cell through Bax. *Cancer Biol, Ther.* 2005; 4: 2005.
127. (a) Clauson-Kaas N, Tyle Z. Preparation of cis and trans 2,5 dimethoxy-2-(acetamidomethyl)-2,5-dihydrofuran, of cis and trans 2,5-dimethoxy-2-(acetamido)-tetrahydrofuran and of 1-phenyl-2-(acetamidomethyl)-pyrrole. *Acta Chem. Scand.* 1952; 6: 667. (b) Elming N, Clauson-Kaas, N. The preparation of pyrroles from furans. *Acta Chem. Scand.* 1952; 6 : 867.
128. Bertamino A, Aquino C, Simona Musella et al. Design and synthesis of spirotryprostatin-inspired diketopiperazine systems as potential cell cycle modulators from prolyl spirooxindolethiazolidine derivatives. *Bioorg Med Chem.* 2010; 18 :4328-37.
- 129.(a) Sherr CJ. Cancer Cell Cycles, *Science* 1996, 274, 1672-7; (b) Sandal T. Molecular aspects of the mammalian cell cycle and cancer. *Oncologist* 2002; 7: 73-81.
- 130.(a) Hung DT, Jamison TF, Schreiber SL. Understanding and controlling the cell cycle with natural products. *Chem. Biol.* 1996; 3: 623-629. (b) Crews CM, Shotwell JB. Small-molecule inhibitors of the cell cycle: an overview. *Prog. Cell Cycle Res.* 2003, 5, 125-33.
131. Osada, H. J. Bioprobes for investigating mammalian cell cycle control. *Antibiot.* 1998; 51: 973-82.
132. Von Nussbaum F, Danishefsky SJ. A Rapid Total Synthesis of Spirotryprostatin B: Proof of its relative and absolute stereochemistry *Angew. Chem., Int. Ed.* 2000; 9: 2175-78.
133. Onishi T, Sebahar PR, Williams RM. Concise, asymmetric total synthesis of spirotryprostatin A. *Org. Lett.* 2003; 5: 3135-7.

134. Miyake FY, Yakushijin K, Horne DA. Preparation and synthetic applications of 2-halotryptophan methyl esters: synthesis of spirotryprostatin B. *Angew. Chem., Int. Ed.* 2004; 43: 5357-60.
135. Wilson RM, Danishefsky SJ. Small molecule natural products in the discovery of therapeutic agents: the synthesis connection. *J. Org. Chem.* 2006; 71: 8329-51.
136. Gomez-Monterrey I, Campiglia P, Carotenuto A, Califano D, Pisano C, Vesce L, Lama T, Bertamino A, Sala M; Mazzella di Bosco A, Grieco P, Novellino E. Design, synthesis, and cytotoxic evaluation of a new series of 3-substituted spiro[(dihydropyrazine-2,5-dione)-6,3'-(2',3'-dihydrothieno[2,3-b]naphtho-4',9'-dione)] derivatives. *J. Med. Chem.* 2007; 50: 1787-98.
137. Dillman R L, Cardellina II J H. An unusual sulfur-containing diketopiperazine from the bermudian sponge *tedania ignis*. *J. Nat. Prod.* 1991; 54: 1159.
138. Grunwald, E. Reaction Coordinate and Structure-Energy Relationships *Prog. Phys. Org. Chem.* 1990;17: 55.
139. Fields GB. Methods in Molecular Biology. Peptide Synthesis Protocols. Methods for Removing the Fmoc Group. Pennington, M. W., Dunn, B. M., Eds., doi: 10.1385/0-89603-273-6:17.
140. Isidro-Llobet A, Guasch-Camell J, Alvarez M, Albericio F. *Eur. J. Org. Chem.* 2005,32: 3031. and references cited therein.
141. Gomez-Monterrey I, Bertamino A, Porta A, Carotenuto A, Musella S, et al. Identification of the Spiro(oxindole-3,30-thiazolidine)-Based Derivatives as Potential p53 Activity Modulators. *J. Med. Chem.* 2010; 53: 8319–8329.
142. Vousden K H, Lu X. Live or Let Die: The Cell's Response to p53. *Nat. Rev. Cancer* 2002; 2: 594–604.

143. Levine A J. P53, The Cellular Gatekeeper for Growth and Division. *Cell* 1997; 88: 323–331.
144. (b) Olivier M, Lees R, Hollstein M, Khan MA, Harris CC, Hainaut P. The IARC TP53 Database: New Online Mutation Analysis and Recommendations to Users. *Hum. Mutat.* 2002; 19,:607–614.
145. (a) Freedman DA, Wu L, Levine AJ. Functions of theMDM2 oncoprotein. *Cell. Mol. Life Sci.* 1999; 55: 96–107. (b) Momand J, Wu HH, Dasgupta G. MDM2 master regulator of the p53 tumor suppressor protein. *Gene* 2000; 242: 15–29.
146. Juven-Gershon T, Oren M. Mdm2: The ups and downs. *Mol. Med.* 1999; 5: 71–83.
147. (a) Haupt Y, Maya R, Kazaz A, Moshe O. Mdm2 promotes the rapid degradation of p53. *Nature* 1997; 387: 296–299. (b) Kubbutat MHG, Jones SN, Vousden KH. Regulation of p53 stability by Mdm2. *Nature* 1997; 387: 299–303.
148. (a) Fakharzadeh SS, Trusko SP, George DL. Tumorigenic potential associated with enhanced expression of a gene that is amplified in a mouse tumor cell line. *EMBO J.* 1991; 10: 1565– 1569. (b) Oliner JD, Kinzler KW, Meltzer PS, George DL, Vogelstein B. Amplification of a gene encoding a p53-associated protein in human sarcomas. *Nature* 1992; 358: 80–83.
149. Bottger A, Bottger V, Sparks A, Liu WL, Howard SF, Lane DP. Design of a synthetic Mdm2-Binding mini protein that activates the p53 response in vivo. *Curr. Biol.* 1997; 7: 860–869.
150. (a) Chen L, Lu W, Agrawal S, Zhou W, Zhang R, Chen J. Ubiquitous induction of p53 in tumor cells by antisense inhibition of MDM2 expression. *Mol. Med.* 1999; 5: 21–34. (b) Zhang Z, Li M, Wang H, Agrawal S, Zhang R. Antisense Therapy Targeting MDM2 oncogene in prostate cancer: effects on proliferation, apoptosis,

- multiple gene expression, and chemotherapy. *Proc. Natl. Acad. Sci. U.S.A.* 2003; 100: 11636–11641. (c) Wang H, Nan L, Yu D, Agrawal S, Zhang R. Antisense anti-MDM2 oligonucleotides as a novel therapeutic approach to human breast cancer: In vitro and in vivo activities and mechanisms. *Clin. Cancer Res.* 2001; 7: 3613–3624.
151. (a) Wasylyk C, Salvi R, Argentini M, Dureuil C, Delumeau I, Abecassis J, Debussche L, Wasylyk B. P53 mediated death of cells overexpressing MDM2 by an inhibitor of MDM2 interaction with p53. *Oncogene* 1999; 18: 1921–1934. (b) Chene P, Fuchs J, Carena I, Furet P, Garcia-Echeverria C. Study of the cytotoxic effect of a peptidic inhibitor of the p53-Mdm2 interaction in tumor cells. *FEBS Lett.* 2002; 529: 293–297.
152. (a) Klein C, Vassilev LT. Targeting the p53-MDM2 interaction to treat cancer. *Br. J. Cancer* 2004; 91: 1415. (b) Vassilev LT. p53 Activation by small molecules: Application in Oncology. *J. Med. Chem.* 2005; 48:4491–4499.
153. (a) Chen J, Marechal V, Levine A.J. Mapping of the p53 and Mdm-2 Interaction Domains. *Mol. Cell. Biol.* 1993; 13: 4107–4114. (b) Kussie PH, Gorina S, Marechal V, Elenbaas B, Moreau J, Levine AJ, Pavletich NP. Structure of the MDM2 oncoprotein bound to the p53 tumor suppressor transactivation domain. *Science* 1996; 274: 948–953.
154. (a) Murray JK, Gellman SH. Targeting protein-protein interactions: Lessons from p53/MDM2. *Biopolymers* 2007; 88: 657–686. (b) Shangary S, Wang S. Small-molecule inhibitors of the MDM2-p53 protein-protein interaction to reactivate p53 Function: A Novel Approach for Cancer Therapy. *Annu. Rev. Pharmacol. Toxicol.* 2009; 49: 223–241.
155. (a) Zhao J, Wang M, Chen J; Luo A, Wang X, Wu M, Yin D, Liu Z. The initial evaluation of non-peptidic small-molecule

- HDM2 inhibitors based on p53-HDM2 complex structure. *Cancer Lett.* 2002, 183, 69–77.
156. Galatin PS, Abraham DJ. A nonpeptidic sulfonamide inhibits the p53-mdm2 interaction and activates p53-dependent transcription in Mdm2-overexpressing cells. *J. Med. Chem.* 2004; 47: 4163–4165.
157. Grasberger BL, Lu T, Schubert C, Parks DJ, Carver TE, Koblisch H.K, Cummings MD, LaFrance LV, Milkiewicz KL, Calvo RR, et al. Discovery and cocrystal structure of benzodiazepinedione HDM2 antagonists that activate p53 in cells. *J. Med. Chem.* 2005; 48: 909–912.
158. Vassilev LT, Vu BT, Grave B, Carvajal D, Podlaski F, Filipovic Z, Kong N, Kammlott U, Lukacs C, Klein C, Fotouhi N, Liu, E. A. In vivo activation of the p53 pathway by small-molecule antagonists of MDM2. *Science* 2004, 303, 844–848.
159. (a) Ding K., Lu Y, Nikolovska-Coleska Z, Qui S, Ding Y, Gao W, Stuckey J, Krajewski K et al . Structure-based design of potent non-peptide MDM2 inhibitors. *J. Am. Chem. Soc.* 2005; 27: 10130–10131.
(b) Yu S, Qin D, Shangary S, Chen J, Wang G, Ding K, McEachern D, et al. Potent and orally active small- molecule inhibitors of the MDM2-p53 interaction. *J. Med. Chem.* 2009; 52:7970–7973.
160. Issaeva N, Bozko P, Enge M, Protopopova M, Verhoef LG, Masucci M, Pramanik A, Selivanova G. Small molecule RITA binds to p53, blocks p53-HDM-2 interaction and activates p53 function in tumors. *Nat. Med.* 2004; 10: 1321–1328.
161. Galliford CV, Scheidt KA. Pyrrolidinyl-spirooxindole natural products as inspirations for the development of potential therapeutic agents. *Angew. Chem., Int. Ed.* 2007; 46: 8748–8758.

162. Domling A. Small molecular weight protein-protein interaction antagonists; An insurmountable challenge? *Curr. Opin. Chem. Biol.* 2008; 12: 281–291.
163. Miskolczi I, Zekany A, Rantal F, Linden A, Kover K, Gyorgydeak Z. Diastereo- and regioisomeric bicyclic thiohydantoin from chiral 1,3-thiazolidine-2,4-dicarboxylic acids. *Helv. Chim. Acta* 1998; 81:744–753.
164. Kerr J FR., Wyllie AH, Currie AR. Apoptosis: A basic biological phenomenon with wide-ranging implications in tissue kinetics. *Br. J. Cancer* 1972; 26: 239–257.
165. Jaanicke RU, Sprengart ML, Wati MR, Porter AG. Caspase-3 is required for DNA fragmentation and morphological changes associated with apoptosis. *J. Biol. Chem.* 1998; 273: 9357–9360.
166. Germain M, Affar EB, D'Amours D, Dixit VM, Salvesen GS, Poirier GG. Cleavage of automodified Poly(ADP-ribose) polymerase during apoptosis. *J. Biol. Chem.* 1999; 274: 28379–28384.
167. (a) D'Silva L, Ozdowy P, Krajewski M, Rothweiler U, Singh M, Holak TA. Monitoring the effects of antagonists on protein-protein interactions with NMR spectroscopy. *J. Am. Chem. Soc.* 2005; 127: 13220–13226. (b) Krajewski M, Rothweiler U, D'Silva L, Sudipta Majumdar S, Klein C, Holak TA. An NMR-based antagonist induced dissociation assay for targeting the ligand-protein and protein-protein interactions in competition binding experiments. *J. Med. Chem.* 2007; 50: 4382–4387.